FABRICATION OF HIGH INFRARED REFLECTIVE TEXTILES BY MAGNETRON SPUTTERING TECHNOLOGY

MIAO DAGANG

Ph.D

The Hong Kong Polytechnic University

2015

The Hong Kong Polytechnic University
Institute of Textiles and Clothing

Fabrication of High Infrared Reflective Textiles by Magnetron Sputtering Technology

Miao Dagang

A thesis submitted in partial fulfilment of the requirements
for the degree of Doctor of Philosophy

October 2014

CERTIFICATE OF ORIGINALITY

I hereby declare that this thesis is my own work and that, to the best of my knowledge and belief, it reproduces no material previously published or written, nor material that has been accepted for the award of any other degree or diploma, except where due acknowledgement has been made in the text.

_________________________________ (Signed)

______MIAO DAGANG__________ (Name of student)

To my beloved parents and wife

Abstract

The growing demand for energy conservation in recent years has been accompanied by an increasing interest in high infrared reflective textiles for heat shielding applications. Traditional heat shielding textiles are mainly produced by laminating a layer of metal onto the fabric. However, there are few scientific studies on producing high infrared (IR) reflective textiles through coating of nano films onto textiles. Therefore, in this project, the aim is to fabricate and investigate innovative high IR reflective textiles by using magnetron sputtering technology.

A systematic investigation is presented in this project, where aluminum doped zinc oxide (AZO)/Ag/AZO multilayer films are deposited onto polyester fabric to obtain a high IR reflectance on its surface. In the study, the surface morphology, crystal structure, chemical composition, ultraviolet (UV)-visible transmittance, electrical and IR properties of the prepared samples are investigated by using Atomic Force Microscopy, Scanning Electron Microscope, X-ray Diffraction, Spectrophotometer, a four-point probe system and Fourier Transform infrared spectroscopy, respectively. An examination of the coated films shows that:

(1) AZO films with a highly *c*-axis oriented wurtzite structure are successfully prepared by using radio frequency (RF) magnetron sputtering. The average visible transmittance and IR reflection rates (from 1.5 to 25 μm) of the deposited films are 84.8% and 30%;

(2) among all of the structures based on AZO and Ag films, the AZO/Ag/AZO sandwich structure exhibits the property of having the highest IR reflection. The AZO/Ag/AZO multilayer film with AZO layers that are 30 nm in thickness and an inner layer of Ag that is 15 nm in thickness shows the highest rate of IR reflection of 97% on a glass substrate and 96% on a PET substrate. In this multilayer film, the inner layer of Ag starts to form a continuous film at a thickness of around 10 nm. The thickness of the Ag layer is also inversely proportional to the film sheet resistance and directly proportional to the IR reflection rate of the film.

(3) In the AZO/Cu/AZO films, the inner layer of copper (Cu) starts to form a continuous film at a thickness of around 11 nm. The AZO/Cu/AZO film samples exhibit a visible transmittance of 60% - 80% and the sample with a Cu inner layer of 15 nm in thickness shows the highest rate of IR reflection of 67% in the far infrared radiation (FIR) region; and

(4) the polyester fabrics coated with AZO/Ag/AZO films (with an Ag inner layer that is 15 nm in thickness) have good water resistance (CA=91.5°) and superior air permeability (17.1 ml/s/cm^2 at 100 Pa) compared to the polyester fabric without any coating. The coated fabrics also exhibit excellent UV protection from UV radiation (UPF=40.64), and demonstrate a high rate of IR reflection of 95% - 96%.

The high IR reflectance and unique properties of AZO/Ag/AZO coated polyester fabrics make them a promising candidate for use in high IR reflective textile products in the future.

Publications

Referred SCI Journals

[1] **D. G. Miao**, S. X. Jiang, S. M. Shang and Z. M. Chen, "Effect of heat treatment on infrared reflection property of Al-doped ZnO films," *Sol. Energy Mater. Sol. Cells.,* vol. 127, pp. 163-168, 2014. (IF: 5.030)

[2] **D. G. Miao**, S. X. Jiang, H. M. Zhao, S. M. Shang and Z. M. Chen, "Characterization of AZO and Ag based films prepared by RF magnetron sputtering," *J. Alloys Compd.,* vol. 616, pp. 26-31, 2014. (IF: 2.726)

[3] **D. G. Miao**, S. X. Jiang, S. M. Shang and Z. M. Chen, "Infrared reflective properties of AZO/Ag/AZO trilayers prepared by RF magnetron sputtering," *Ceram. Int.*, vol. 40, pp. 12847-12853, 2014. (IF: 2.086)

[4] **D. G. Miao**, S. X. Jiang, S. M. Shang and Z. M. Chen, "Highly transparent and infrared reflective AZO/Ag/AZO multilayer film prepared on PET substrate by RF magnetron sputtering," *Vacuum,* vol. 106, pp. 1-4, 2014. (IF: 1.426)

[5] **D. G. Miao**, S. X. Jiang, S. M. Shang, Z. M. Chen and J. Liu, "Infrared reflective property of AZO films prepared by RF magnetron sputtering," *Mater. Technol.* vol. 29, pp. 321-325, 2014. (IF: 0.746)

[6] **D. G. Miao**, S. X. Jiang, S. M. Shang, H. M. Zhao and Z. M. Chen,

"Transparent conductive and infrared reflective AZO/Cu/AZO multilayer film prepared by RF magnetron sputtering," *J. Mater. Sci.-Mater. Electron.* vol. 25, pp. 5248-5254, 2014. (IF: 1.966).

[7] **D. G. Miao**, H. M. Zhao, Q. X. Peng, S. M. Shang and S. X. Jiang, "Fabrication of high infrared reflective ceramic films on polyester fabrics by RF magnetron sputtering," *Ceram. Int.* vol. 41, pp. 1595-1601, 2015. (IF: 2.086)

[8] **D. G. Miao**, S. X. Jiang, H. M. Zhao, S. M. Shang and P. Zhu, "Fabrication of high infrared reflective AZO/Ag/AZO films on polyester fabrics," *J. Mater. Sci.-Mater. Electron.* vol. 26, pp. 1198-1204, 2015. (IF: 1.966)

[9] **D. G. Miao**, A. S. Li, S. X. Jiang, and S. M. Shang, "Fabrication of infrared reflective Ag and AZO/Ag/AZO films on cotton fabrics for solar control," *Ceram. Int.* vol. 41, pp. 6312-6317, 2015. (IF: 2.086)

[10] **D. G. Miao**, H. M. Zhao, A. S. Li, and S. M. Shang, "A novel rapid electropulsing treatment on AZO thin ceramic films," *Ceram. Int.* vol. 41, pp. 8235-8240, 2015. (IF: 2.086)

[11] **D. G. Miao**, H. W. Hu, A. S. Li, S. X. Jiang and S. M. Shang, "Fabrication of porous and amorphous TiO2 thin films on flexible textile substrates," *Ceram. Int.* vol. 41, pp. 9177-9182, 2015. (IF: 2.086)

[12] **D. G. Miao**, H. W. Hu, and L. Gan, "Fabrication of high infrared reflective

Al-doped ZnO thin films through electropulsing treatment for solar control," *J. Alloys Compd.,* vol. 639, pp. 400-405, 2015. (IF: 2.726)

[13] **D. G. Miao**, S. X. Jiang, D. D. Zhao and R. H. Guo, "Microstructure and adhesive properties of TiO_2 coating to PU and PVC leathers," *J. Text. Inst.* DOI:10.1080/00405000.2014.951189, 2014. (IF: 0.770)

[14] **D. G. Miao**, S. X. Jiang, H. M. Zhao, S. M. Shang and Z. M. Chen, "Preparation of Antibacterial Microfiber," *Indian J. Fibre Text. Tes.* (Accepted). (IF: 0.778)

[15] S. X. Jiang, **D. G. Miao** and D. D. Zhao, "Adhesive properties of S.S to PU and PVC leathers," *Int. J. Cloth. Sci. Tech.*, vol. 26, pp. 108-117, 2014. (IF: 0.333)

[16] S. X. Jiang，**D. G. Miao**, G. M. Yang, A. S. Li, Z. M. Chen and S. M. Shang, "Fabrication of Ag thin film on polyester fabric by roll to roll magnetron sputtering system," *J. Mater. Sci.-Mater. Electron.* vol. 26, pp. 3364-3369, 2015. (IF: 1.966)

[17] Z. M. Chen, **D. G. Miao**, S. X. Jiang, R. H. Guo and B. J. Xin, "Y_2O_3: Eu^{3+} luminescent thin film deposited on quartz fiber by electron beam evaporation technology," *J. Mater. Sci.-Mater. Electron.* vol. 26, pp. 4113-4118, 2015. (IF: 1.966)

Referred Conference Papers

[1] **D. G. Miao**, S. X. Jiang, S. M. Shang, Z. M. Chen, "A Study of Infrared Radiation Stealth Textiles," 12th Asian Textile Conference, Donghua University, Shanghai, Proceeding, October 24-26, 930-933, 2013.

[2] **D. G. Miao**, S. X. Jiang, S. M. Shang, Z. M. Chen, "A Study of Antibacterial Microfiber Properties," 12th Asian Textile Conference, Donghua University, Shanghai, Proceeding, October 24-26, 157-160, 2013.

Oral Presentations

[1] D. G. Miao, "Fabrication of low infrared emissivity textiles by RF magnetron sputtering," the 8th ITC Research Student Seminar, The Hong Kong Polytechnic University, 4 December, 2013.

[2] D. G. Miao, "Characterization of AZO/Ag/AZO coated polyester fabric by RF magnetron sputtering," Textile Summit and Research Student Conference, University of Leeds, 24-26 April 2014.

Acknowledgements

First of all, I would like to express my sincerest gratitude to my supervisor, Dr Jiang Shou-xiang Kinor, for his expertise, inspirational encouragement and invaluable help towards my study at the Hong Kong Polytechnic University. His indefatigable dedication to research and enthusiasm in scientific pursuits has inspired me. His dialectical philosophical views in general have contributed to this study.

Great tribute is to be given to my co-supervisor, Dr. Shang Songmin, for his guidance and suggestions toward my research. His comprehensive knowledge and professional views have guided this study.

Special thanks to my wife and my lovely son for their encouragement and support throughout the study. I would also like to thank my diligent parents and parents-in-law for their love. Without their care and understanding, this could not have been achieved.

I would also like to express my appreciation to Prof. Tao Xiao-ming for her support in the experimental work. I am also indebted to the colleagues in my research group, with whom I have had the great pleasure to work with.

Finally, I gratefully acknowledge the grant from the Hong Kong Innovation and Technology Commission (ITP/012/11TP, Dr. Harry Lee (Manager Director of TAL Apparel), and Mr. Yu Rong Zhan (President of Kaiping Xindi Dyeing Mill Co., Ltd.), and thank the Research Committee of The Hong Kong Polytechnic University for providing me with a scholarship.

Table of contents

List of Figures

List of Tables

Abbreviations

AATCC	American Association of Textile Chemists and Colorists
AFM	Atomic Force Microscope
ASTM	American Society for Testing and Materials
AZO	Aluminum doped zinc oxide
FIR	Far Infrared Radiation
IR	Infrared Radiation
ITO	Indium Tin Oxide
MIR	Middle Infrared Radiation
NIR	Near Infrared Radiation
PET	Polyethylene terephthalate
RF	Radio Frequency
SEM	Scanning electron microscopy
TCO	Transparent conductive oxide
UPF	Ultraviolet protection factor
XRD	X-ray diffraction

Chapter 1 Introduction

1.1 Background

In recent years, there has been increasing interest in the fabrication of solar films for automobiles and architectural glass. The sun is the primary heat source of the earth; it provides light and heat in the form of electromagnetic radiation, and the radiation is mainly distributed in a wavelength range from 0.25 to 2.5 μm, due to absorption by the atmosphere. Among them, 50% of the energy is in the near infrared (NIR) region (0.72-2.5 μm) [1]. Besides, the substances that absorb solar energy will also emit heat in the form of thermal infrared (IR) radiation which is another important indirect heat source from solar energy, and the wavelengths of this kind of radiation range from 2.5 to 20 μm [2]. Under the exposure of the sun, solar energy can easily penetrate into a room through common window glass, and thus the indoor temperature will gradually increase. Currently, it is found that in many developed countries, the energy consumed to reduce the temperature is more than 20% of the total energy consumption [3]. Therefore, the demand for energy conservation makes solar films ever more significant as a result of the decrease in non-renewable energy resources.

There are three methods by which heat can be transferred. These processes are known as conduction, convection and radiation [4]. This study is mainly focused on the radiation heat from solar energy. The growing demand for heat shielding has been accompanied by increasing scholarly interest in thin films that are highly visible transparent and NIR reflective [5]. Transparent conductive oxides (TCOs) are one of the potential candidates for use in energy conservation films due to their highly visible transparency and high concentration of free electrons [6-9]. Aluminum doped zinc oxide (AZO) is an emerging TCO material and has been extensively investigated for substituting the widely used yet costly Indium Tin Oxide (ITO), because of its rich storage, non-toxicity, reaction stability in hydrogen plasma as well as due to the ease of its synthesis and processing [10]. AZO has a wide-band gap, and is a degenerate n-type semiconductor with very large concentrations of electrons [11]. These characteristics render AZO with unique properties throughout the electromagnetic radiation spectrum. With photon energies above the band gap, which generally occurs in the ultraviolet (UV) range, AZO is therefore highly UV absorbing. In contrast, AZO becomes highly transparent in the visible range, and in the IR spectrum, its free electrons readily respond to electromagnetic field plasma oscillations and provide it with metallic optical properties beyond the plasma frequency, which even extends well into the microwave region. Nevertheless, the best NIR reflectance of AZO films can only be obtained when heating treatments are employed during or after the deposition process, which increases the overall cost of the solar material fabrication. In order to acquire the desired IR reflection rate and maintain high transmittance, TCO/Metal/TCO multilayer films have recently received renewed interest as a highly promising resource in solar materials [12]. In this case, silver

(Ag) is the optimal metal because of its low resistivity (approximately 1.6×10^{-6} Ω.cm).

Nowadays, most of the thin films that are NIR reflective are deposited onto rigid glass or polyester films to fabricate heat shielding glass and window-films. In considering the fragile and complicated replacement of shielding glass, the development of high IR reflective textiles is becoming more important. Textiles are one of the most important materials in the world, owing to their unique properties of flexibility, wearability and permeability.

With the development of nanotechnology and the advent of synthetic fibers, textile materials have been extensively studied and engineered to meet the demands for a variety of functional fabrics [13]. In recent years, researchers and engineers have tried various techniques, such as traditional textile finishing technologies, chemical plating [14-16], and physical vapor deposition [17] and magnetron sputtering deposition [18,19] to prepare a nanostructured surface on textiles, thus improving the surface properties and expanding their applications. Magnetron sputtering deposition has been proven to be one of the most promising technologies to produce nanostructured textile materials due to the advantages of low processing temperature, stability in quality, high deposition rate, multi-functionality [20,21] and higher bonding strength between the coating and substrate [22].

Currently, energy conservation textiles, such as heat shielding curtains, tents and umbrellas, are mainly developed by coating a layer or several layers of metal onto the textile, and the most popular is aluminum (Al). However, energy conservation textiles prepared by using the above conventional method have drawbacks. For instance, they have low penetration of visible light, reflect visible light which may show pollutants, limit air permeability, and have a stiff hand feel. These drawbacks have restricted the application of conventional energy conservation textiles. Moreover, most current studies are focused on high performance IR reflective glass, but there has not been a systematic investigation on high IR reflective textiles. Therefore, this research focuses on the development of novel high IR reflective textiles which have AZO and metal deposited onto their surface by using magnetron sputtering technology.

1.2 Objectives

High IR reflective textiles are an innovative kind of functional material that can reflect the heat from solar energy and the heat emitted from other objects. It can be used for heat shielding due to their high IR reflectivity.

In this study, AZO and Ag are primarily candidates for coating target materials in sputtering experiments to prepare high IR reflective textiles. Radio frequency (RF) magnetron sputtering technology is chosen as the optimal method to deposit materials with high IR reflection onto textile substrates. AZO/Ag/AZO trilayers are sputtered deposited as the functional films on the innovative textile. One of the most important aspects of developing high IR reflective textile is the investigation of the deposition mechanism which significantly influences the optical property of the developed textile. In addition, the IR property of AZO and the AZO/Ag/AZO films will be systematically investigated, which is an innovative research in the area of TCOs. In considering the cost of Ag, copper (Cu) will also be investigated as a substitute for Ag as the inner layer material. The related performances of the high IR reflective textiles will be assessed and evaluated, and this research will also contribute to developing high IR reflective textiles, specifically those with magnetron sputtered coatings, for the industry and eventual use by the mass market.

The following primary objectives will be achieved in this study:

(1) to develop an innovative way to coat high IR reflective textiles with AZO and Ag films by using RF magnetron sputtering;

(2) to explore the structural, electrical, optical and IR properties of the AZO and AZO/Ag/AZO coated multilayer films;

(3) to investigate the properties of the AZO/Cu/AZO coated multilayer films and provide an option that would have acceptable IR properties at a relatively

reasonable cost; and

(4) to evaluate the performance and properties of the prepared high IR reflective textiles in terms of an elaborated appearance with broad applications.

1.3 Project significance and values

In this project, the aim is to provide novel high IR reflective textiles coated with AZO/Ag/AZO films, and explore an effective deposition process that would contribute to the development of such textiles. Advanced high IR reflective textile products could be developed by using magnetron sputtering technology to produce AZO/Ag/AZO multilayer films. AZO/Cu/AZO multilayer films will also be studied as an alternative with a more reasonable cost to fabricate products with an acceptable rate of IR reflection. There is a lack of research in the development of a deposition process of high IR reflective films for functional textile products, thus constituting a research gap.

The significance of the project is as follows.

(1) The developed innovative textiles have high IR reflectance, which not only can isolate the heat from solar energy, but also that emitted from other substances to achieve energy conservation.

(2) The developed high IR reflective textiles have high UV absorption and IR reflection. They can be used as both UV protective and energy conservation textiles.

(3) Magnetron sputtering technology can be easily used on large functional textiles and characterized by a waterless process and less pollution to the environment compared to wet chemical-based finishing methods. It is therefore a potentially green production process.

(4) The results from this project will effectively contribute to the local textile and clothing industries by expanding the technological applications for their products and improving the added value of their products. The results may also help to improve the competitiveness of local textile companies.

The innovativeness of this project is described below.

(1) AZO has been widely studied for its visible transmittance and NIR reflection; the study is innovative in taking the initiative to analyze the characteristics of its MIR and FIR properties, and therefore contributes to developing a heat shielding textile.

(2) Hitherto, there have been no reports on the coating of visibly transparent materials onto high IR reflective textile through the use of magnetron

sputtering technology. The development of high IR reflective textiles that have multi-layer depositions of AZO/Ag/AZO and AZO/Cu/AZO films is considered to be innovative research in the textile field. The resultant products will not only provide a novel textile with a heat shielding property, but also encourage the use of a waterless process; that is, magnetron sputtering technology in the textile field.

(3) The explored optimal parameters of the magnetron sputtering technique can be further applied to develop tailored high IR reflective textiles that are suitable for different applications.

1.4 Structure of the thesis

Chapter 1 gives a brief introduction on the background of high IR reflective textiles and the historical development of coating technologies. It also highlights the advantages of using TCO and metal in preparing high IR reflective textiles and the innovativeness of applying magnetron sputtering technology in fabric processing. Along with the research problem, the objectives of this research as well as project significance and value are also put forth.

Chapter 2 is a review on the performance and application of high IR reflective coatings. The properties of AZO and TCO/metal/TCO films are introduced and the fabrication technologies of high IR reflective textiles are reviewed. Current developments in high infrared reflective textiles and the advantages of magnetron sputtering are also reviewed.

In Chapter 3, the methodology of the research work will be provided. An outline of the experiment design, introduction of the RF magnetron sputtering system, and discussion of the deposition procedures and characterization methods of the coating films will also be given.

The focus of Chapter 4 is on the preparation and characterization of AZO films deposited onto glass substrates. The properties of the deposited AZO films are then investigated in terms of IR reflection.

In Chapter 5, AZO and Ag based films that are deposited onto glass substrates will be examined. The deposition and characterization of Ag, AZO/Ag, Ag/AZO and AZO/Ag/AZO films will be outlined. After comparing the properties of the deposited films, the optimal film structure with better IR reflection is selected for further study.

In Chapter 6, the optimal film structure, that is, AZO/Ag/AZO, is applied and deposited onto glass and PET substrates respectively. The properties of the deposited multilayer films are investigated as a function of the thickness of the Ag layer. The evolution of the inner layer of Ag is also analyzed in this chapter.

The properties of AZO/Cu/AZO multilayer films that are deposited onto glass substrates are studied in Chapter 7. The evolution of the inner layer of Cu is also investigated with respect to IR reflectance.

The high IR reflective films are then applied onto polyester fabric to fabricate high IR reflective textiles, as discussed in Chapter 8. The IR properties, as well as other physical properties of the coated polyester fabric, are investigated.

Finally, Chapter 9 provides the general conclusions and some suggestions for possible future research work.

Chapter 2 Literature review

2.1 Introduction

This chapter begins with a review of the literature on high IR reflective textiles, which includes work that addresses high IR reflective coatings and the current development of IR textiles. Studies on TCO/metal/TCO multilayer structures will then be reviewed, followed by a discussion on the vacuum deposition used in textile modification. The purpose of this literature review is to provide an understanding of the previous research work in this area and a rationale for using a TCO/metal/TCO multilayer for high IR reflective textiles as well as demonstrate that there are research gaps in the current area of study.

2.2 Infrared reflective textiles

Currently, high IR reflective textiles are commercially available, and these are widely used in heat shielding products. Most of the textiles are made to be IR reflective by using high IR reflective coatings through traditional textile finishing methods.

2.2.1 Infrared reflective coatings

On the market, most commercial energy conservation textiles are made by using textile coating technologies [23-30]. In the production process, the high IR reflective coatings are laminated onto textiles through physical or chemical methods. The coatings mainly contain metal, and semiconductor and conductive polymers. Among all of the coatings, metal is the most outstanding due to its excellent IR reflectivity performance. At present, the metal coatings contain gold (Au), Ag, Al, Cu, Zn, platinum (Pt), cobalt (Co) and nickel (Ni). Among them, Al and Cu are the optimal elements as they are abundantly available and reasonable in cost. Moreover, some of the metal coated high IR reflective textiles are already available on the market.

With regard to semiconductor coatings, the most commonly used types are those of diamond, silicon (Si), Germanium (Ge) and some of Groups Ⅲ-Ⅳ chemicals, such as SnO_2, In_2O_3, ZnO, Ga_2O_3 and CdO [31]. Wang and Yu [32] found that ITO coatings made with high temperature sintering have low IR emissivity when the proportion is about 5%. By comparing the IR emissivity of all of the coatings in their work, Ma et al. [33] reported that AZO has a much higher visible transparency and IR reflection than ITO, which makes it a promising coating with low IR emissivity considering its low cost, higher stability and simplicity in doping.

In addition, conductive polymers have also attracted increasing attention due to their electrical and optical characteristics as both a metal and inorganic semiconductor, as well as having the machinability of common organic polymers.

After doping, the IR reflective ability of the conductive polymers will be largely improved.

Currently, many researchers are dedicated to investigating the properties of high IR reflective coatings and many useful results have been reported. Some researchers [34,35] found that the shape and size of the metal coatings have an obvious influence on IR emissivity. They stated that the wavelength size of the low IR emissivity coatings should be shorter than the MIR and FIR but longer than the NIR wavelength. When the incident wavelength is shorter than the plasma frequency, the material will be highly transparent, and when the incident wavelength is longer than the plasma frequency, the material will be highly reflective [36,37].

Yang et al. [38] prepared high IR reflective coatings by using polyurethane (PU)/titania/silica multilayered core-shell composite micro-spheres. They reported that the IR emissivity values are reduced along with an increase in the covering layers. Hu et al. [39] prepared high IR reflective coatings with good thermal resistance by using epoxy-siloxane and Al as the adhesive and pigment, respectively. They indicated that the composite coatings still have low emissivity after thermal ageing and thermal shock resistance testing. Zhu et al. [40] investigated the characterization of lactate-intercalated Co-iron (Fe) layered double hydroxides (LDHs) and exfoliated nanosheet films with high IR reflection.

They stated that the IR emissivity values of the Co-Fe LDHs are lower than those of Zn-Al due to the special electron configuration of Co and Fe. Yan and Xu [41] studied the synergy effect of silane and cetiltrimethylamonium bromide (CTAB) on the corrosion-resistance of high IR reflective Cu/PU coatings formed on tinplate. They indicated that the interfacial interaction between Cu and PU is improved by the synergy effect, thus benefiting from the dispersion of Cu and the low porosity of the Cu/PU coating, which maintains high IR reflectivity and increases the corrosion resistance of the Cu/PU coating formed on the tinplate. They [42] also studied the surface modification of Cu with Ag by ball-milling on the corrosion resistance of the high IR reflective coatings. They argued that the structure maintains high IR reflectivity and at the same time, enhances the anti-corrosion performance of the coating. Wu and Yu [43] prepared a low IR emissivity coating by using modified Al powder and PU as the metallic pigment and adhesive respectively. The coating showed a lower emissivity and excellent optical properties. The IR emissivity of the composite coating increased with increased thickness, and approached a constant value when the thickness was more than 80 μm. Yuan et al. [44] analyzed the visible/IR optical properties of Al/Fe_3O_4 core-shell magnetic composite pigments. They suggested that these pigments can be used as a novel high IR reflective pigment to improve the multispectral compatibility of high IR reflective coatings.

Kato et al. [45] studied the visible and near IR properties of thin Ag films deposited onto a ZnO substrate. They found that the optical property of low emissivity coatings is determined by the resistivity and surface roughness of the thin Ag films. The light absorbance was reduced with decreases in the resistivity of the thin Ag films. The surface plasmon polariton of the thin Ag films influenced the optical property when the surface became rough. Del Re et al. [46] examined the optical properties of AlN/ZrN/AlN low emissivity coatings, and stated that ZrN films have a high reflectivity in the IR range (85%) and AlN films have a high transmission in the visible range (90%). Lee et al. [47] prepared multi-period low-emissivity filters for display application with a TiO_2/Ti/Ag/TiO_2 multilayer structure. The prepared samples could be used for a display application in that the transmittance of the multilayer structure can be drastically reduced in the NIR region, and the sheet resistance can be low enough to be used for electromagnetic wave shielding. Yuste et al. [48] investigated the visible transmittance of low emissivity titanium nitride (TiN) based coatings for solar thermal applications. They found that the deposition of multilayer structures increases the original transmittance obtained by single TiN coatings by 30%. Chiba et al. [49] analyzed the low-emissivity of a coating of a diamond-like amorphous carbon (DLC)/Ag-alloy multilayer on glass. They found that the coating has a low emittance of less than 0.1 from black body radiation at 297 K and exhibits a transparent heat mirror property embedded in the DLC films. Meszaros et al. [50] studied the effect of thermal annealing on the mechanical properties of low-emissivity multilayer-coatings for architectural applications. It was reported that treatment in an inert atmosphere appears to generally result in lower levels of tensile stress and rupture strength as compared to treatment in an oxidizing atmosphere. Ando and Miyazaki, and Ando et al. [51,52] investigated the moisture resistance of Ag-based low-emissivity coatings. They found that the AZO/Ag/AZO coatings have better moisture resistance than the untreated ones.

It was also reported that aside from good physical and mechanical properties, the adhesion agent should also have high IR reflection to produce high IR reflective products [53]. Wang et al. [54] reported the use of pure, epoxy modified, fluorinated and epoxy modified fluorinated PUs as organic adhesives to prepare high IR reflective coatings with an extremely low emissivity near 0.10 at 8-14 μm. Yuan et al. [55] investigated the influence of binder viscosity on controlling IR emissivity in low emissivity coatings. They stated that low resin viscosity is helpful for aggregating pigment and reducing the thickness of the top polymer layer near the surface, thus reducing the IR emissivity.

With reference to the literature review, it is evident that high IR reflective coatings have been widely studied. However, the application of high IR reflective coating onto fabrics has been mainly focused on the use of traditional textile finishing methods, and therefore, the development of an innovative means for producing high IR reflective textiles still needs to be further studied.

2.2.2 Development of infrared textiles

Aside from textiles with low IR emissivity coatings, some researchers have also carried out studies on IR textiles. Zhang [56] reported that polyethylene terephthalate (PET) textiles prepared by chemical plating with the use of Ni, Cu and Ag can obtain low IR emissivity. At the same time, a fabric with better electrical conductibility and effective electromagnetic shielding can also be obtained. However, chemical plating is a highly polluting process; it cannot fulfill the needs of green production.

Li [57] proposed that low IR emissivity textiles could be possible prepared by coating mono-dispersed spherical silicon dioxide particles onto cotton. Li also found that surface temperature of the fabric with a deeper color is higher than that of the fabric surface with a lighter color. The spherical silicon dioxide particles could increase the IR reflection of these cotton fabrics and the temperature is one degree lower than that of the untreated fabric. This is an innovative study in the use of spherical silicon dioxide particles as an IR reflection agent, but the study result indicates that further research is needed.

Zhang et al. [58] presented a mathematical model for measuring the transmittance of IR radiation through fabrics in the range of 8-14 μm at different ambient temperatures. They found that the IR transmittance through cotton fabric is less than 65%, and for PET fabric, less than 75%. In the relationship between

IR transmittance and fabric thickness, a linear relationship between transmittance and area density was obtained. Xu et al. [59] investigated the IR absorption of textile materials. They found that the textile temperature decreases in accordance with Lambert-Beer's law from the front surface to the backside when the textile was positioned in the direction of the IR irradiation. The results showed that there are some differences in IR absorbing ability among different textiles. Silk can absorb irradiation more effectively than cotton and wool. Polyester textiles absorb less IR energy than the mentioned textiles. These studies show that there is a basic relationship between textiles and IR transmittance/absorption, which would be a useful guide for future research.

Li et al. [60] prepared a new type of insulation coating agent for textile by using nano-TiO_2 and phase-change microencapsules as functional fillers. The results showed that the thermal insulation textiles can be maintained at 23-26 ℃ under simulated summer sunlight in 2 hours. Moreover, the finished fabrics also have a high ultraviolet protection factor (UPF) value above 50+ and anti-water pressure higher than that of European standards. In this study, a multifunctional textile is prepared with an insulation coating agent, which is a good example of a study on the development of multifunctional textiles.

As mentioned above, traditional high infrared reflective textiles are produced by using textile coating technologies, and the most common high IR reflective coatings are those with metal. The metal coatings have low penetration of visible light, reflect visible light which may show pollutants, but in some cases, visible transparency is necessary, such as for heat shielding curtains. Consequently, TCOs come into play due to their highly visible transparency and high IR reflection.

2.3 Transparent Conductive Oxides

TCOs are widely used in solar energy applications and also potential materials for use as energy conservation films due to their highly visible transparency and high concentration of free electrons.

2.3.1 Aluminum-doped zinc oxide

AZO is one of the most important TCOs. It has been widely investigated due to its highly visible transmittance and electrical conductivity.

2.3.1.1 Zinc Oxide

Zinc oxide (ZnO) is a ceramic material and used early on in history, for instance, as a precursor material for brass manufacturing in old China. In 1810, it was discovered by Dr. Bruce in Franklin (New Jersey, USA) as red oxide of zinc. In 1845, it was first named as zincite by Haidinger [61]. The two elements that make up ZnO are abundant in quantity; the content of Zn and O in the earth crust is 132 ppm and 49.4%, respectively. This is very important for large-scale applications of ZnO, for example, as transparent electrodes in thin film solar cells and advantageous in abundance over ITO, which is the dominant transparent electrode material today, wherein there is only 0.1 ppm of In in the earth crust.

ZnO is a compound semiconductor which crystallizes in the hexagonal wurtzite structure, as described by Bragg in 1914, just shortly after the discovery of X-ray diffraction [62]. The crystal structure is shown in Figure 2.1 with two different views. In the hexagonal unit cell of ZnO, which contains two ZnO molecules, the Zn atoms are tetrahedrally surrounded by oxygen atoms. The Zn-O distances in the c-direction are a little shorter than those to the other three oxygen atoms.

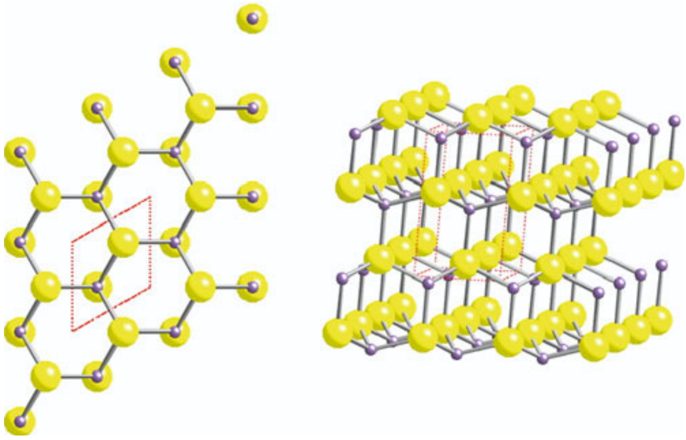

Figure 2.1 Two views of the crystal structure of ZnO. Left: View along the c-axis on the oxygen terminated (001) plane. Right: Perspective view perpendicular to the c-axis. The upper side is the oxygen terminated (001) plane, the bottom plane is zinc terminated (001). Large balls: oxygen, small balls: zinc. The unit cell is shown as dotted lines

2.3.1.2 Optical and electrical properties of ZnO

Figure 2.2 shows the optical reflection, transmittance and absorption spectra of ZnO coated onto glass, which exhibits the key spectral features of a ZnO material [63]. First, the material is quite transparent, about 80% in the visible portion of the spectrum (400-800 nm). Across this spectral region where the sample is transparent, there are oscillations because interference effects from the thin films can be seen in both the transmittance and reflection spectra. The short wavelength that is cut off in the transmittance at about 300 nm is due to the fundamental band gap excitation from the valence band to the conduction band as depicted in the right panel of Figure 2.2. The gradual long wavelength decreases in the transmittance starting at 1000 nm and the corresponding increases in the reflection starting at 1500 nm are due to the collective oscillations of conduction band electrons known as plasma oscillations or plasmons for short.

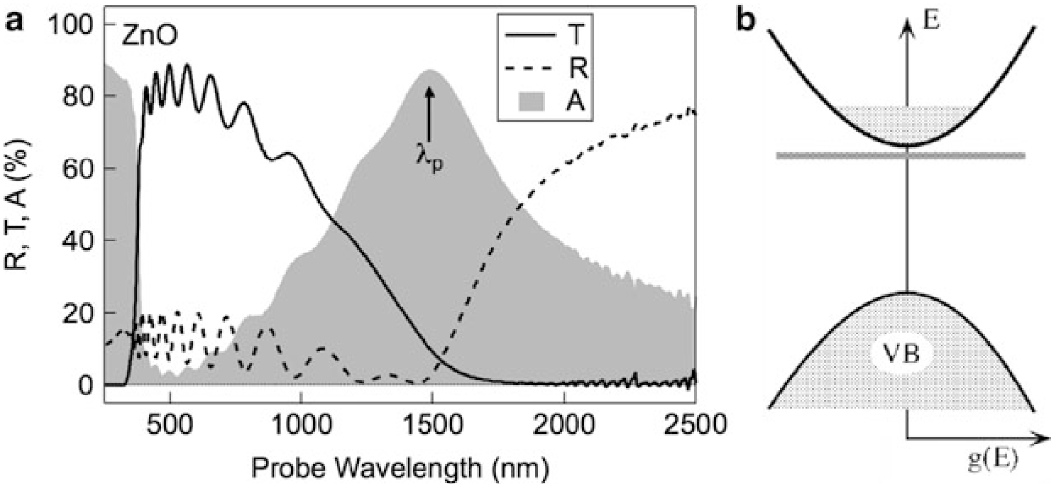

Figure 2.2 Optical spectra and schematic electrical structure of ZnO

2.3.1.3 Bonding concept of Al doping of ZnO

In the doping process, it was assumed that the Al doped atoms were built in onto zinc lattice sites, and spending the additional electrons not required for the bonding to the conduction band in accordance with the following equation (M means metal) [64]:

$M_2O_3 \longleftrightarrow 2\,M_{Zn} + 2e + 2O_O + 1/2O_2$;

thus leading to the following oxygen partial pressure dependence of the electron concentration [e]:

$[e] = [M_{Zn}] \sim P_{O2}^{-1/8}$

In the doping process, Al atoms will be substituted for the Zn atoms. Two of the three valence electrons from the Al atoms replace two electrons of the Zn atom to complete the bonding arrangement. Since all valence bonds or valence band states are fillers, the third electron must go into other band states. However, the third electron is attracted to the net positive charge in the Al atom core, and this produces a series of allowed energy levels in the forbidden band gap just below the conduction band. The energy separation between these levels and the conduction band is sufficiently small such that at room temperature, the attraction can be overcome and the electron will be free to move in the conduction band. Therefore, the conductivity of ZnO will be largely improved due to Al doping.

To obtain unique visible and IR properties, the TCO must be prepared under high temperatures by undergoing heat annealing, which limits its applications [65-75]. In order to solve this high temperature problem in the production process, a TCO/metal/TCO multilayer structure is designed to fabricate highly visible transparency and an IR reflective coating at room temperature.

2.3.2 TCO/metal/TCO multilayer structures

TCO/metal/TCO is an emerging IR reflective material used in the solar energy field; it is also possibly a new material for high infrared reflective textiles.

2.3.2.1 TCO/metal/TCO

Recently, a type of multilayer film that consists of several layers of metal and semiconductor has been investigated as a substitute for the widely implemented TCOs in various applications, such as transparent electrical contacts or electrodes in flat panel displays, touch screens, thin film solar cells, and electrochromic devices [76-96].

There is a wide range of requirements for such TCO/metal/TCO layers depending on the specific application. First, a certain sheet resistance is needed in order to develop electrical conductivity. The required sheet resistance range is from 400-700 Ω/sq for electrodes on touch screens to those less than 10 Ω/sq for large flat panel displays and thin film solar cells [97]. Secondly, another very important property is the transmittance of the layers in the spectral range. The range can be determined by the quantum efficiency of the absorber material for solar cells, by the sensitivity of the human eye, or the reflective to infrared radiation used for heat mirrors and energy saving windows. In spite of the different requisites for specific applications, there are generally two basic factors used to define the TCO/metal/TCO layers: (1) the band gap energy of the oxide must be above 3.1 eV, which renders the oxide transparent in visible light and the transmittance to be more than 80%, and (2) the metal oxide must be susceptible to degenerate doping so that carrier densities of 10^{20}-10^{21} cm^{-3} can be achieved [98-116].

Generally, TCOs are degenerate n-type semiconductors with intrinsic doping by native donors such as oxygen vacancies and/or interstitial metal atoms and additional extrinsic doping by donor impurities [117,118]. There is an inherent limitation in the metal oxide conductivity, and the requirement of transparency and the fundamental scattering mechanism establish an absolute limit to TCO resistivity of about 4×10^{-5} Ω.cm [119]. Actually, it is difficult to approach this resistivity limit owing to additional scattering mechanisms caused by neutral impurities, grain boundaries, or other forms of structural disorders which depend on the inherence of specific materials and details of the preparation procedure [120].

The most well-known TCOs are ITO, fluorinedoped tin oxide (FTO), and AZO [121-140]. ITO dominates the market in high-end electronics and constitutes the most common usage of indium. This is due to the outstanding combination of its optical and electrical properties: an intrinsic band gap of 3.7 eV and electrical resistivity near 2×10^{-4} Ω.cm when deposited at temperatures above 250°C [141]. However, indium is a rare metal and increasing demand combined with its natural scarcity is reflected in its market value [142]. Under this context, indium consumption can be significantly lowered by reducing the thickness of the ITO layer by incorporating other very thin metal films with a very low resistivity of about 10^{-6} Ω.cm [143,144]. Actually, the ITO/Ag/ITO structure can achieve a sheet resistance that is less than 5 Ω/sq and a visible transmittance above 85% with an overall thicknesses of less than 100 nm [145-147]; however, a thickness of more than 400 nm would be required for single-layer ITO electrodes with a resistivity of 2×10^{-4} Ω.cm to obtain the same amount of sheet resistance.

In the ITO/Ag/ITO structure, the key element that contributes to sheet resistance is the Ag layer which has excellent electrical properties and can be made thin enough to provide sufficient visible transmittance. Similar performances have been obtained with other TCO/metal/TCO structures such as AZO/Ag/AZO [148], ZnO/Ag/ZnO [149], InZnSnOx/Ag/InZnSnOx [150], AZO/Ag/FTO [151] and InZnOx/Ag/ InZnOx [152].

Indium is an expensive rare earth element used in the dominant transparent electrode material (ITO) today, wherein the content of this metal is only 0.1 ppm in the earth crust. Therefore, it is important to investigate AZO/Ag/AZO multilayer films as a substitute for the more costly ITO films.

2.3.2.2 AZO/Ag/AZO

AZO/Ag/AZO multilayer films are derived from TCO/metal/TCO structures and widely studied as a substitute for the most costly ITO films. To date, there has been research work with many useful results reported on the AZO/Ag/AZO multilayer structure [153,154].

For instance, Sahu et al. [155,156] prepared AZO/Ag/AZO trilayers by using electron beam evaporation. They found that the trilayers show satisfactory properties of low resistance and high transmittance for applications as transparent conductive electrodes. They also indicated that the trilayers exhibit low sheet resistance of 5.34 Ω/sq and transmittance of more than 85% after thermal treatment. Park et al. [157] and Sutthana et al. [158] both innovatively prepared AZO/Ag/AZO films by using direct current (DC) magnetron sputtering for solar cell applications. Crupi et al. [159] investigated the optimization of AZO/Ag/AZO structures prepared by RF magnetron sputtering. They found that an AZO film as thin as 20 nm is an excellent barrier to Ag diffusion and the inclusion of a thin

Ag layer of 9.5 nm in thickness leads to the maximum enhancement of the electro-optical characteristics. In addition, Wu et al. [160] studied the influence of the thickness of the Ag layer in thin AZO/Ag/AZO films, and found that when the thickness of the Ag layer is 10 nm, the transmittance is more than 70% for wavelengths above 400 nm. When the thickness of the Ag layer is 10 nm, the resistivity is as low as 3.71×10^{-4} Ω.cm. Qi et al. [161] prepared AZO/Ag/AZO multilayer TCO films by using pulsed laser deposition (PLD) and DC/RF sputtering at room temperature.

All of the prepared samples showed a sheet resistance below 5 Ω/sq and maximum visible transmittance of about 85% with a total thickness less than 100 nm. Therefore, the substitution of ITO by using alternative TCOs has become easier with AZO/Ag/AZO structures, because the Ag inlayer can largely reduce the overall resistivity even though the electrical property of AZO is not optimum.

2.3.2.3 AZO/Cu/AZO

Compared to Ag, the most conductive metal, Cu, has an only slightly higher resistivity of about 1.7×10^{-6} Ω.cm, and therefore Cu can be a good substitute due to its cost and availability. In view of the more reasonable cost and acceptable optical and electrical properties, AZO/Cu/AZO multilayer films have also been consequently studied by researchers.

Jung et al. [162] prepared AZO/Cu/AZO multilayer thin films on a polyethersulfone substrate at room temperature. They indicated that the multilayer films deposited onto a flexible substrate show low sheet resistance and stable mechanical properties as compared with single oxide layers. A sheet resistance of 12 Ω/sq, and average visible transmittance of 80% were acquired by the AZO (50 nm)/Cu (9 nm)/AZO (50 nm) multilayer films. Song et al. [163] studied the effects of the thickness of the Cu layer on the properties of AZO/Cu/AZO multilayer films. They found that the critical thickness of the Cu layer is 8 nm, and a multilayer film with an AZO layer of 40 nm in thickness and Cu layer of 8 nm in thickness provides a sheet resistance of 12 Ω/sq and average visible transmittance of 84%. Wang et al. [164] analyzed Cu-based AZO multilayer films that had transparent conductivity and NIR reflectance. They suggested that the critical thickness of the Cu layer is about 7 nm, and the highest NIR reflection of about 40% can be acquired by the AZO/Cu/AZO multilayer film with a Cu inner layer that is 7 nm in thickness.

Lin and Huang [165] also explored the optical structure of AZO/nano-layer metals/AZO sandwich structures, in which the nano-layer metals were Al, Cu and Ag. They found that compared to Cu and Al, the multilayer film with an inner layer of Ag shows the lowest resistivity of 8.9×10^{-5} Ω.cm and the highest average visible transmittance of 81% when the thickness of the Ag layer was kept at approximately 9 nm.

The above studies on TCO/metal/TCO multilayer films are all based on the use of rigid glass substrates to fabricate high infrared reflective textiles through TCO/metal/TCO coatings. Therefore, the literature on TCO/metal/TCO multilayer films prepared on flexible substrates also needs to be reviewed, as follows.

2.3.2.4 TCO/metal/TCO on flexible substrates

Currently, the majority of the production of flat panel displays and thin film solar cells is based on glass substrates which provide rigid support and can withstand the temperatures required for successive production processes [166,167]. In order to meet the expectations for the growing needs of renewable energy and flexible electronics, it has become necessary to substitute flexible plastics for rigid glass as the base substrate [168-170]. This is explained by the fact that the handling of polymer foils of some tens or hundreds of micrometers in thickness is much easier than panes of glass with similar thicknesses. Polymer foils are lighter than glass and flexible, thus allowing low-cost mass production by roll to roll based continuous fabrication processes [171,172].

Thermoplastic polymers have a cost advantage, but cannot withstand the temperatures required for some widely used production steps in semiconductor processing. Currently, it is difficult to make high quality transparent electrodes from the widely used TCOs because the necessary temperatures for achieving low electrical resistivity cannot be applied to flexible substrates. Nevertheless, temperature may not be an issue for TCO/metal/TCO structures because optimum electrical conductivity can be obtained without substrate heating. This is a good solution for flexible electronics and also a promising technology for functional metallic textiles in that high performance films can be prepared by sputtering at room temperature.

Vacuum sputtering is extensively used for TCO deposition onto large areas of glass [173], and also applied to roll to roll deposition of TCO films onto plastics with a large area [174,175]. This technology will be further elaborated in the next section.

2.4 Surface coating technology

Magnetron sputtering is a surface coating technology; an effective technology that produces stable thin films at a high deposition rate. It has been extensively used in architectural glass, and has high potential for preparing functional textiles.

2.4.1 Sputtering

The sputter deposition of films, which is often referred to as sputtering, was first reported in 1852 by Grove [176]. Edison patented a sputtering deposition process that deposited Ag onto wax photograph cylinders in 1904 [177]. It has since been significantly improved to the point that in the last 50 years, sputtering has been widely used to deposit films onto architectural glass, hard drive platters, integrated circuits, and many other applications [178]. The sputtering process is the physical deposition of atoms from a target onto a substrate. It is a glow discharge or a plasma process, which uses ionized gas atoms accelerated by an electric field to erode the target material, which then condense from the gas phase on a work substrate where the film is grown. To attract positive ions, a strong negative field is applied to the target; hence the sputter deposition source is also referred to as the cathode.

Magnetron sputtering refers to the sputtering which places magnets behind a sputtering target. The magnetic field extends into the ambient gas in front of the target, and influences the trajectories of moving charge particles by the Lorentz force caused by the both the magnetic and electric fields [179]. The electrons concentrate near the sputtering target, therefore increasing the amount of ionization in the working gas. The higher degree of ionization in the plasma effective area lowers its resistance, increasing the ion flux (current) relative to the target bias (voltage), and effectively increases the sputtering rate and broadens the operating pressure range. The magnetron sputtering deposition process is shown in Figure 2.3.

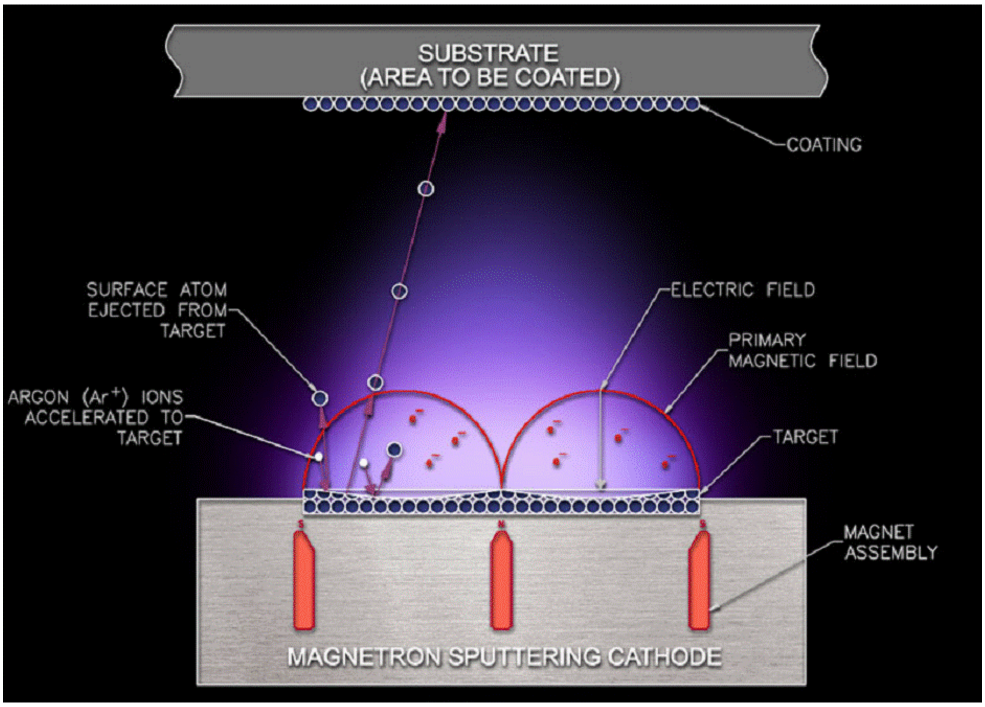

Figure 2.3 Schematic of magnetron sputtering deposition process [180]

Among all the sputtering methods, RF sputtering is one of the most popular; it can be used to deposit material from insulating targets which is different from DC sputtering which can only be used to deposit conductive targets. For instance, Thornton [181] detailed film-atom condensation as a three step process. First, incident atoms transfer kinetic energy to the lattice and become loosely bonded adatoms. Second, the adatoms diffuse over the surface and due to energy transfer, are eventually desorbed or trapped in low-energy lattice sites. Third, the incorporated atoms achieve final positioning within the lattice via bulk diffusion. Moreover, there are three commonly observed nucleation and growth types as follows.

(1) formation of three-dimensional island growth, better known as the Volmer-Weber growth mode, where nucleation is heterogeneous and associated with substrate defects and texture. Growth of the nuclei leads to island formation and coalescence into a continuous film with either a columnar or isotropic microstructure (this is dependent on the deposition conditions previously mentioned in the structure zone models).

(2) Frank-Van der Merwe growth mode, where nucleation is homogeneous. The arriving adatoms stick virtually anywhere onto a uniform crystalline substrate. The adatoms that follow these arriving adatoms complete the monolayer rather than clustering to form islands. This type of growth leads to epitaxy.

(3) Stranski-Krastanov growth mode, which describes a higher advanced intermediate model with continuous layers that form before island formation. As described above, typical puttered thin films, unless deposited at high temperatures (T/ TM > 0.50) or annealed, are columnar in nature.

2.4.2 Advantages of sputter deposition

Sputter deposition is a controlled process of thin film growth. It can be done under different vacuum conditions that vary from below 10^{-5} Torr up to approximately 50 mTorr. Sputter deposition can deposit films of elements, alloys and compounds from either conductive or insulating targets onto different substrates. There are also many other advantages of using sputter deposition, see [182].

One of the major differences between sputtering and thermally excited thin-film preparation methods, such as chemical vapor deposition and evaporation, is the much higher energy released onto the target atoms. The high kinetic energy increases the thermal surface mobility of the sputtered atoms, thus allowing increased rearrangement of the atoms on the substrates, and consequently improving the film properties. The target is generally cooled and will not be affected by the energy of the ejected particles from the momentum transfer of the bombarding ions. Therefore, with the use of only a small amount of heat, sputter deposition becomes an appropriate process to deposit films onto heat sensitive substrates, such as textile fabric. Sputtering deposition therefore provides the possibility of creating new functional textiles, and has already been studied by researchers.

2.4.3 Textiles with sputter deposited thin films

Thin films can be placed onto a variety of textiles by using different sputtering techniques, such as RF, DC reactive and middle frequency reactive sputtering. Comprehensive studies have been carried out on textiles with sputter deposited thin films, and many types of functional textiles have been created, thus making sputtering a promising technique for future similar applications.

The deposition of nanostructured multilayer films onto textile substrates can be applied to make smart functional textiles. These textiles have great potential for applications that range from solar control films to electromagnetic shielding and electronic sensors [183]. Jiang et al. [18] studied the surface functionalization of nanostructured Ag-coated polyester fabric by magnetron sputtering. They found that the surface function of Ag-coated polyester fibers is highly versatile, and the coated fabrics provide excellent UV protection, and exhibit excellent hydrophobicity and good antibacterial performance. Yip et al. [21] compared the characterization of metallic textiles deposited by magnetron sputtering and traditional metallic treatments. The results showed that magnetron sputter coated fabrics have better or similar physical and mechanical properties. Other researchers [184,185] also studied fibers/fabrics coated with Ag through the use of magnetron sputtering. They found that the coated fibers/fabrics have good antibacterial ability, and this ability is primarily determined by the thickness of the Ag film. All of the studies demonstrate that sputter coating has opened up new possibilities in the modification of textile materials and is a promising method for achieving multifunctional fabrics.

Wei et al. [186] analyzed the surface characterization of Cu coated fibers/fabrics. They reported that the sputtered nanoparticles are well deposited onto the textile substrates, and the functions of the coated textiles are largely affected by the sputtering parameters. In addition, the interfacial bonding between the substrate and sputtered Cu was also evaluated. It was found that plasma pretreatment and heating during the sputtering process obviously improve the adhesion between the substrate and Cu.

Deng et al. [187] applied AZO films onto nonwoven substrates by using RF magnetron sputtering. In their study, the influence of the deposition time on the structural, optical, and electrical properties of AZO films was investigated. The results showed that the nonwovens with deposited AZO films have better UV absorption, and the average visible transmittance is approximately 50%. However, the electrical resistance is very high, which is a common problem of sputter coated textiles due to the discontinuous films caused by the structure of the textiles. They also studied the characterization of sputter coated ZnO films on nonwoven material. They found that the size of the ZnO grains is determined by the sputtering time, pressure and time, respectively [188].

After a review of high IR reflective textiles, TCO/metal/TCO multilayer structures and magnetron sputtering, the research gaps have been identified and will be discussed in the next section.

2.5 Research gaps

Based on the extensive literature review carried out in this study, the following research gaps are identified.

Currently, most efforts by researchers are dedicated to studies on the visible transmittance and electrical resistivity of AZO [189-196] and only a few studies have referred to IR reflection [197]. Among the limited research, AZO films were reported to have high visible transmittance (about 80% - 85%) and NIR reflectance (about 50% - 70% at 2500 nm). Therefore, AZO may be desirable for application in electromagnetic interference (EMI) shielding coatings, and heat/microwave reflective coatings for windows. As reported by Zhao et al. [197] in their study, reflectance spectra only up to 2500 nm were investigated due to equipment limitations, and the doped ZnO is a promising IR-reflective material. Therefore, it is important to further examine the MIR and FIR reflection properties of AZO films.

As mentioned above, to date, studies have only focused on the NIR reflection of AZO films, and little attention has been devoted to the IR reflection property of Ag, AZO/Ag, Ag/AZO and AZO/Ag/AZO films, especially IR reflections under 20 μm which is the main region of solar energy and thermal IR radiation from the absorbed solar energy of other substances [2]. Therefore, it is significant to further investigate the IR reflection properties of AZO and Ag based films and selects a proper film structure for further applications of high IR reflective coatings.

AZO/Ag/AZO multilayer films deposited onto rigid glass substrates without post thermal annealing have been extensively studied in recent years because they combine innovative properties with both high visible transparency and electrical conductivity [198-200]. However, few studies have referred to their IR reflection. Therefore, it is essential to investigate the IR reflection of AZO/Ag/AZO films for future development of low emissivity coatings. At the same time, the IR properties of AZO/Cu/AZO films have not been fully analyzed. It is therefore also important to explore the IR properties of AZO/Cu/AZO films to fabricate products with an acceptable IR reflectivity and reasonable cost.

As is commonly known, glass is heavy and fragile, and this is especially problematic for certain applications, such as automobile solar films and electronic maps, where flexibility and lightweight materials are required. As a result, there is the need to find alternative options, and study the innovativeness of depositing AZO/Ag/AZO multilayers onto flexible substrates, such as PET film and textile materials.

High IR reflective textiles currently prepared by using conventional methods have some limitations; they have low visible light transparency, a stiff hand feel and limited air permeability, and reflect visible light which may show pollutants.

Therefore, it is innovative to study the fabrication of novel high IR reflective textiles to address these limitations by depositing AZO/Ag/AZO multilayer films onto textile fabric via magnetron sputtering.

Therefore, a systematic scientific study needs to be conducted to fill the research gaps.

2.6 Summary

Previous research work on high IR reflective textiles has been based on the examining of high IR reflective coatings, current high IR reflective textiles, TCO/metal/TCO multilayer structures, vacuum deposition techniques and developments in the application of vacuum deposition techniques on textiles. Vacuum deposition is a novel technique applied to textile materials to efficiently produce fabrics with multi-functional properties. It involves the application of an ever-widening range of functional films to a wide range of fabrics.

Consequently, based on an extensive literature review, the following research gaps have been identified: (1) there is a lack of research work on the MIR and FIR reflection of AZO films deposited using magnetron sputtering; (2) few in the literature have focused on the IR reflection of AZO and Ag based films; (3) studies on the IR reflection of AZO/Ag/AZO and AZO/Cu/AZO multilayer films are limited; and (4) there is no work that has reported on the deposition of AZO/Ag/AZO and AZO/Cu/AZO multilayer films onto textile fabrics. It is therefore important to address these research gaps in studying vacuum deposition techniques to produce high IR reflective textiles.

Chapter 3 Research methodology

3.1 Experimental outline

In this project, AZO, Ag and Cu based films are deposited onto different substrates by RF magnetron sputtering to fabricate high IR reflective textiles with commercially available AZO (ZnO 98 wt.%: Al_2O_3 2 wt.%), Ag (99.99%) and Cu (99.99%) targets. The design of the research is shown in Figure 3.1.

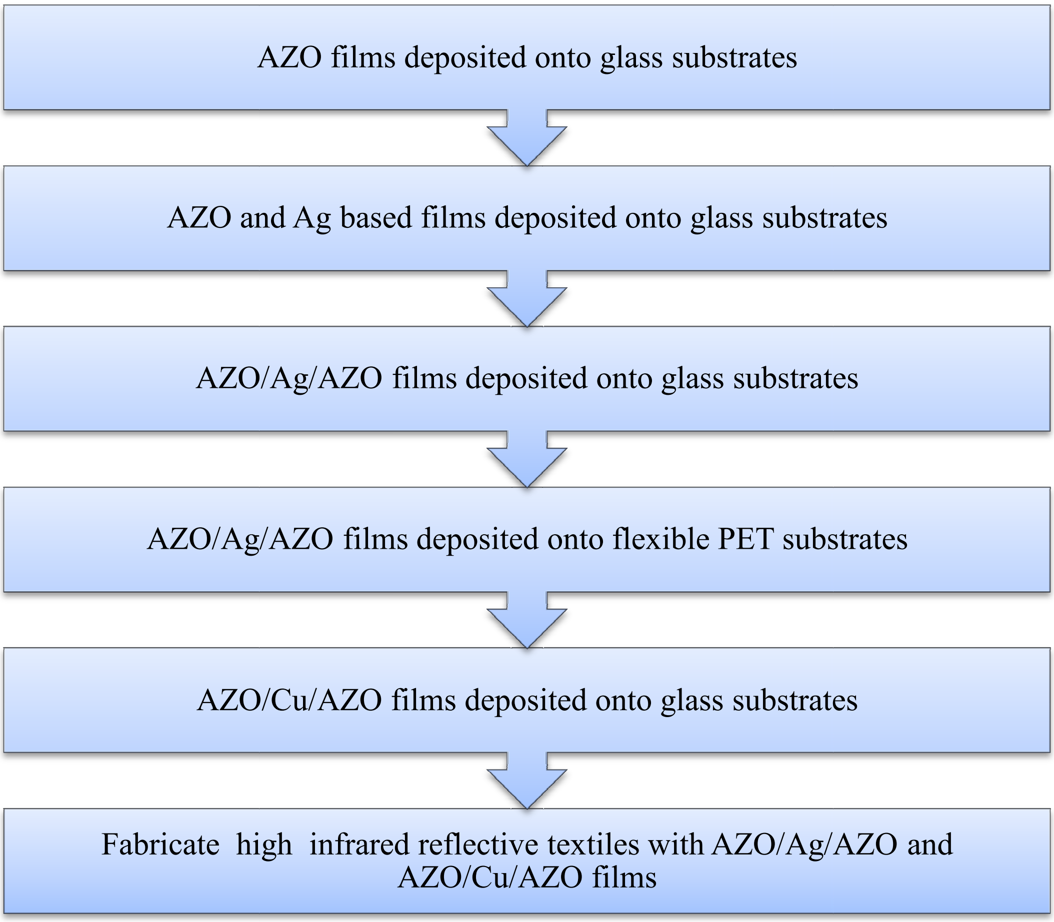

Figure 3.1 Scheme of the experimental process

First, AZO films will be deposited onto glass substrates to examine the IR reflection properties of the deposited films. Second, different AZO and Ag based structures will be designed to explore a better film structure for high IR reflective coatings. Third, the selected film structure will be extensively deposited onto glass substrates; the thickness of the deposited films will be systematically investigated in terms of the IR reflection of the coatings. Fourth, the selected film structure will be deposited onto a flexible PET substrate to examine the IR reflection with regard to furthering studies on high IR reflective textiles. Fifth, Cu will be applied as the inner layer material to substitute for the more costly Ag, and the Cu multilayer film will be deposited onto a glass substrate to investigate its IR reflection. Finally, the multilayer films will be deposited onto polyester fabric to fabricate a high IR reflective textile.

3.2 Materials

The targets were: AZO (ZnO 98 wt.%: Al_2O_3 2 wt.%, Ag (99.99%) and Cu (99.99%). All the targets were purchased from Zhongnuo Advanced Material Technology Co., Ltd.

The substrates were: Borofloat borosilicate glass (thickness: 1 mm), polyester (PET) film (DuPont, thickness: 0.25 mm) and polyester fabric (Xindi China; Yarn fineness: 75D; Warp density: 90; Weft density: 90; Fabric weight: 64.50 g/m^2).

3.3 Radio frequency magnetron sputtering system

RF magnetron sputtering deposition was carried out at room temperature which would avoid damaging the substrates with the high temperature generated during the sputtering process. The equipment used was a self-designed sputtering system. Images of the equipment are shown in Figure 3.2. The system is made of stainless steel, and equipped with a load-locked vacuum system to generate the high vacuum required for sputter deposition. The typical base pressure of the system is approximately 8×10^{-5} Pa.

Figure 3.2 RF magnetron sputtering system

The system originally has two RF and one DC planar source, with each handling a 9 cm target in a sputter up geometry. For uniformity of research, the system with two RF planar sources is applied in this study. The targets used were: ZnO: Al_2O_3 (98 wt.%: 2 wt.%), Ag (99.99%) and Cu (99.99%). A magnetron that is 9 cm in diameter was applied on the top of the targets to closely confine the electrons to the target and increase the sputter rate. The targets and the magnets were cooled by using chilled water and the distance between the substrate and target was 10 cm.

The RF power was supplied by a SY 500W RF generator which can provide an RF of 13.56 MHz. The RF power was applied onto the target through an impedance matching network.

A molecular pump (model KYKY FF-160/620C) and a rotary pump provided the high vacuum environment and rough pumping, respectively. A mass flow controller was used to regulate the flow of the argon (Ar) gas, and in conjunction with the throttling valve to generate a controlled gas ambient system for sputter deposition. During the deposition, the substrate holder was rotated at a speed of 100 rpm to ensure that the nano particles were uniformly attached onto the substrate.

3.4 Deposition procedure

In this project, Borofloat borosilicate glass, polyester (PET) film (DuPont, thickness: 0.25 mm) and polyester fabric (75D/180T 90*90, 64.50 g/m^2) are used as the substrates. Prior to deposition, the substrate materials were first immersed into an acetone solution for 30 min to remove organic solvents and dust, and then rinsed with a spray of deionized water. After that, the samples were dried at a temperature of 50°C and conditioned in accordance with ASTM D1776-04 before sputtering and measurement. The substrates were placed inside the vacuum chamber which was then evacuated to a base pressure of 5×10^{-4} Pa. Other deposition parameters were varied in accordance with the requirements of the different films.

3.5 Characterization of the coated films

(1) Film thickness

The film thickness was controlled by sputtering time, and represented by deposition velocity curves which were drawn after a series of film deposition. To measure the thickness of the deposited film, tape was used on a part of the substrate. After the deposition, the tape was carefully removed, thus yielding a well defined trench step which was equivalent to the thickness of the film. An Alpha-Step 500 (Tencor) profilometer was used to measure the depth of the trench, and five times of measurements on different places and at different deposition times for each sample were conducted. In addition, observation of the film cross sections was also carried out by using a scanning electron microscope (JEOL-7100F) to calibrate the film thickness. The accuracy of the film thickness is better than ±5% as estimated according to the cumulative results which were obtained by multiple measurements on different places and at different times after the deposition process for each sample.

(2) Atomic Force Microscopy

Atomic Force Microscopy (AFM) micrographs were taken with a Bruker Nanoscope 8 microscope. Samples that were roughly 10×10 mm in size were attached onto a steel sample mount with double sided tape, and placed onto the magnetic holder on the instrument. The micrographs were taken in the tapping mode in air and scanned in the x-y directions. The height was also measured for each micrograph. All of the images and data were taken from the height measurements. The root mean square roughness (Rq) of the prepared samples was calculated by using NanoScope Analysis software V1.2.

(3) Scanning Electron Microscope

Scanning Electron Microscope (SEM) images were taken by using a JEOL-7100F microscope.

(4) X-Ray Diffraction

X-ray diffraction spectra were collected by using a Rigaku SmartLab powder diffractometer with Cu Kα radiation (λ=0.154 nm) to analyze the crystal phases and structure of the coated films. The standard setting for the X-ray generator was 45 kV at 200 mA. The θ/2θ spectra were collected with a step scan over a 2θ range of 30° to 70°, a step size of 0.02°, and the scanning speed was 5°/min.

(5) Electrical property

The sheet resistance of the coated films was detected by a four-point probe system (Suzhou Jingge, ST-2258A). Five times of measurements on different places for each sample were conducted.

(6) UV-VIS Spectrophotometry

Optical spectrophotometry was carried out by using a Lambda 18 spectrophotometer, from the UV region into the near IR region in order to obtain UV/visible transmittance spectral features. Transmittance spectra were collected at normal incidence by using double beam geometry with a sampling and a reference beam. For all measurements, the reference path was left open and the background spectrum of the substrate material was not moved.

(7) Ultraviolet radiation penetration

UV transmittance through a substance is the crucial factor for determining the UV protection properties of a substance. The ultraviolet protection factor (UPF) is used to illustrate the amount of UV protection provided to skin by a substance. UPF is defined as the ratio of the average effective UV irradiance for unprotected skin to the UV irradiance protected by the test specimen. A higher value indicates better UV protection properties provided. The value of the UPF was recorded and the results of the UV protection materials were classified according to the rated UPF.

The UV radiation penetration of the coated films was evaluated by a UV-visible spectrophotometer (Varian, Cary 300 Conc) over wavelengths that ranged from 280 to 400 nm. The UPF results were determined by using the methods described in AATCC 183-2010.

(8) Contact angle

The contact angle (CA) measurements were conducted by using a CA meter (model CAM-Moric; Tantec Inc.). Samples (2.0 cm×2.0 cm) were taken from the coated fabrics and placed onto the observation platform. A water drop of 5 μl was placed onto the tested sample and the CA was measured by manual manipulation of the protractor on the apparatus. The measurements were taken on the side of the water droplet 1 min after its placement. The results were assessed by conducting measurements on three individual locations on three different fabric samples. The statistical mean and standard deviation of the characterization data were then calculated for presentation purposes.

(9) Air permeability

Air permeability measurements were taken by using an air permeability tester (SDL International, M021S) in accordance with ISO 9237:1995. The testing area was 5 cm^2 and the pressure drop across the testing area was 100 Pa. Repeat the test on five different samples prepared under the same sputtering condition, and two times of test on each sample.

(10) Infrared properties

IR transmittance and reflection measurements of the samples were completed by using a Perkin Elmer Spectrum 100 spectrometer. A fixed angle (16°) specular reflectance accessory was used to measure the coated glass and PET samples and a diffuse reflection accessory was used to measure the coated textiles.

Chapter 4 Preparation and characterization of AZO films[i]

4.1 Introduction

Based on the problems mentioned in the literature and also the research gaps discussed in Chapter 2, the preparation and analysis of AZO films will be discussed in this chapter. In order to study the basic deposition parameters, RF powers of 100, 150 and 200 W are applied to prepare the samples. After preparation, AFM, SEM, XRD, and UV-VIS spectrophotometry are conducted, and the film resistivity and IR reflection/transmittance spectra of the coated films are examined, to investigate the properties of the AZO films.

4.2 Preparation of AZO films on glass substrates

In order to acquire the basic properties of AZO films, RF magnetron sputtering was conducted to prepare AZO film on glass substrates at room temperature. Based on the capabilities of the sputtering system in this project, and other research results [201-212], the following deposition parameters were chosen (as shown in Table 4.1).

---

[i] *Parts of this chapter have been published in* ***Solar Energy Materials and Solar Cells*** *and* ***Materials Technology.***

Table 4.1 Deposition parameters of AZO films

RF power	100 W	150 W	200 W
Base pressure	5×10^{-4} Pa	5×10^{-4} Pa	5×10^{-4} Pa
Ar flow rate	40 sccm	40 sccm	40 sccm
Working pressure	0.5 Pa	0.5 Pa	0.5 Pa
Sputtering time	10, 30, 50 and 70 min	10, 30, 50 and 70 min	10, 30, 50 and 70 min

4.3 Characterization of AZO films

4.3.1 Film thickness and deposition velocity curve analysis

The thickness of the AZO coated films determined under various deposition parameters is shown in Table 4.2 and Figure 4.1 (sample number is included for further experiments and discussion). As shown in the results, all of the AZO films grow at a linear speed under different RF power levels in that the film thickness increases with increases in deposition time, except for the samples prepared under an RF of 100 W, for which the deposition line is not quite linear. The average deposition speed under RFs of 150 W and 200 W was determined to be 3.58 and 5.87 nm/min, which supports that the deposition speed is directly proportional to the sputtering power.

Ar atoms were ionized and accelerated under an electrical field to bombard the

AZO target. A higher RF power can provide more ionized Ar atoms with higher speed; therefore, more AZO atoms with high kinetic energy would be sputtered out, and thereafter deposited onto the glass substrate. This would explain the relationship between the sputtering power and deposition speed. When the RF power was 100 W, the kinetic energy of the sputtered AZO atoms was limited, and not all could be deposited onto the substrate. Therefore, the deposition velocity curve is not as linear as that of the films deposited under RFs of 150 W and 200 W.

Table 4.2 Film thickness (nm) of AZO coated films

RF power	100 W	150 W	200 W
10 min	20(#1)	38(#5)	63(#9)
30 min	67(#2)	111(#6)	180(#10)
50 min	86(#3)	174(#7)	294(#11)
70 min	142(#4)	248(#8)	394(#12)

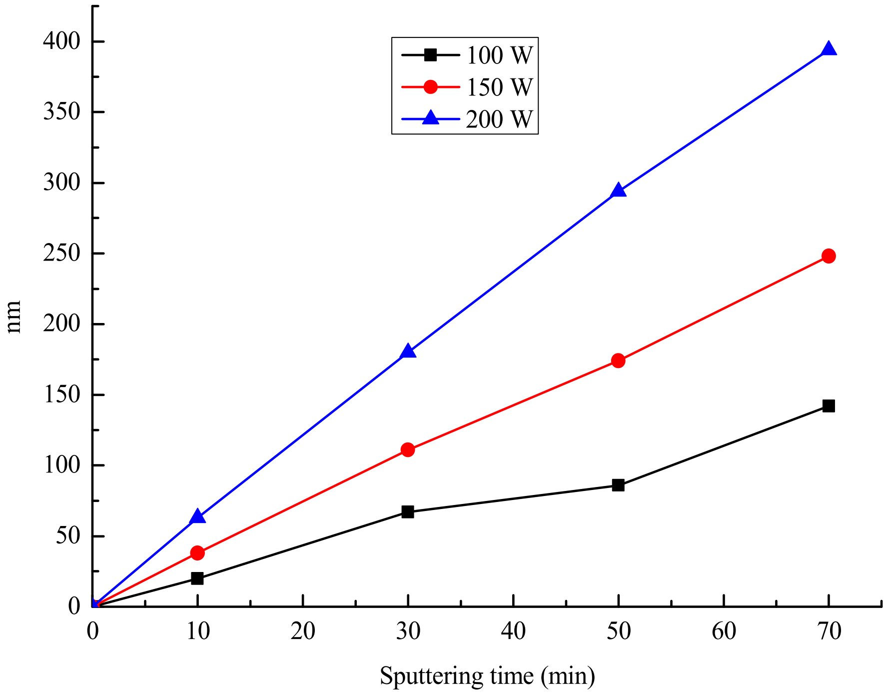

Figure 4.1 Deposition velocity curve of AZO films under RFs of 100, 150 and 200 W

4.3.2 Crystal structure of AZO coated films

The XRD spectra of the coated samples are shown in Figure 4.2. In the spectra, it is clear that only the pure phase of ZnO (002) can be detected on the coated films. The deposited films exhibit a highly *c*-axis orientation which is revealed by the height of the (002) peak, thus reflecting the wurtzite structure of the AZO film. It can also be observed that the intensity of the ZnO (002) peaks is significantly enhanced with increased sputtering time and RF power. The intensity of the ZnO (002) peaks is affected by the both film thickness and crystal size. As discussed in in Section 4.3.1, film thickness increases with an increase in the sputtering time and power. Therefore, thicker AZO films would show higher ZnO (002) peak intensity. The analysis of the grain size of the coated films is discussed in the following section.

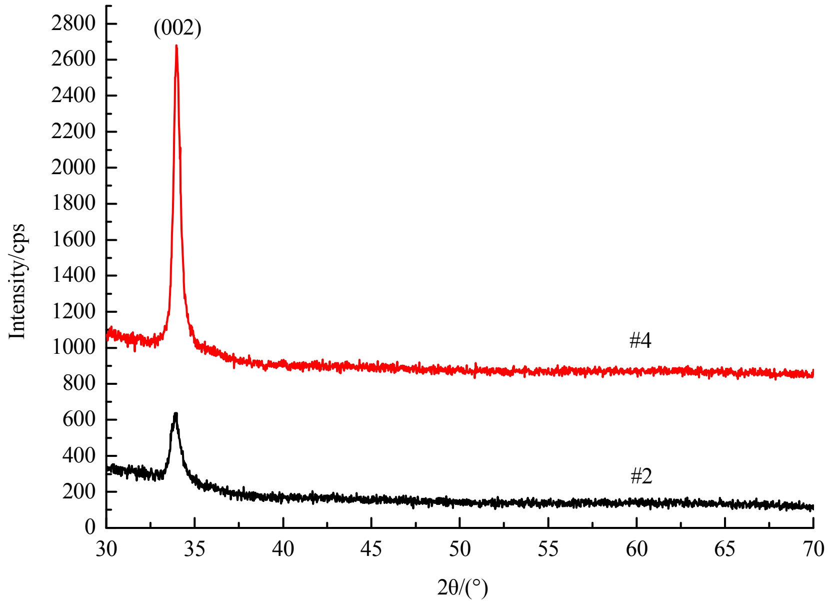

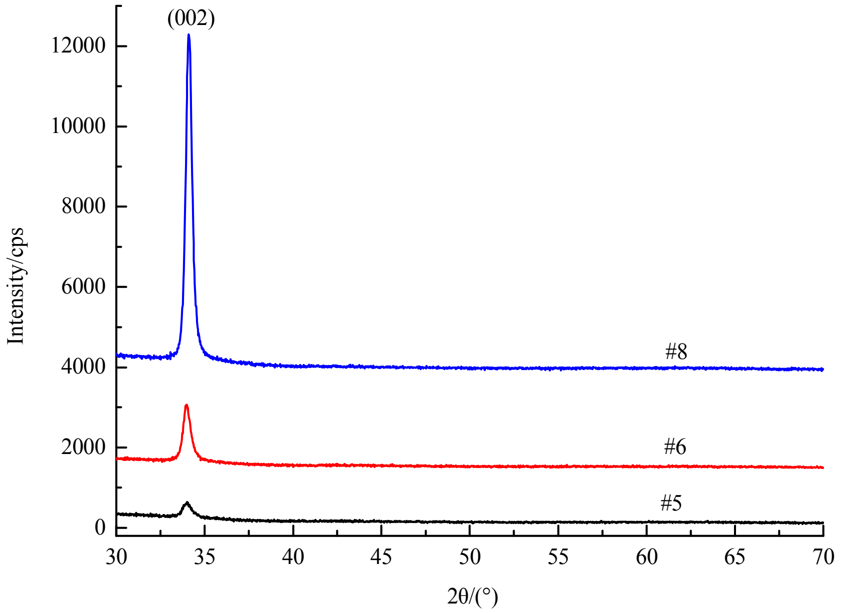

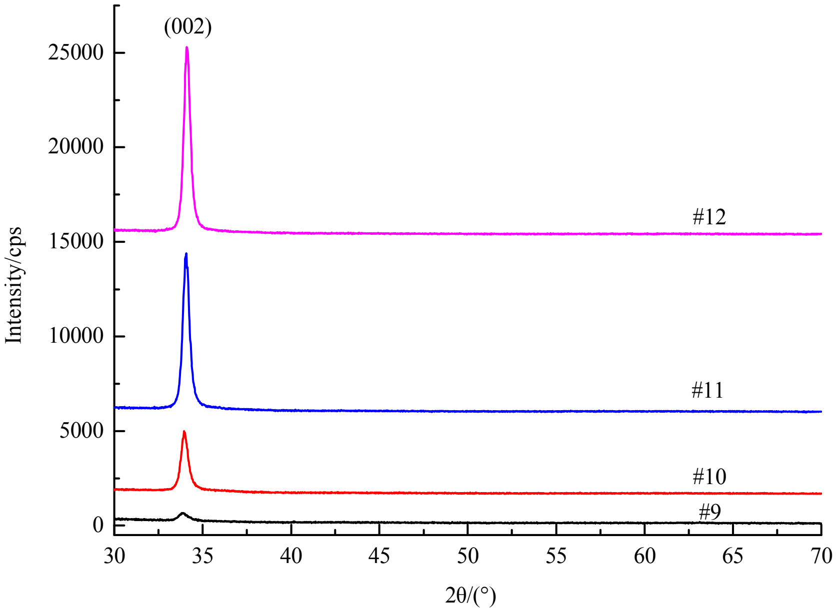

Figure 4.2 XRD spectra of AZO coated samples

The grain size along the (002) longitudinal direction can be determined by using the well-known Scherrer equation [213]. The results are shown in Table 4.3. As shown in the table, the grain size is closely related to the sputtering time and RF power, in that the grain size increases as the sputtering time and power are increased. In addition, the largest grain size of the coated films is 20 nm prepared under an RF of 150 W.

Grain size is determined by the energy of the particles deposited onto the substrate; substrate; high energy particles are more inclined to form grains with a larger size. size. With increases in the sputtering power, the kinetic energy of the sputtered particles will be increased and at the same time, the energy of the deposited particles will also be improved with accumulation of sputtering time. Therefore, the grain size of the AZO coated films would increase with increases in sputtering sputtering time and power. However, when the sputtering power is too high, the deposited film could also be sputtered out by the sputtered particles, which causes causes degeneration of the coated film. This phenomenon is why the largest grain size is obtained in Sample 8.

Table 4.3 Grain size of AZO coated films

Sputtering time	100 W	150 W	200 W
10 min	13.8 nm	14.8 nm	16.2 nm
30 min	15.0 nm	17.1 nm	17. 9 nm
50 min	15.9 nm	18.6 nm	19.2 nm
70 min	18.3 nm	20.0 nm	19.8 nm

4.3.3 Surface morphology of AZO coated films

The AFM images of Samples 5 and 8 are shown in Figure 4.3. In the figure, AZO particles can be detected on both samples. Furthermore, the AZO particles on Sample 8 are much larger than those on Sample 5. With an increase in the sputtering time, more particles would be sputtered onto the substrate and the deposited particles would aggregate into larger sized particles. The surface roughness of Samples 5 and 8 was 0.91 and 3.81 nm, which was determined by using NanoScope Analysis software V1.2. This result indicates that the surface of Sample 5 is much smoother than that of Sample 8, which is due to the aggregation of the small particles.

The SEM images of Samples 5 and 8 are shown in Figure 4.4. It is obvious that the particles on Sample 5 are much smaller in size than those on Sample 8, which is consistent with the AFM images. The AZO particles on Sample 5 are about on average, 20 nm in size; in contrast, the particles on Sample 8 are about 70 nm in size. Both the AFM and SEM images prove that nano-sized AZO particles are well deposited onto the glass substrates by RF magnetron sputtering at room temperature.

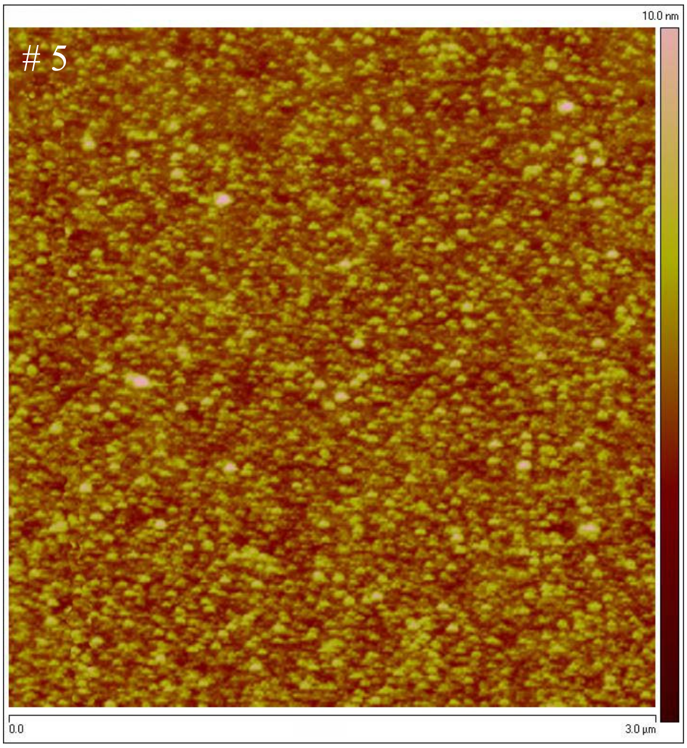

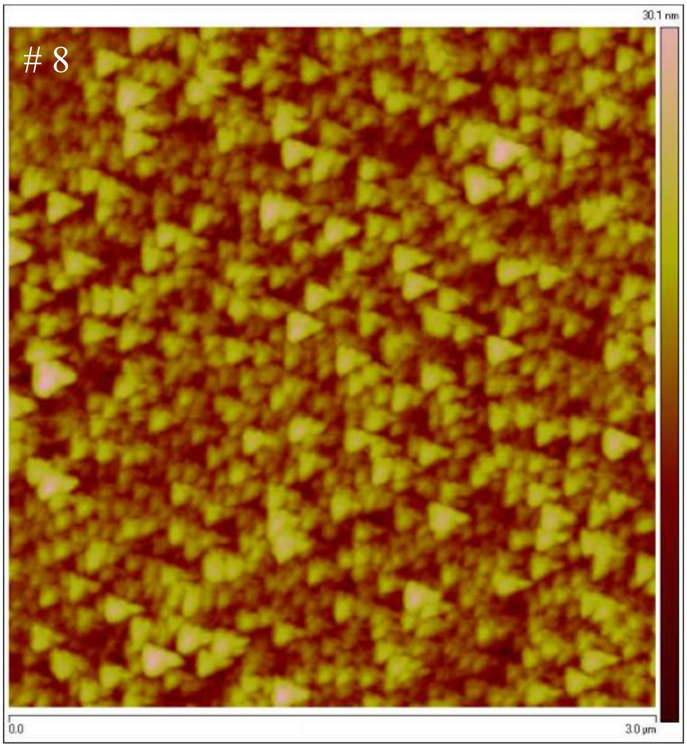

Figure 4.3 AFM images of AZO films deposited under an RF of 150 W for 10 min (Sample 5) and 70 min (Sample 8)

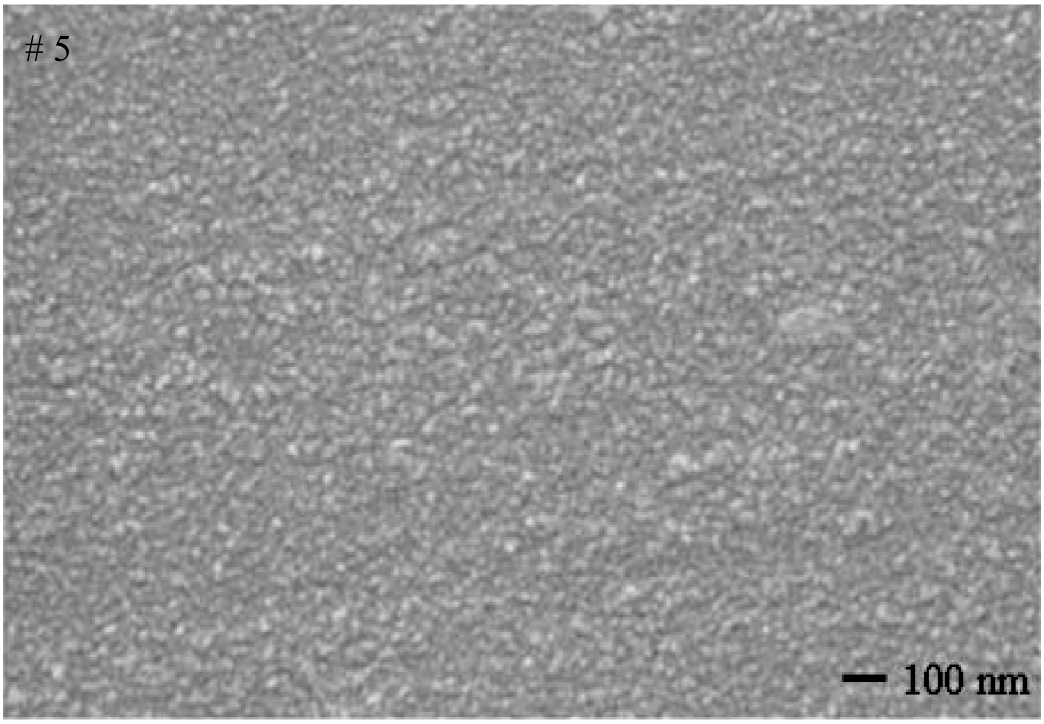

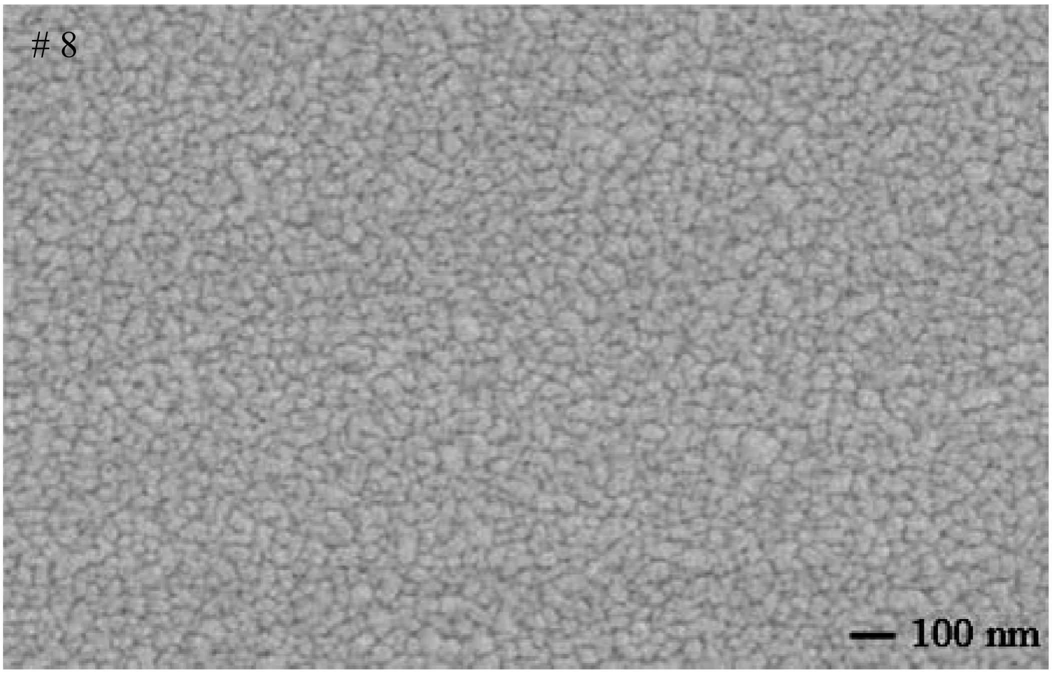

Figure 4.4 SEM images of AZO films deposited under an RF of 150 W for 10 min (Sample 5) and 70 min (Sample 8)

4.3.4 Electrical properties of AZO coated films

Table 4.4 shows the electrical properties of Samples 6 and 8. It can be seen that the film resistivity decreases with increases in the film thickness. The relationship between resistivity, Hall mobility and carrier concentration can be described by the following equation, in which resistivity is inversely proportional to carrier concentration and mobility:

$$\rho = \frac{1}{\sigma} = \frac{1}{ne\mu}$$

where ρ is the resistivity, n is the carrier concentration, μ is the mobility, and e is the electron charge. The carrier concentration and Hall mobility are affected by crystal lattice deficiencies and grain boundaries; better crystallization would reduce the crystal lattice deficiencies and grain boundaries, and increase the carrier concentration and Hall mobility. The results from testing the electrical properties proved that Sample 8 has better crystallization than Sample 6, which is consistent with the XRD results provided in Section 4.3.1.

Table 4.4 Electrical properties of AZO samples, Samples 6 and 8

Sample	Resistivity (ohm-cm)	Hall mobility (cm^2/v-s)	Carrier concentration (cm^3)
6	0.684	0.575	$1.59*10^{19}$
8	0.0399	2.71	$5.77*10^{19}$

4.3.5 UV-VIS properties of AZO coated films

The UV-VIS spectra of the AZO coated films are shown in Figure 4.5. As shown in the figure, all of the samples show a high transmittance of about 80% (uncoated glass 90.5%) in the visible range and the transmittance is also affected by the film thickness. Table 4.4 shows the average visible transmittance (in a wavelength region of 400 to 800 nm) of the coated samples. Among all of the samples, the films coated under an RF of 150 W have relatively high visible transmittance, which could be due to an appropriate deposition speed and better crystallization.

Table 4.4 Average visible transmittance of AZO coated samples

Sputtering time	100 W	150 W	200 W
10 min	89.1%	83.3%	78.4%
30 min	79.9%	81.8%	83.9%
50 min	78.5%	84.8%	80.8%
70 min	82.2%	81.9%	83.3%

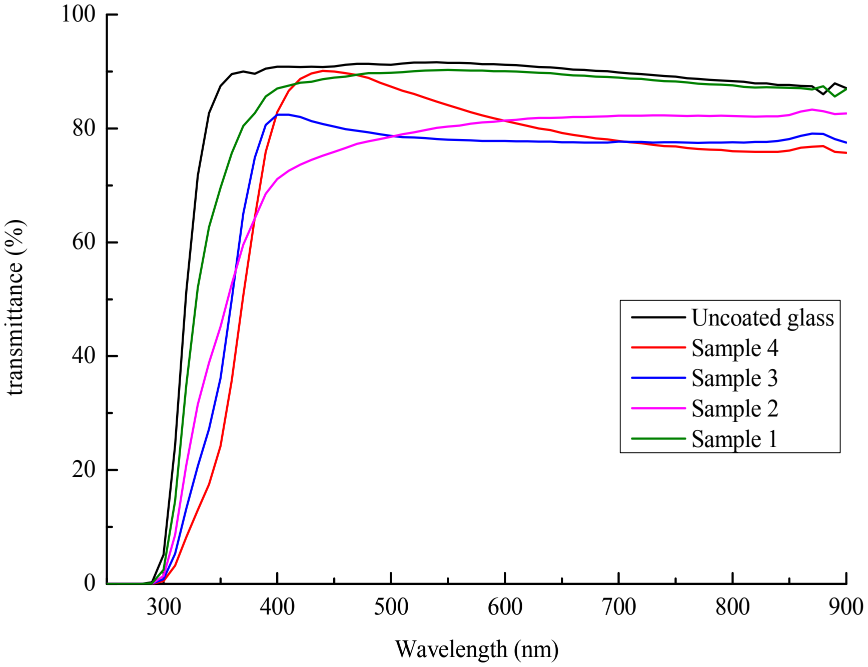

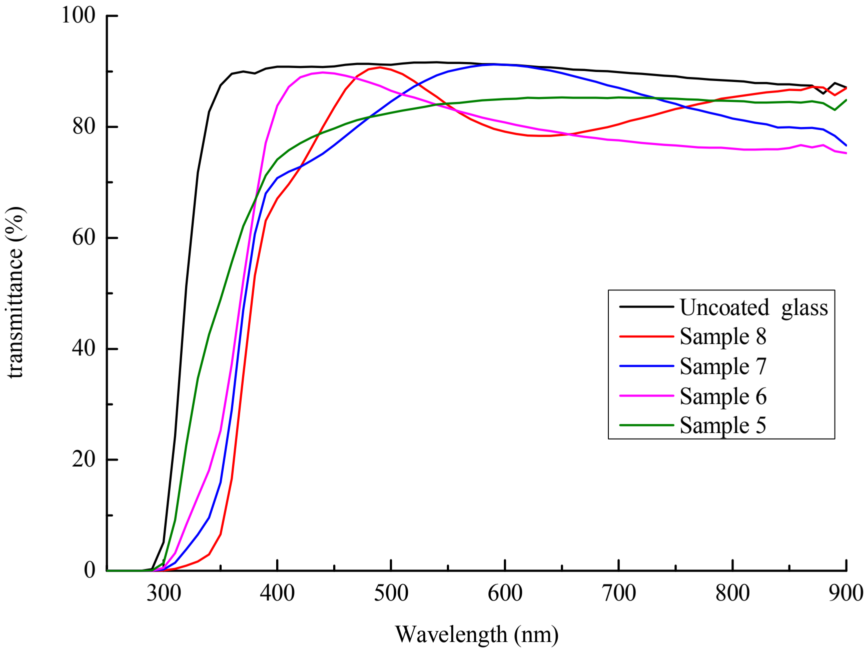

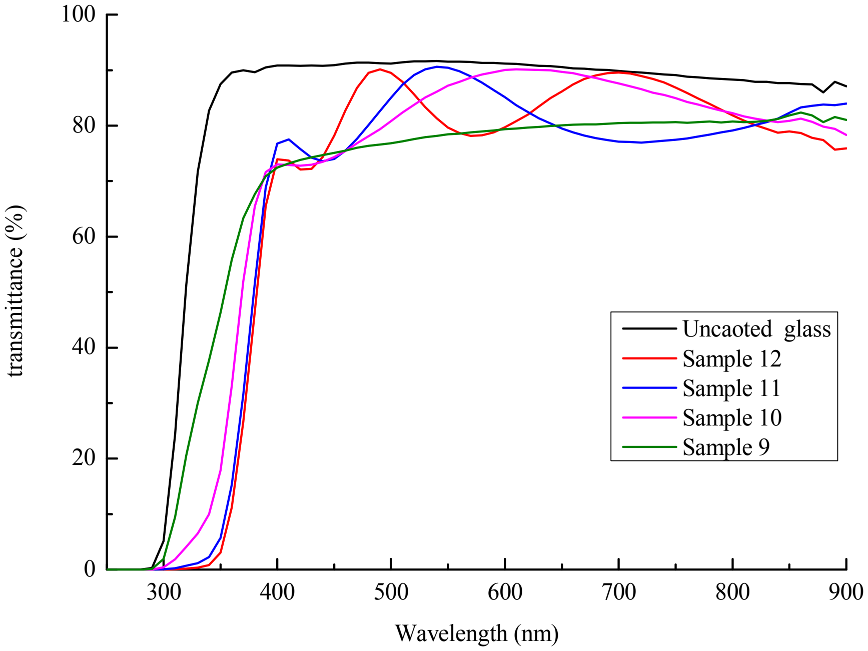

Figure 4.5 UV-VIS spectra of AZO coated samples

4.3.6 Infrared properties of AZO coated films

Figure 4.3 shows the IR reflection and transmittance properties of uncoated glass, and Samples 6 and 8. In the figure, the IR reflection of Sample 6 does not show any obvious improvement compared to that of the uncoated glass. For Sample 8, the average rate of the IR reflection of the whole band range is approximately 30%, which is higher than that of the uncoated glass by about 10%. It can also be noticed that there is a large IR reflection band at around 9.5 μm, which is the reflection region of the uncoated glass. In this region, the IR reflection of the uncoated glass is greater than that of the coated films due to film interference.

IR reflection is caused by the interactions between IR electromagnetic waves and free carriers in the AZO film in that the free carriers would reflect the IR photons. Sample 8 has much higher free carriers than Sample 6, and more free carriers would mean more IR photons will be reflected; therefore, Sample 8 exhibits better IR reflection than Sample 6. In considering the relationship between free carriers and film resistivity, it could be deduced that IR reflection is inversely proportional to film resistivity.

In the transmittance spectra, the transmittance of the coated samples is lower than that of the uncoated glass, and the IR transmittance tends to zero when the IR wavelength is longer than 5 μm caused by the high IR absorption of the uncoated glass in this wavelength region. Sample 8, which has films with greater thickness, shows the lowest IR transmittance; this is contrary to the IR reflection result. Based on the law of energy conservation, when more IR electromagnetic waves penetrate a substance, this means that fewer would be reflected.

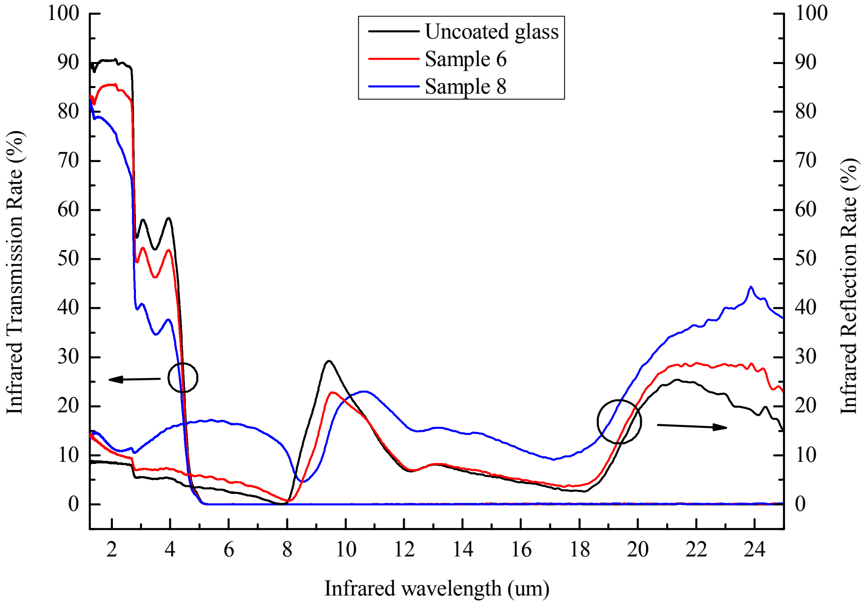

Figure 4.6 IR transmission and reflection spectra of uncoated glass, AZO samples prepared under an RF of 150 W for 30 min (Sample 6) and 70 min (Sample 8)

4.4 Summary

AZO films are deposited onto glass substrates under different sputtering parameters. The film deposition speed, surface morphology, crystal structure, UV-visible transmittance, and electrical and IR properties of the AZO coated films have been investigated. The results indicate that the average deposition speed under an RF power of 150 W and 200 W is linear, and they are determined to be 3.58 and 5.87 nm/min, respectively. The AFM and SEM images illustrate that the deposited particles increase in size with sputtering time, and nano-sized AZO particles are obtained through RF magnetron sputtering. The crystal structure analysis indicates that the AZO coated films exhibit a highly *c*-axis orientation with a wurtzite structure. The peak intensity of ZnO (002) and film grain size increase with increased sputtering time. The UV-VIS spectra show that all of the prepared samples have a high transmittance of about 80% (uncoated glass 90.5%) in the visible range and the transmittance is also affected by the film thickness. Samples coated under an RF of 150 W have relatively high visible transmittance, which is due to an appropriate deposition speed and better crystallization. The results of testing the electrical and IR properties indicate that the average rate of IR reflection of Sample 8 is approximately 30% in the whole band range, which is higher than that of the uncoated glass of 10%. As expected, the sample with the highest IR reflection shows the lowest IR transmittance. It can also be observed that film resistivity is inversely proportional to IR reflection.

In summary, an RF of 150 W is the optimal sputtering power for deposition of AZO films at room temperature with the use of the current sputtering system. The prepared AZO samples show higher IR reflection than the uncoated glass, but the reflection is still considered to be low, so it is not sufficient for developing high IR reflective textiles. Consequently, further studies will need to be conducted, and these will be described in the following chapters.

Chapter 5 Preparation and characterization of AZO and Ag based films[ii]

5.1 Introduction

As reported in Chapter 4, AZO films deposited at room temperature have low IR reflection, which is not appropriate for use in high infrared reflective textiles. Therefore, based on the literature review, AZO/Ag/AZO multilayer films are taken into consideration instead, as they may potentially be good enough to provide low emissivity coatings. In order to confirm the suitability of the film structure, Ag, AZO/Ag, Ag/AZO and AZO/Ag/AZO films are prepared and analyzed. After preparation, the crystal structure, surface morphology, electrical properties, visible transmittance, UPF and infrared transmittance/reflection properties of the coated films are systematically investigated.

5.2 Preparation of AZO and Ag based films on glass substrates

In order to choose a suitable type of coating for high infrared reflective textiles that could be potentially marketed in the future. Ag, AZO/Ag, Ag/AZO and AZO/Ag/AZO films were deposited onto Borofloat borosilicate glass substrates at room temperature by using an RF magnetron sputtering apparatus. In

---

[ii] *Parts of this chapter have been published in the* ***Journal of Alloys and Compounds****.*

considering the capabilities of the sputtering system in this study, and other research results [159,160], the deposition parameters of the Ag and AZO films (AZO films will be deposited with the selected parameters in Chapter 4) are shown in Table 5.1. The samples used in this study are listed in Table 5.2. In each group, the AZO layer was fixed at 30 nm and Ag layers were deposited at a thickness of 5, 10 and 15 nm, respectively. The film thickness was controlled by the deposition velocity, and the results are shown in Figure 5.1 by means of a deposition velocity curve.

Table 5.1 Deposition parameters of AZO and Ag based films

	AZO Layer	Ag Layer
Base pressure	5×10^{-4} Pa	5×10^{-4} Pa
RF power	150 W	10, 30 and 50 W
Ar flow rate	40 sccm	25 sccm
Working pressure	0.5 Pa	0.25 Pa

Table 5.2 AZO and Ag based samples used in this study

Group 1	Group 2	Group 3	Group 4
Glass/Ag	Glass/AZO/Ag	Glass/Ag/AZO	Glass/AZO/Ag/AZO
Ag (5 nm)	AZO/ Ag (5 nm)	Ag (5 nm)/AZO	AZO/Ag (5 nm)/AZO
Ag (10nm)	AZO/ Ag (10 nm)	Ag (10 nm)/AZO	AZO/Ag(10 nm)/AZO
Ag (15nm)	AZO/ Ag (15 nm)	Ag (15 nm)/AZO	AZO/Ag(15 nm)/AZO

As shown in Figure 5.1, the Ag films deposited under RFs of 30 and 50 W have linear deposition velocity curves. The film thickness of the samples deposited under an RF of 10 W is less than the lower limits of measurement capable of the Alpha-Step 500 when the deposition time is less than 20 min. After calculation, the average deposition speed of the Ag film under RFs of 30 and 50 W is 1.0 and 3.2 nm/min, respectively. In considering that the prepared Ag film was thin, an RF of 30 W was selected for the deposition of the Ag films so as to more easily control the film thickness.

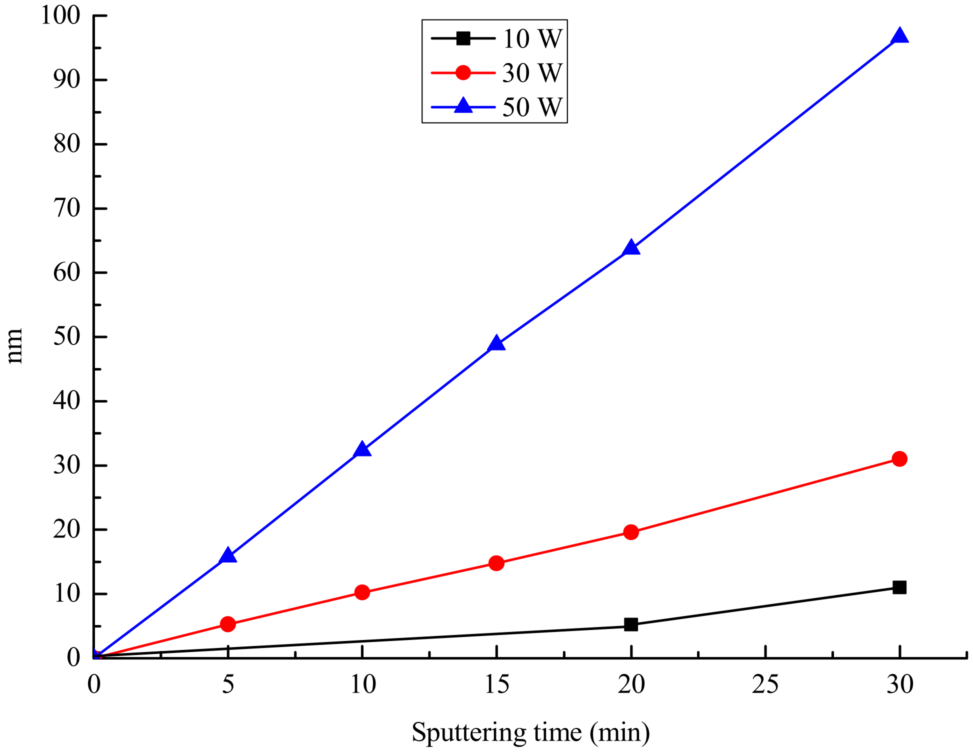

Figure 5.1 Velocity curve of Ag film deposition at RFs of 10, 30 and 50 W

5.3 Characterization of AZO and Ag based films

5.3.1 Crystal structure analysis

The XRD spectra of the coated samples as a function of the thickness of the Ag layers are shown in Figure 5.2. As demonstrated, a weak Ag (111) peak of the Ag and Ag/AZO films can only be detected when the thickness of the Ag layer is 15 nm. The results suggest that the Ag layers have limited crystallization ability on a glass substrate, and acceptable crystallization takes place when their thickness is greater than 10 nm. In Group 2 with the AZO/Ag films, strong peaks of Ag (111) and ZnO (002) can be observed, and the Ag (111) peaks can be detected in all three samples, which indicate that Ag shows better crystallization ability when deposited onto an AZO substrate as opposed to a glass substrate. This phenomenon can be explained when the surface of the glass and AZO substrates are compared, as follows.

As shown in Figure 5.3(a), the surface of the glass substrate is flat and its roughness is estimated to be 0.33 nm. When there are few nucleation centers for the Ag particles to form islands, and the transformation from island to continuous film is slow, thus the crystallization of Ag particles on glass would not be as ideal as on substrates with many nucleation centers that have the same thickness. In Figure 5.3(b), the surface of the AZO film (30 nm) is identified to be rougher than glass with a roughness of 0.94 nm. The deposited AZO particles most likely acted as nucleation centers for the Ag particles, thus resulting in the crystallization of the Ag particles.

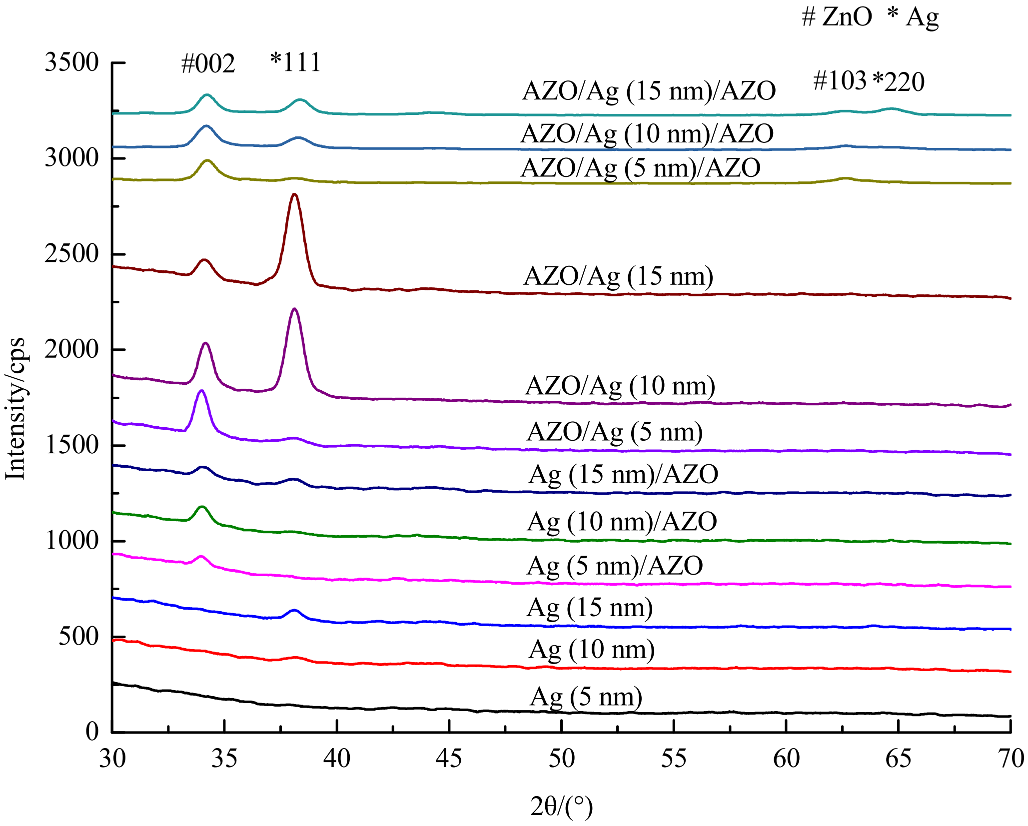

Figure 5.2 XRD spectra of coated AZO Ag based samples

In Group 4 with the AZO/Ag/AZO multilayer films, strong ZnO (002) peaks along with weak ZnO (103) peaks were observed, which indicate the polycrystalline nature of the AZO thin layers. In addition, strong Ag (111) and weak Ag (220) peaks were also detected which prove the crystallization of the Ag layer. It could also be proven that the Ag layer in the AZO/Ag/AZO multilayer films showed superior crystallization as opposed to other films, which is supported by the detection of the Ag (220) peak.

By comparing all of the samples with an AZO layer, it was found that the intensity of the ZnO (002) peaks changes as a function of the thickness. The intensity first increased to its highest value with an Ag layer of 10 nm and then slightly decreased with an Ag layer of 15 nm. In the AZO/Ag/AZO and Ag/AZO samples, the Ag layer of 10 nm had better crystallization than the Ag layer of 5 nm, so the crystallization of the AZO film deposited onto the Ag layer would also be improved. In the AZO/Ag film, the intensity changes of the ZnO (002) peaks were also affected by the changes in the thickness of the Ag layer. The top Ag layer had further crystallization at a thickness of 10 and 15 nm rather than at 5 nm. The increasing amount of Ag may have dominated some of the ZnO information, thus the intensity of the ZnO (002) peak decreased with increasingly thickness of the Ag layer.

5.3.2 Surface morphology analysis

AFM images of the AZO/Ag and AZO/Ag/AZO coated samples are shown in Figure 5.4, and the roughness (Rq) of all the prepared samples is shown in Table 5.3. For each sample, the scanned area is 2×2 μm. As presented in Table 5.3, the films with an Ag layer of 10 nm have the lowest surface roughness in each group, except for the Ag film which decreased in surface roughness with increasing thickness of the Ag layer. The surface roughness of the samples is attributed to the variation in the Ag layer. A rough surface and lack of crystallization would result when the Ag layer is not thick enough [214].

As discussed in the XRD results, the Ag film showed low crystallization on the glass substrate, and could not form a continuous layer at a thickness of 10 nm, so the surface roughness of the Ag films varied differently from the other groups. In Figure 5.4, the images shown are consistent with the roughness results, in that the samples with an Ag layer of 10 nm have the smoothest surface and the roughness is slightly increased with an Ag layer of 15 nm.

Table 5.3 Roughness (Rq) of the AZO samples coated with Ag

Sample	Ag layer thickness (5 nm)	Ag layer thickness (10 nm)	Ag layer thickness (15 nm)
Ag films	3.03	2.42	2.00
AZO/Ag films	3.37	2.58	2.60
Ag/AZO films	1.67	1.57	1.95
AZO/Ag/AZO films	2.61	1.48	1.52

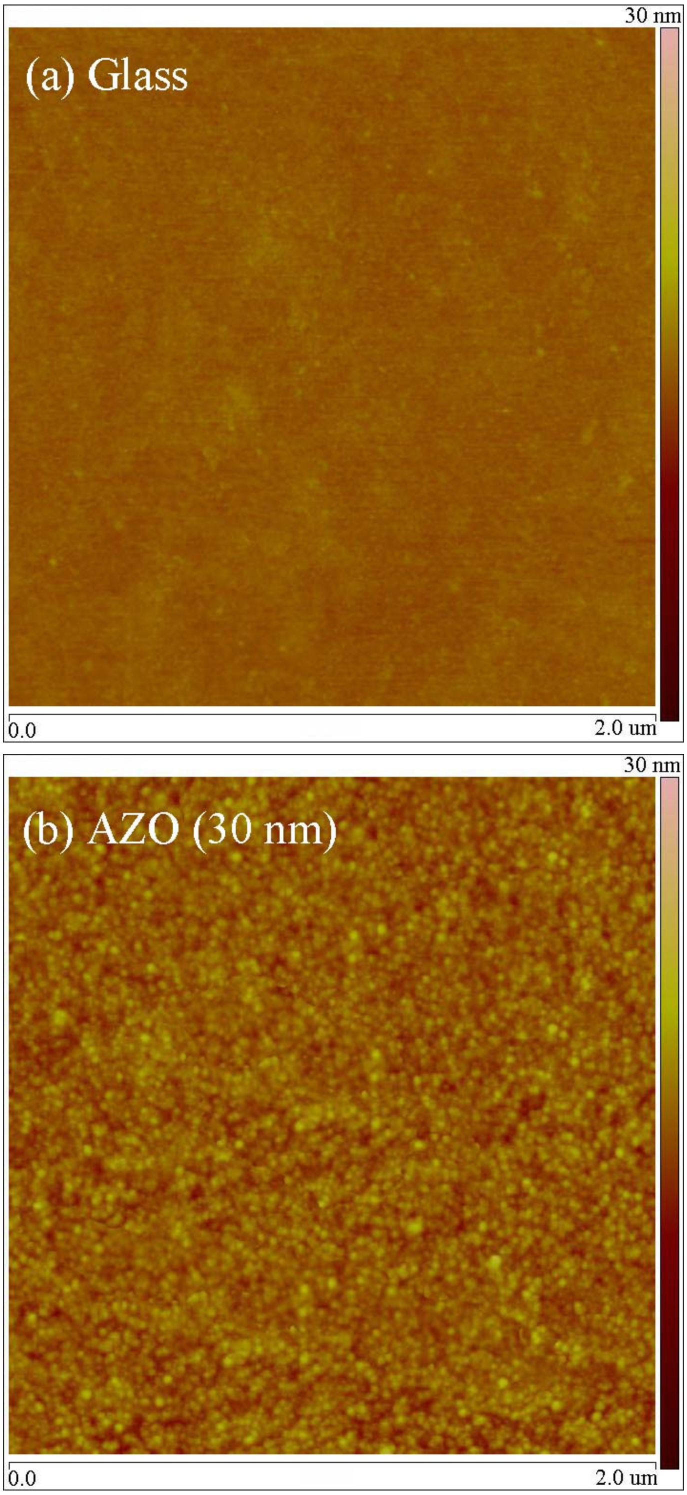

Figure 5.3 AFM images of uncoated glass and AZO film (30 nm)

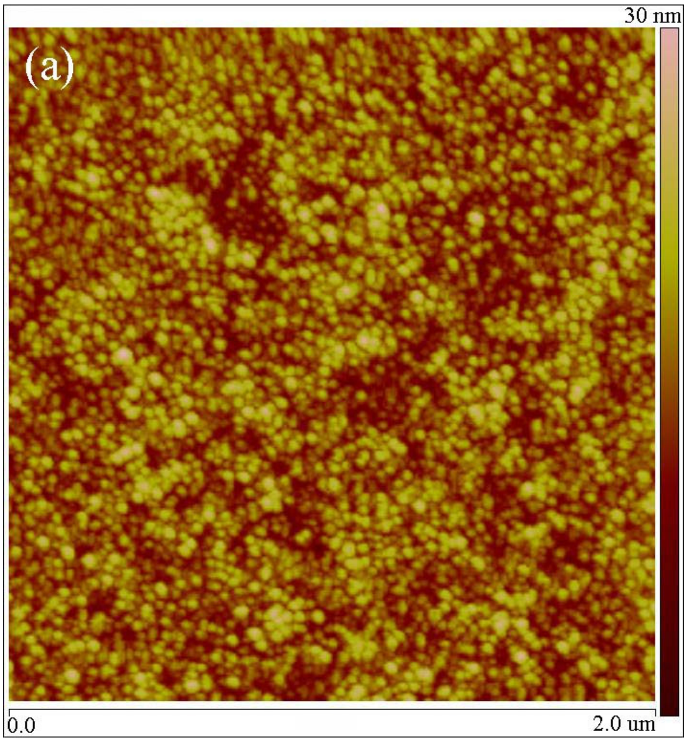
(a)
30 nm
0.0
2.0 um

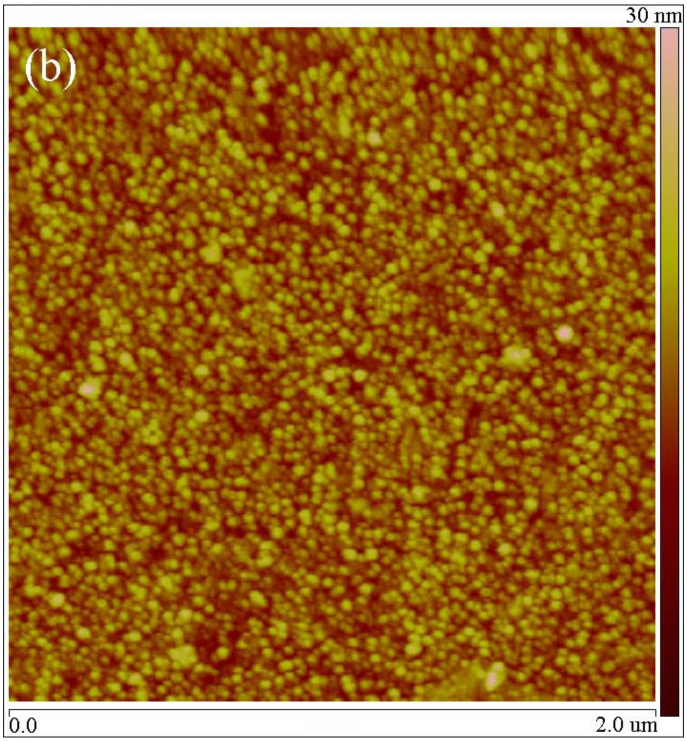
(b)
30 nm
0.0
2.0 um

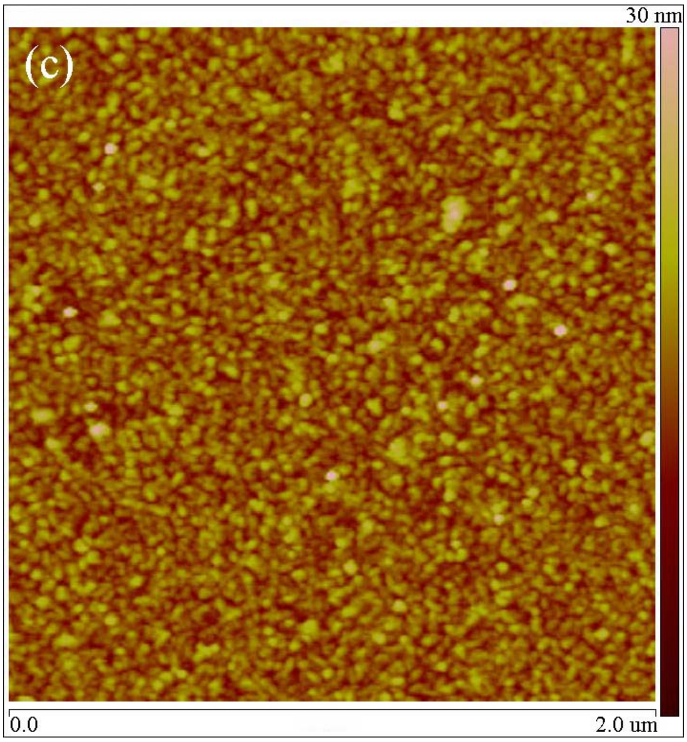
30 nm
(c)
0.0
2.0 um

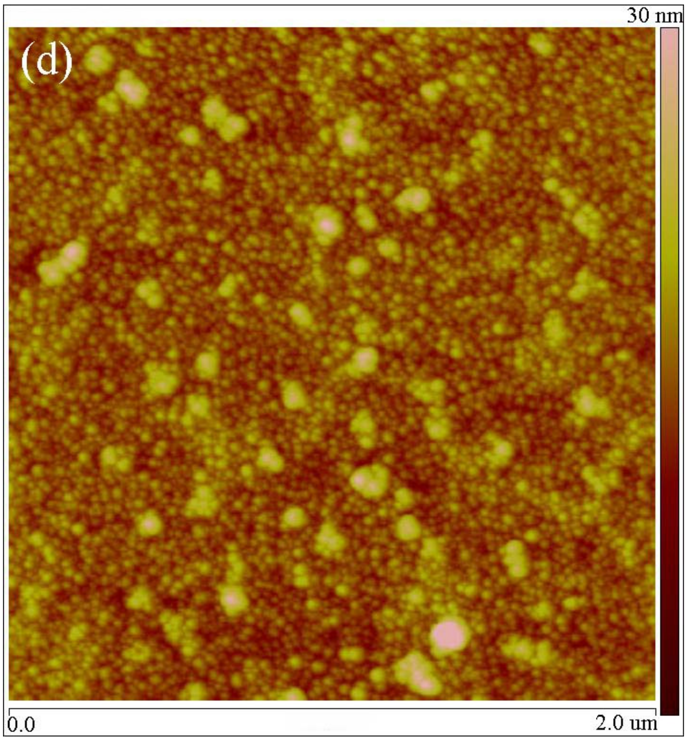
30 nm
(d)
0.0
2.0 um

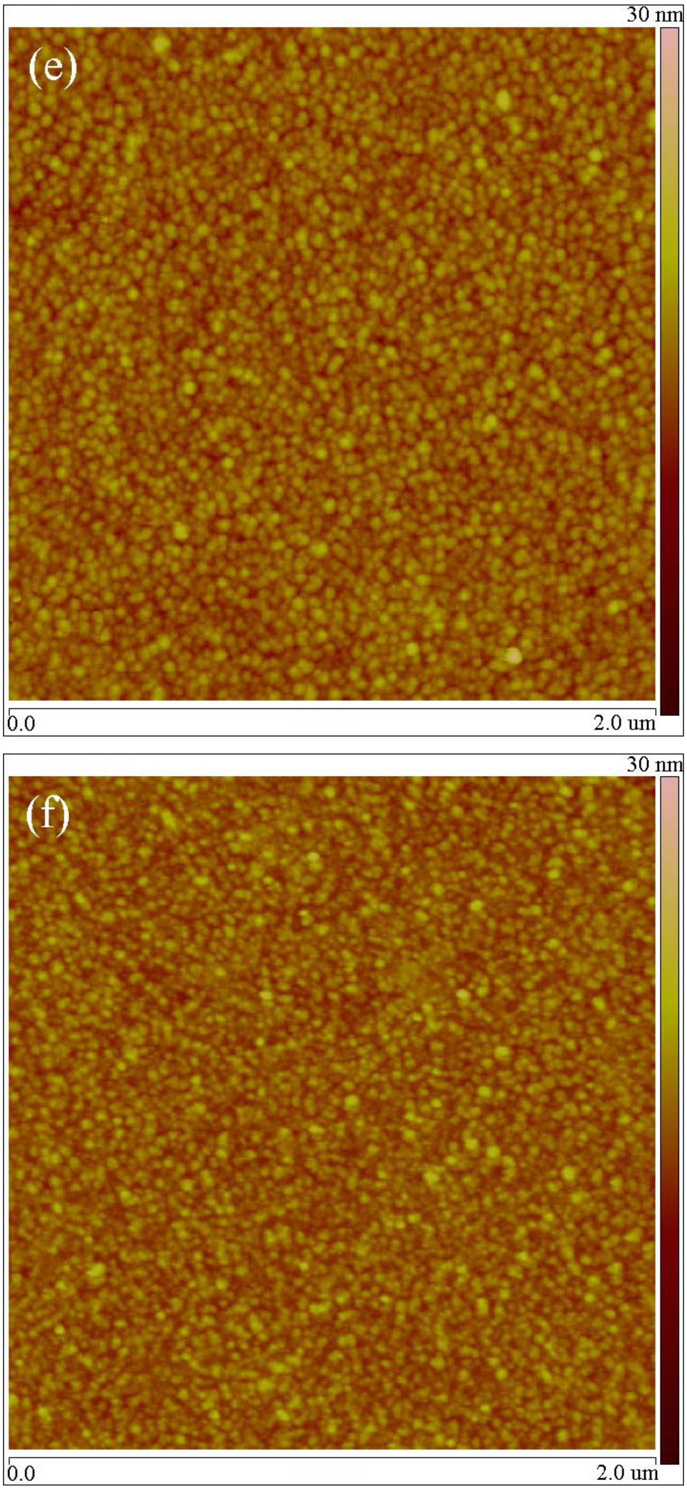

Figure 5.4 AFM images of coated samples: (a) AZO/Ag (5 nm); (b) AZO/Ag (10 nm); (c) AZO/Ag (15 nm); (d) AZO/Ag (5 nm)/AZO; (e) AZO/Ag (10nm)/AZO and (f) AZO/Ag (15 nm)/AZO

5.3.3 Electrical properties analysis

The sheet resistance of the coated samples is calculated as a function of the thickness of the Ag layer, as shown in Table 5.4. In each single group, the sheet resistance is decreased with increases in the thickness of the Ag layer, as expected, and the lowest sheet resistance of about 3.21 Ω/sq is acquired with the AZO/Ag (15 nm)/AZO sample, which is much lower than that of the pure AZO film with a thickness of 60 nm.

A simple parallel model can be used to explain the decrease in the sheet resistance resultant of the changes in the thickness of the Ag layer. The measured sheet resistance (Rs) can be defined with the following equation [215]:

$$\frac{1}{Rs} = \frac{1}{R_{AZObot}}(If\ appropriate) + \frac{1}{R_{Ag}} + \frac{1}{R_{AZOtop}}(If\ appropriate)$$

where Rs, R_{AZObot} and R_{AZOtop} are the sheet resistance of the film, and bottom and top AZO layers respectively. Since the resistivity of Ag is much lower than that of AZO, the total resistivity of the film is mainly determined by the thickness of the Ag layer.

In Table 5.4, it can also be observed that the sheet resistance of the Ag, AZO/Ag and Ag/AZO films with an Ag layer of 5 nm is beyond the testing limits of the equipment, which indicates that the Ag particles cannot form a continuous bond with each other at a layer thickness of 5 nm and the Ag particles are not uniformly distributed on the substrate. However, the AZO/Ag/AZO film shows an appropriate sheet resistance with an Ag layer of 5 nm. This could be due to the deposited AZO top layer which helped to form an electric conduction net. When the thickness of the Ag layer is 10 nm and 15 nm, the sheet resistance of the Ag, Ag/AZO, AZO/Ag and AZO/Ag/AZO films gradually declines in each paralleled sample. The results indicate that a continuous Ag layer is obtained when the thickness is higher than or equal to 10 nm. Compared to the other samples, the AZO/Ag/AZO film shows the lowest sheet resistance with the same thickness of the Ag layer, which demonstrates that Ag causes further crystallization on the AZO substrate as opposed to glass, and the top AZO layer also helps to improve the electrical conductivity.

Table 5.4 Sheet resistance※ of coated AZO Ag based samples

Sample	Thickness of Ag layer (5 nm)	Thickness of Ag layer (10 nm)	Thickness of Ag layer (15 nm)
Ag films	> 1.0×10^6 Ω/sq	65.7 Ω/sq	4.5 Ω/sq
AZO/Ag films	> 1.0×10^6 Ω/sq	7.58 Ω/sq	3.8 Ω/sq
Ag/AZO films	> 1.0×10^6 Ω/sq	8.84 Ω/sq	5.16 Ω/sq
AZO/Ag/AZO films	39.9 Ω/sq	6.72 Ω/sq	3.21 Ω/sq

※ Sheet resistance of pure AZO (60 nm) film > 1.0×10^6 Ω/sq

5.3.4 Visible transmittance analysis

The optical transmittance spectra of the prepared samples are shown in Figure 5.5. As shown in the figure, the highest average visible transmittance (from 400 to 800 nm) of the samples can be obtained when the Ag layer has a thickness of 10 nm, except for the Ag films which were acquired when the Ag layer was 15 nm. The highest average visible transmittance of the Ag, AZO/Ag, Ag/AZO and AZO/Ag/AZO films are found to be as 51.4%, 63.7%, 82.8% and 82.5%, respectively.

The optical properties can be attributed to the evolution of the Ag film with deposition time. Zhang et al. [216] reported that Ag particles are deposited as islands with various sizes and randomly distributed onto an AZO substrate at the beginning of the sputtering deposition, and the separated islands would scatter the incident light, thus reducing the light transmittance. The scattering property of the deposited particles is reduced due to decreasing gaps between them because of further sputtering. Finally, the Ag islands form into a continuous film, and serve as a reflection film, so that the transmittance would gradually decrease. As demonstrated by the AFM images, the samples showed the lowest surface roughness with Ag layers of 10 nm, except for the Ag films which showed the lowest surface roughness with Ag layers of 15 nm in thickness. Low surface roughness results in less visible light scattering and more penetration, which well explains the results in Figure 5.5.

It was also observed that the films with Ag on the surface showed much lower visible transmittance than those with AZO on the surface layer. This may be caused by the higher surface roughness of the top Ag layer (see Table 5.3 and Figure 5.4) which would scatter the incident light. In contrast, the films with an AZO top layer exhibited lower surface roughness and a smooth surface (as shown in Table 5.3 and Figure 5.4), so the visible transmittance of these films would be higher.

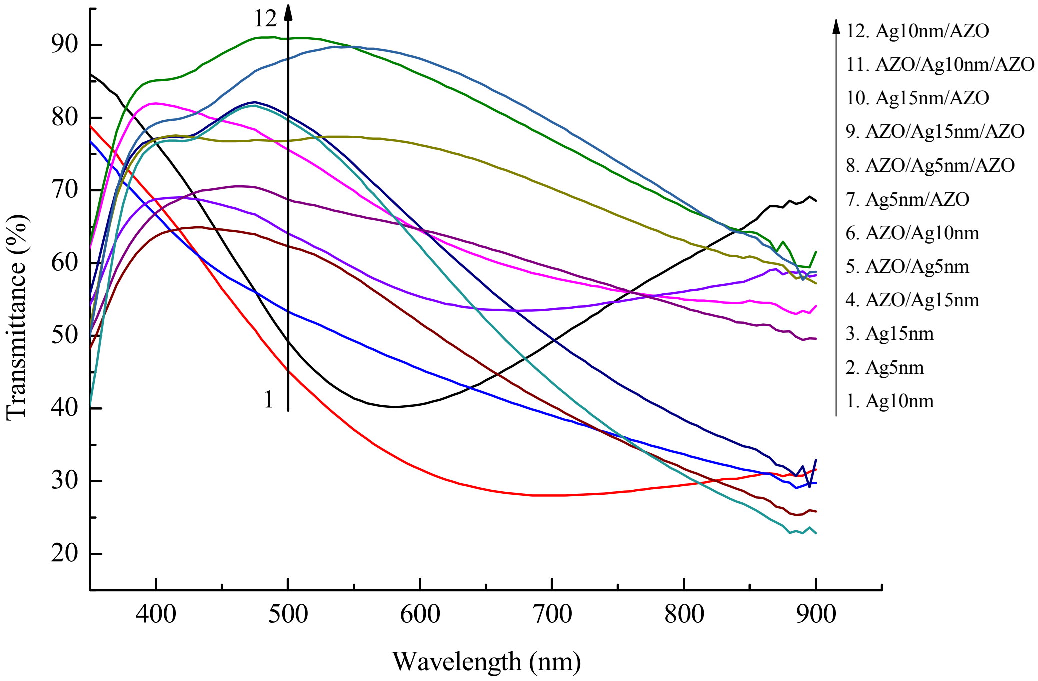

Figure 5.5 Optical transmittance spectra of the coated AZO Ag based samples

5.3.5 Ultraviolet protection factor analysis

The UPF values of the coated samples are listed in Table 5.5. In the table, the

UPF values of all the coated samples are higher than those of uncoated glass and they increase with increases in the thickness of the Ag film for each group. The AZO/Ag/AZO films have the highest UPF values, and the largest value is increased by about 253% compared to the uncoated glass. Among all the samples, single Ag layer films show the lowest UPF value and AZO/Ag/AZO films have the highest UPF value with an Ag layer of the same thickness. It can also be found that the UPF values of the AZO/Ag films are higher than those of the Ag/AZO films. Both the Ag and AZO films have good UV shielding properties, which would be affected by the crystallization of the film. As demonstrated in the XRD results, Ag films deposited onto an AZO substrate have better crystallization than when deposited onto a glass substrate.

Table 5.5 UPF values※ of the coated AZO Ag based samples

Sample	Ag layer thickness (5 nm)	Ag layer thickness (10 nm)	Ag layer thickness (15 nm)
Ag films	4.359	4.544	5.011
AZO/Ag films	6.290	6.882	7.263
Ag/AZO films	5.899	6.069	6.781
AZO/Ag/AZO films	11.564	12.177	15.340

※ UPF value of uncoated glass: 4.338

5.3.6 Infrared property analysis

The IR reflection and transmission properties of the prepared samples are presented in Figures 5.6 and 5.7. It can be observed that the IR reflections of all the coated samples are higher than that of the uncoated glass, except for the Ag (5 nm), AZO/Ag (5 nm) and Ag (5 nm)/AZO films, which are similar to or just slightly higher than that of the uncoated glass. In these films, when the Ag layer with a thickness of 5 nm was deposited onto the substrate, the Ag particles would randomly distribute onto the glass without bonding to each other and IR radiation could easily pass through them. In addition, the scattering property of these three types of films is higher due to the higher surface roughness, thus their IR reflection rate is similar to that of the uncoated glass.

In Figure 5.6, it can be seen that the IR reflection rate increases with increases in the thickness of the Ag layer for each group which indicates that the IR reflection rate is inversely proportional to the sheet resistance. Among all of the samples, the IR reflection rate of the AZO/Ag/AZO films is higher than that of all the other films with an Ag layer of the same thickness, especially the AZO/Ag/AZO film with an Ag layer of 5 nm, which proves that the AZO buffer layer helps to improve the crystallization of the Ag layer. This is coherent with the XRD results. The AZO/Ag/AZO multilayer film with an Ag inlayer of 15 nm shows the highest rate of IR reflection of about 97% in the FIR range.

In Figure 5.7, the transmission spectra demonstrate the reverse phenomenon of the reflection spectra in that all of the coated samples exhibit a lower transmission than that of the uncoated glass. As explained by the energy conservation law, when more IR radiation is reflected, less radiation would penetrate the substance. For the AZO/Ag/AZO sample with an inner layer of Ag that is 15 nm, the IR transmission is less than 7.5% in the NIR region, which is much lower than that of the uncoated glass of about 90%. This is the same when reviewing the AZO transmission spectra in Figure 4.6; the IR transmission tends to zero when the IR wavelength is longer than 5 μm which is caused by the high absorption of the uncoated glass in this IR region.

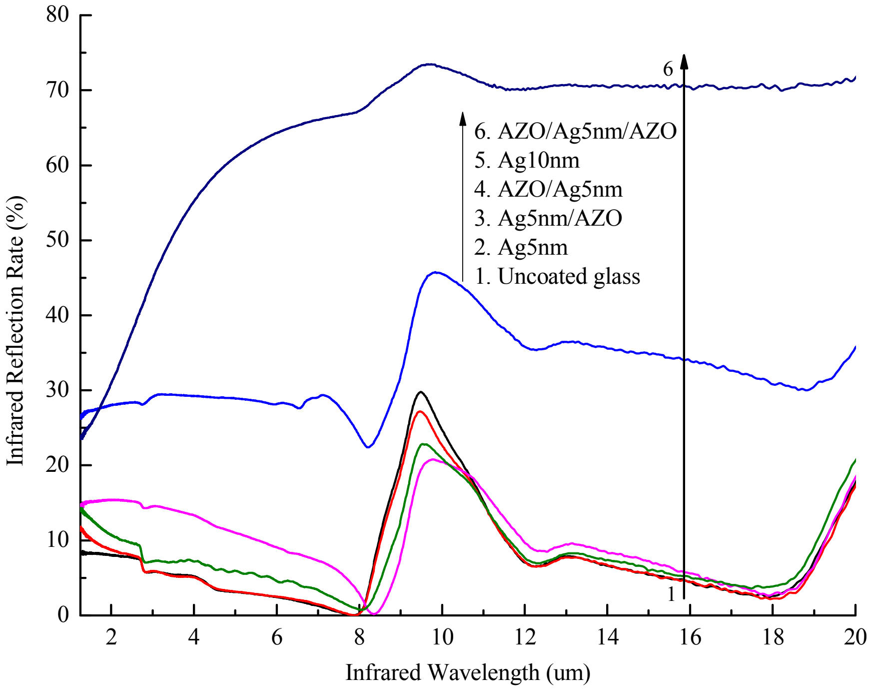

Figure 5.6.1 IR reflection spectra of uncoated glass and the coated AZO Ag based samples

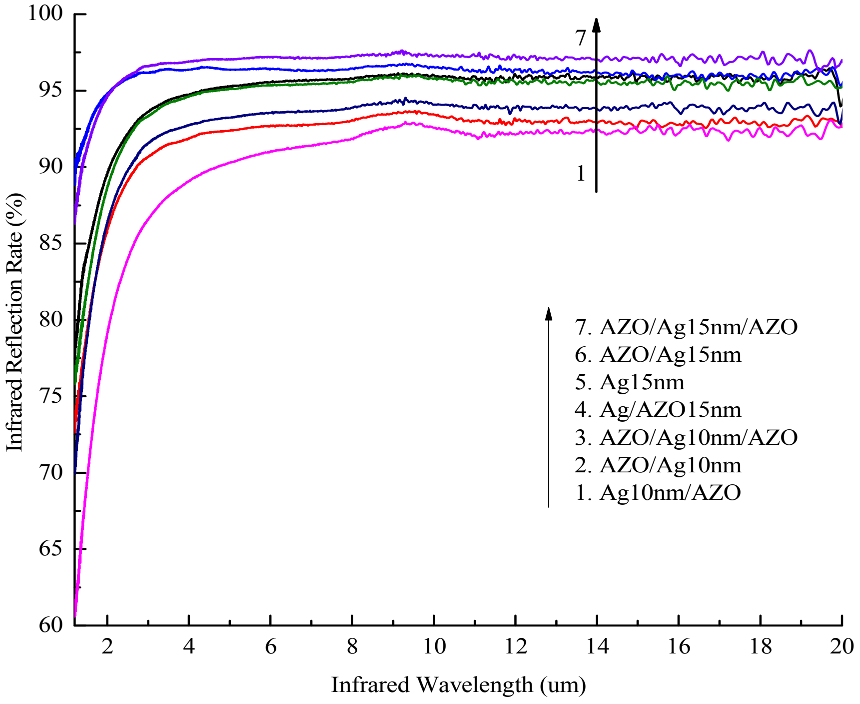

Figure 5.6.2 IR reflection spectra of uncoated glass and the coated AZO Ag based samples

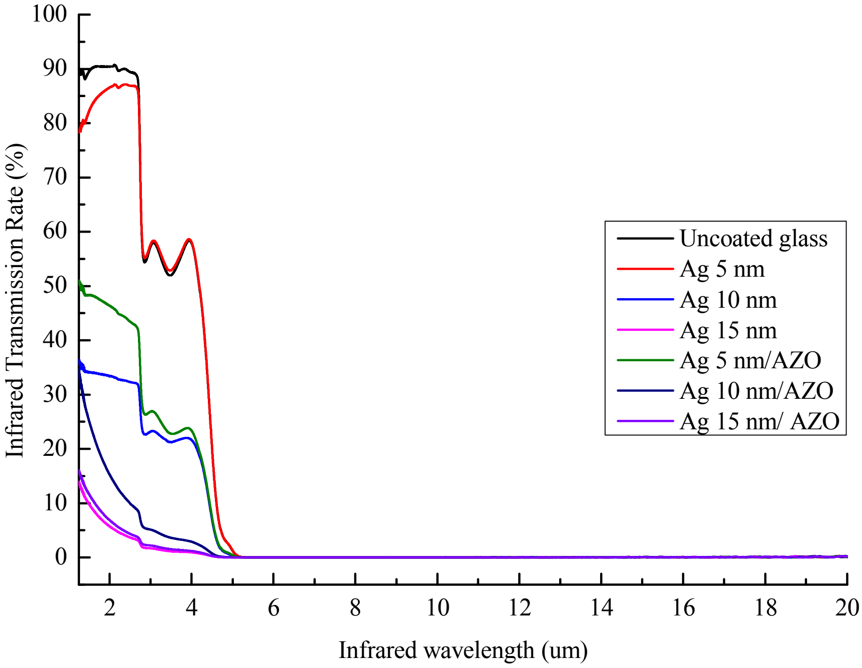

Figure 5.7.1 IR transmittance spectra of uncoated glass and Ag and Ag/AZO coated samples

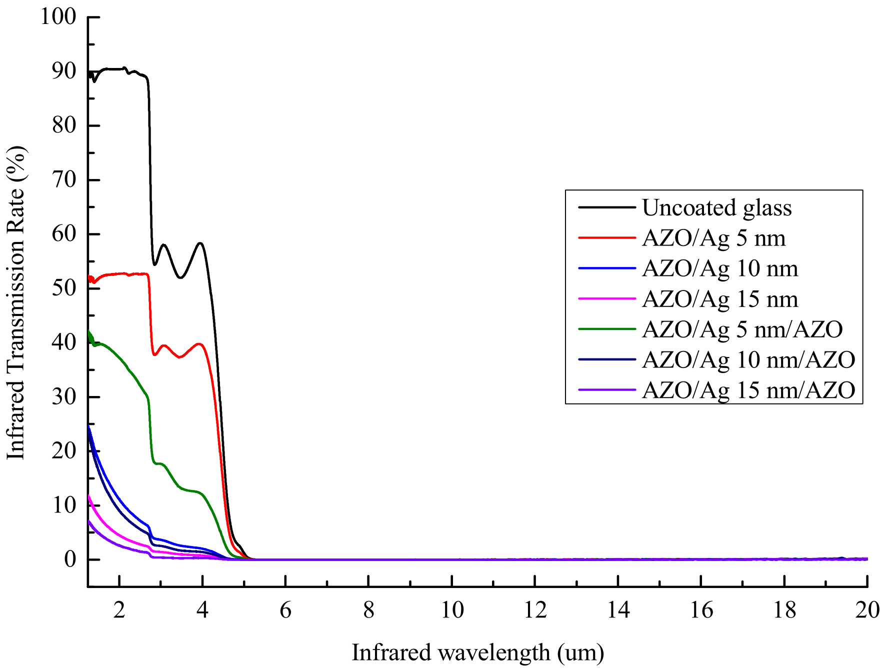

Figure 5.7.2 IR transmittance spectra of uncoated glass and AZO/Ag and AZO/Ag/AZO coated samples

The sheet resistance and IR reflection are mainly determined by the formation of the Ag layer. When the Ag layer is thinner than 10 nm, the Ag particles are randomly distributed on the substrate and do not form a continuous film. At this time, the nano Ag particles mainly work as the scattering center, the films show limited IR reflection and higher sheet resistance. After the forming of a continuous Ag layer, the films would show lower sheet resistance and act as an IR reflective mirror that could reflect most of the incident IR electromagnetic waves. This could also explain about the closely related interactions between electromagnetic waves and conductive materials to the free electrons. When a material contains more free electrons, the IR reflection would be higher. As well, higher free electrons also mean lower electrical resistance.

5.4 Summary

The crystal structure, surface morphology, electrical properties, visible transmittance, UPF and IR properties of the prepared Ag, AZO/Ag, Ag/AZO and AZO/Ag/AZO films have been investigated and discussed in this chapter. The results indicate that the IR reflection rate is inversely proportional to sheet resistance and the IR reflection of the AZO/Ag/AZO multilayer film is higher than that of the other films with an Ag layer that has the same thickness. The film with an IR reflection rate of 97% and sheet resistance of 3.21 Ω/sq has been acquired with an AZO/Ag (15 nm)/AZO structure. Additionally, it has also been observed that the Ag inner layer could start to form a continuous layer at a thickness of around 10 nm and this Ag layer has higher crystallization on an AZO substrate rather than a glass substrate. The AZO/Ag/AZO multilayer film also has a higher average visible transmittance of 82.5% with the presence of a continuous Ag inner layer. The high IR reflective performance, as well as the high visible transmittance of the AZO/Ag/AZO coated films shows that they are a promising means for use in high IR reflective textiles. This will therefore be systematically investigated in the next chapter.

Chapter 6 Characterization of developed and optimized AZO/Ag/AZO films[iii]

6.1 Introduction

As discussed in Chapter 5, the AZO/Ag/AZO multilayer structure is suitable as a coating for developing high IR reflective textiles. In this chapter, the deposition of various thicknesses of AZO/Ag/AZO multilayer films onto glass substrates to investigate the appropriate thickness of each layer for optimal film properties will be first discussed. After that, the selected film thickness will be applied onto a PET substrate to examine the film properties that are deposited onto a flexible substrate, with the considering of further deposition onto flexible textile fabric. After deposition, the crystal structure, surface morphology, electrical properties, visible transmittance, UPF and IR transmittance/reflection properties of the coated films will also be investigated.

6.2 Preparation of AZO/Ag/AZO films

First, in order to confirm the proper thickness of the AZO layer for the multilayer films, AZO layers of 20, 30 and 40 nm were deposited and the Ag inner layer was fixed at 20 nm in each sample. In each sample, both the top and bottom AZO

[iii] *Parts of this chapter have been published in* ***Vacuum*** *and* ***Ceramics international****.*

layers were deposited with the same thickness. After deposition, the films were evaluated by examining the IR reflection spectra, and an appropriate thickness for the AZO layers was selected based on the spectra. Second, after the confirmation of the thickness of the AZO layers, they were fixed at the selected thickness, and the deposition of Ag layers of 5, 7, 9, 10, 11, 13, 15 and 20 nm was carried out on glass substrates. The properties of the coated film as well as the evolution of the Ag inner layer were investigated as a function of the thickness of the Ag layer. Third, the same films were deposited onto flexible PET substrates to evaluate the film properties on a flexible substrate. In order to observe the evolution of the Ag inner layer, substrate/AZO/Ag films were also prepared and analyzed. The deposition parameters of the AZO and Ag layers are shown in Table 6.1.

Table 6.1 Deposition parameters of AZO/Ag/AZO films on glass substrate

	AZO Layer	Ag Layer
Base pressure	5×10^{-4} Pa	5×10^{-4} Pa
RF power	150 W	30 W
Ar flow rate	40 sccm	25 sccm
Working pressure	0.5 Pa	0.25 Pa

6.3 Confirmation of thickness of AZO layers

The IR reflection spectra of the prepared samples with different thicknesses of the AZO layers are shown in Figure 6.1. In the figure, all of the three samples show a high rate of IR reflection between 97% and 99% in the MIR and FIR regions. Among them, the sample with AZO layers of 20 nm shows the lowest IR reflection and the sample with AZO layers of 30 nm shows the highest IR reflection in most of the IR regions. Only in the NIR region did the sample with AZO layers of 40 nm show the highest IR reflection.

Figure 6.2 illustrates the IR transmittance of the AZO/Ag/AZO coated films. All of the three samples show low IR transmittance as expected due to their high IR reflection and the absorption of the glass substrate. As shown in the results, the sample with AZO layers of 30 nm shows the same or higher IR reflection as that with AZO layers of 40 nm, which may be caused by film interference. At the same time, in considering the cost of the multilayer films, both the top and bottom AZO layers are fixed at 30 nm in this project.

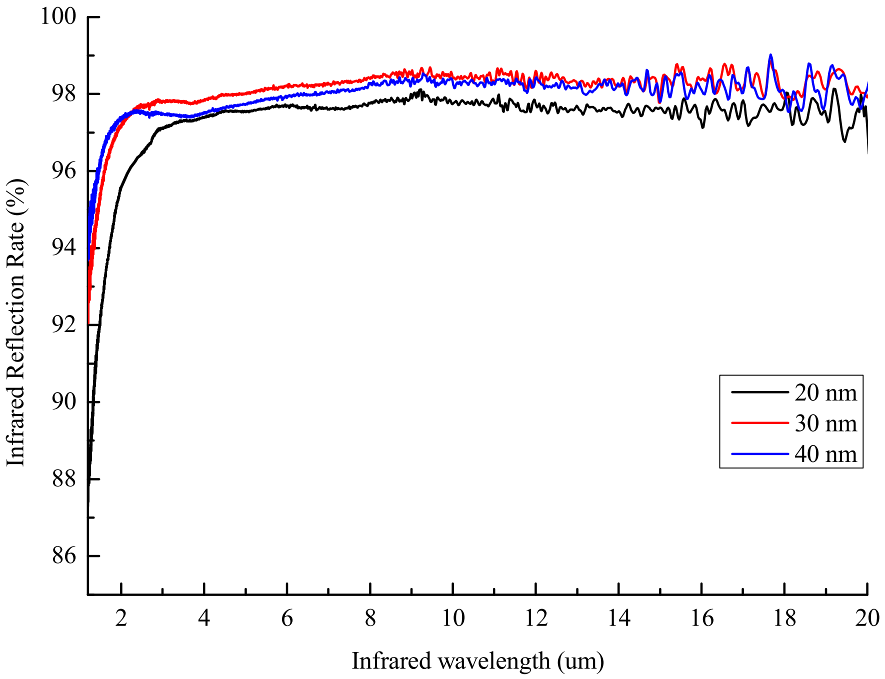

Figure 6.1 IR reflection of the coated samples with different thickness of the AZO layer

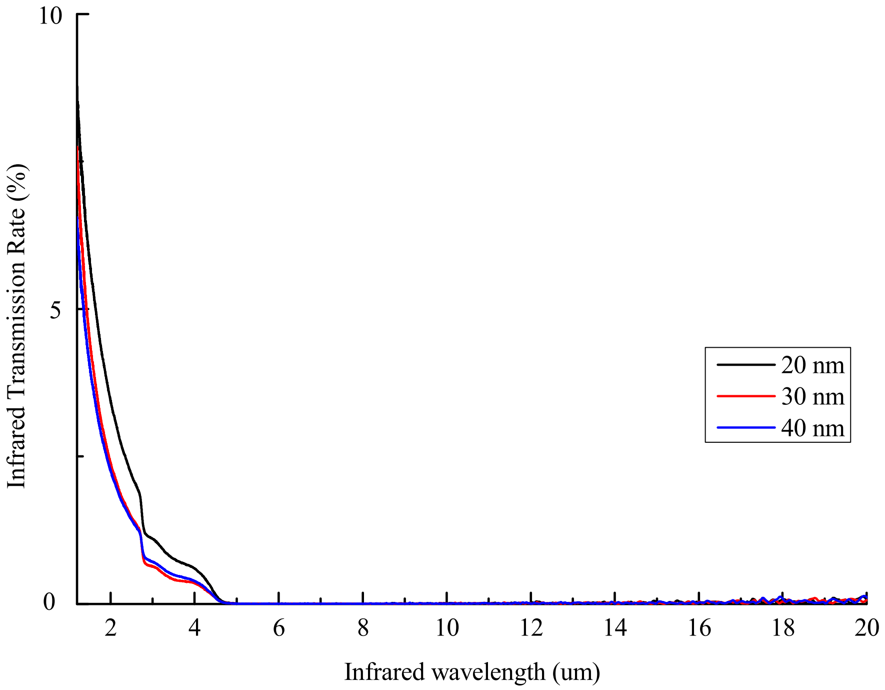

Figure 6.2 IR transmittance spectra of the coated samples with different thickness of the AZO layer

6.4 Characterization of AZO/Ag/AZO films on glass substrates

As stated in Section 6.3, the multilayer films with AZO layers that are 30 nm in thickness have better IR reflection. In the following section, the AZO/Ag/AZO films deposited onto glass substrates will be analyzed with the AZO layers fixed at a thickness of 30 nm. To observe the evolution of the Ag inner layer, glass/AZO/Ag films were also prepared and characterized by using SEM. In the bi-layer samples, the AZO layers were also fixed at a thickness of 30 nm and the deposition of Ag layers of 5, 7, 10 and 13 nm was carried out.

6.4.1 Crystal structure analysis

The XRD spectra of the AZO/Ag/AZO coated multilayer films plotted as a function of the thickness of the Ag layer are illustrated in Figure 6.3. In the figure, strong ZnO (002) peaks along with weak ZnO (103) peaks can be observed in all of the samples, which indicate the polycrystalline nature of the AZO layers. It can also be observed that the intensity of the ZnO (002) peaks is slightly reduced when the thickness of the Ag layer increases from 5 to 15 nm. However, the intensity of the Ag (111) peaks is obviously increased with increases in the thickness of the Ag layers. The increased intensity of the Ag layer indicates the enhancement of Ag crystallization caused by the increases in the thickness of the Ag layer, and at the same time, suppresses the intensity of the ZnO peaks. In the samples, distinct Ag (200) and (220) peaks can be observed when the Ag layer is thicker than 10 nm, which may indicate that the Ag film can obtain good crystallization with the forming of a continuous Ag layer at a thickness of 10 nm.

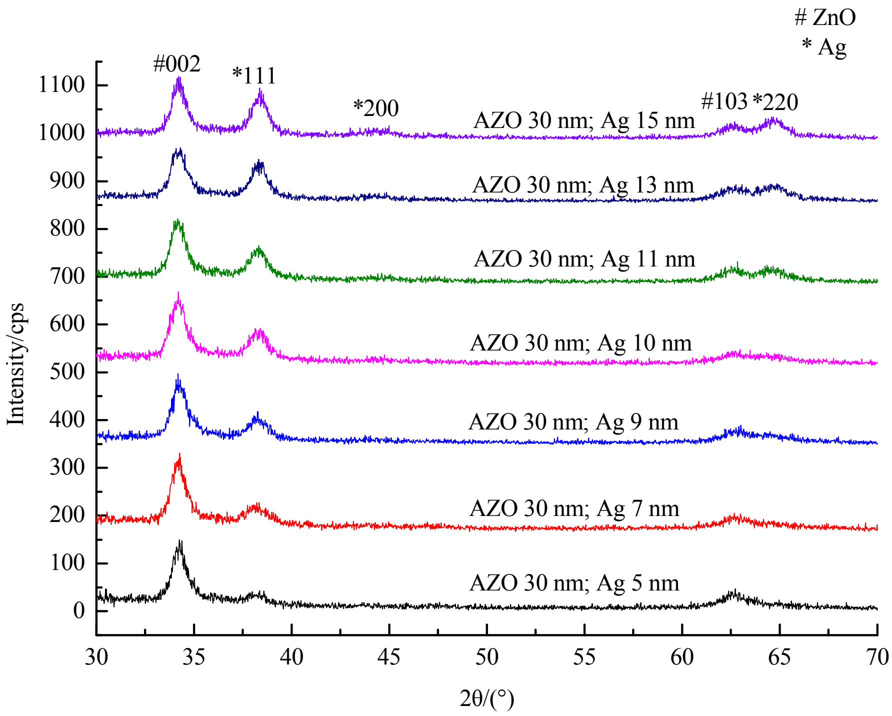

Figure 6.3 XRD spectra of the AZO/Ag/AZO coated samples on glass substrate

6.4.2 Surface morphology analysis

As mentioned in Section 6.4.1, the properties of the coated multilayer films are affected by the changes in the thickness of the Ag inner layer; therefore, SEM imaging of the AZO/Ag films was carried out as a function of the thickness of the Ag layer and the images are shown in Figure 6.4. In Figure 6.4(a), the Ag particles are shown to be non-uniformly distributed onto the AZO substrate and there is almost no bonding between them. The size of the Ag particles is smaller than that observed in the other three images, and the surface of the film is rough. In Figure 6.4(b), it can be seen that the Ag particles begin to bond with each other and the size of the Ag particles is gradually increased. In Figure 6.4(c), the Ag particles become larger and start to form a continuous film with good bonding to each other. In Figure 6.4(d), the particle size of the continuous film further increases. The evolution of the Ag film is consistent with the Volmer-Weber model [217] in that the growth of the nuclei leads to island formation and then coalescence into a continuous film.

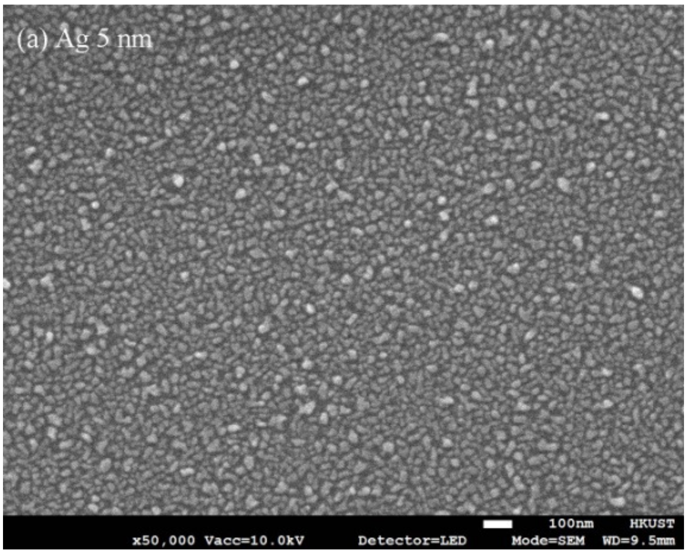

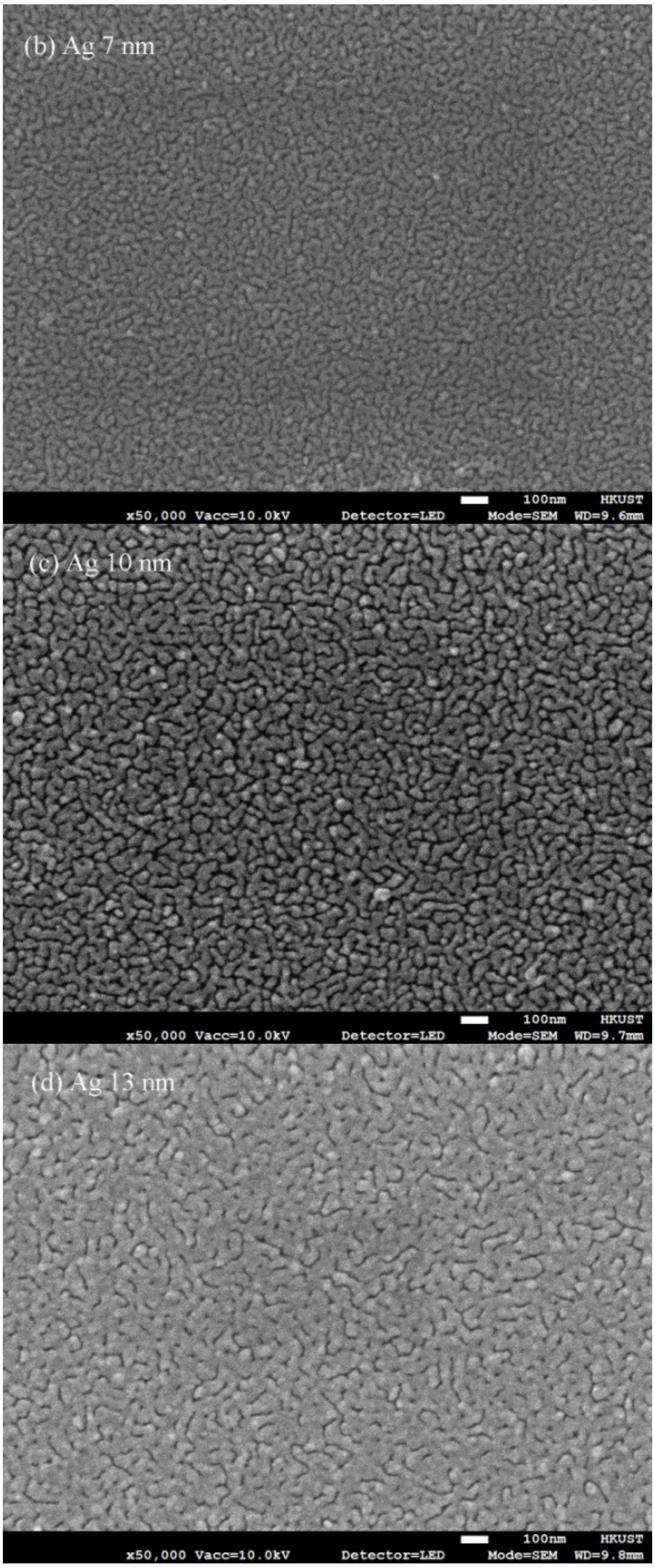

Figure 6.4 SEM images of AZO/Ag films with different thicknesses of Ag layer on glass substrate

Figure 6.5 shows the AFM images (scanning area of 2 μm×2 μm) of the AZO (30 nm)/Ag (5, 7, 10, 13 nm)/AZO (30 nm) films, and the roughness of the samples (determined by using NanoScope Analysis software) are 2.61, 2.05, 1.98 and 2.51 nm, respectively. Similar to the phenomenon shown in the figure, the roughness of the coated samples was reduced with increasing thickness of the Ag layer before the Ag particles formed a continuous film at a thickness of about 10 nm. After that, the roughness of the coated films increased with increased thickness of the Ag layer. The surface roughness of the AZO/Ag/AZO trilayers is attributed to the crystallization of the Ag layer. When the Ag layer was too thin to form a continuous structure, the AZO film that had grown on the discontinuous Ag layer resulted in a rough surface and poor crystallization [214].

A cross section image of the AZO/Ag/AZO multilayer with an Ag inner layer of 15 nm is shown in Figure 6.6. In the figure, the sandwich structure of the multilayer film is evident.

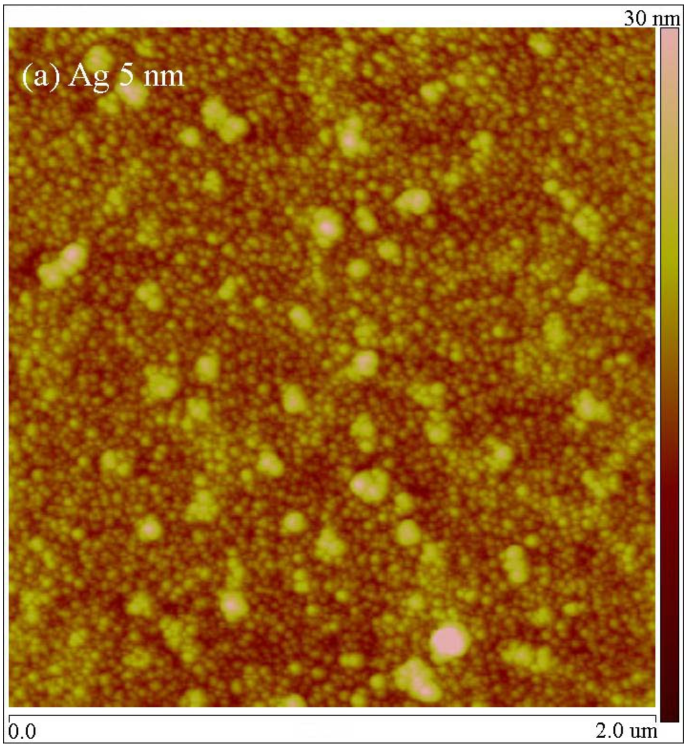
(a) Ag 5 nm
30 nm
0.0
2.0 um

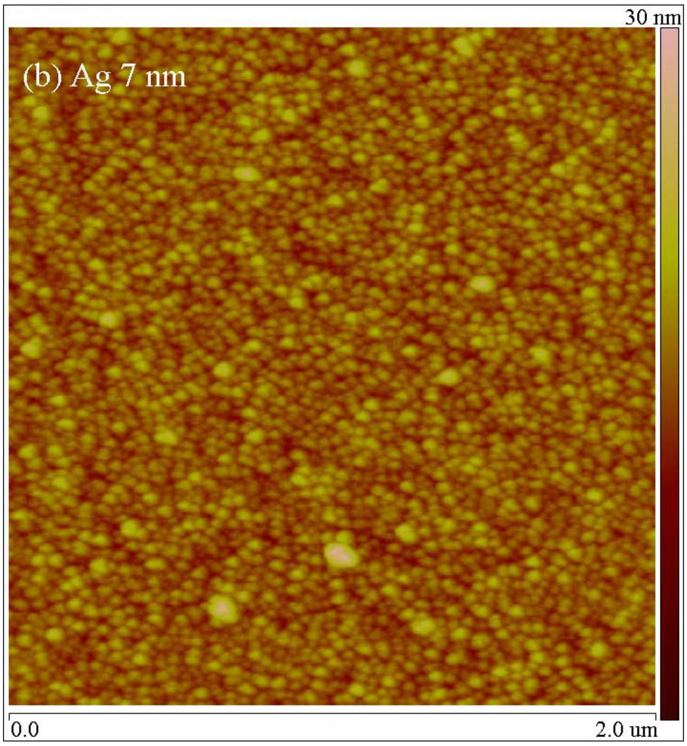
(b) Ag 7 nm
30 nm
0.0
2.0 um

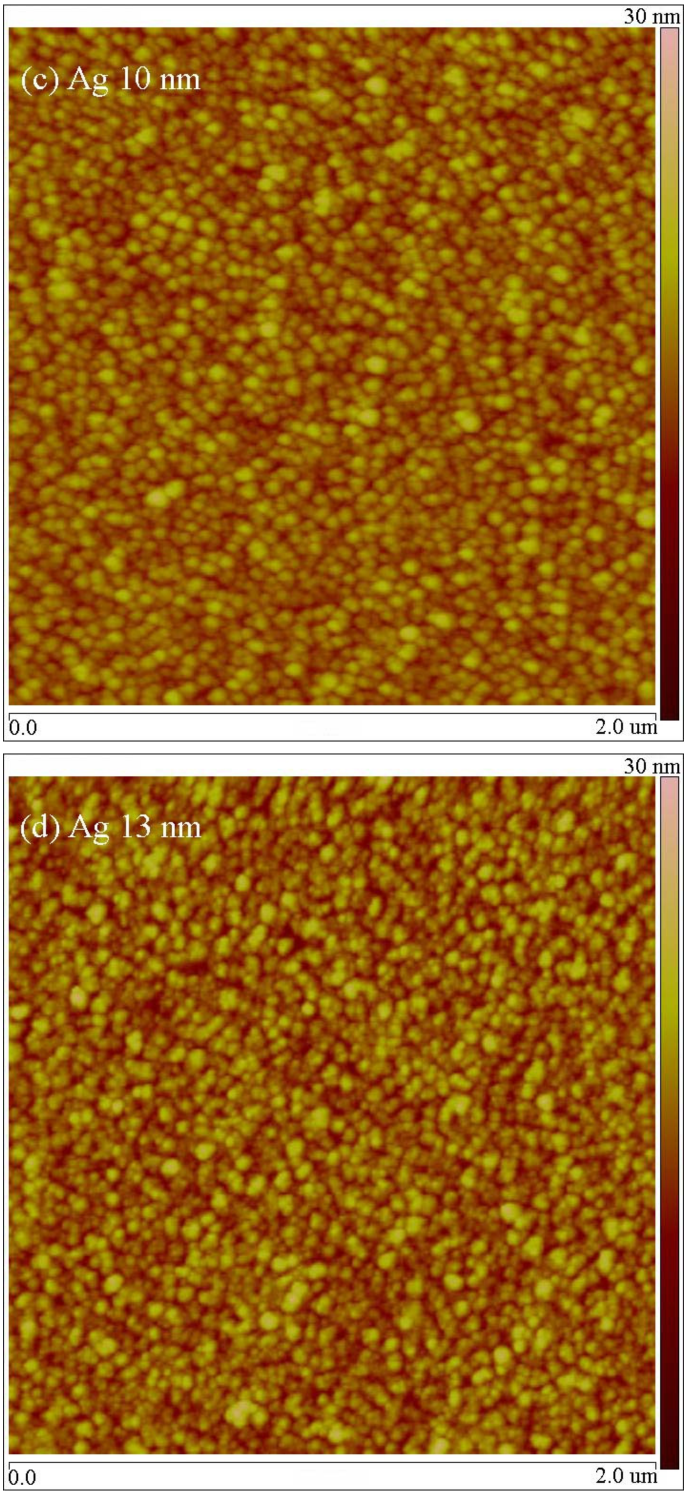

Figure 6.5 AFM images of the AZO/Ag/AZO coated samples on glass substrate

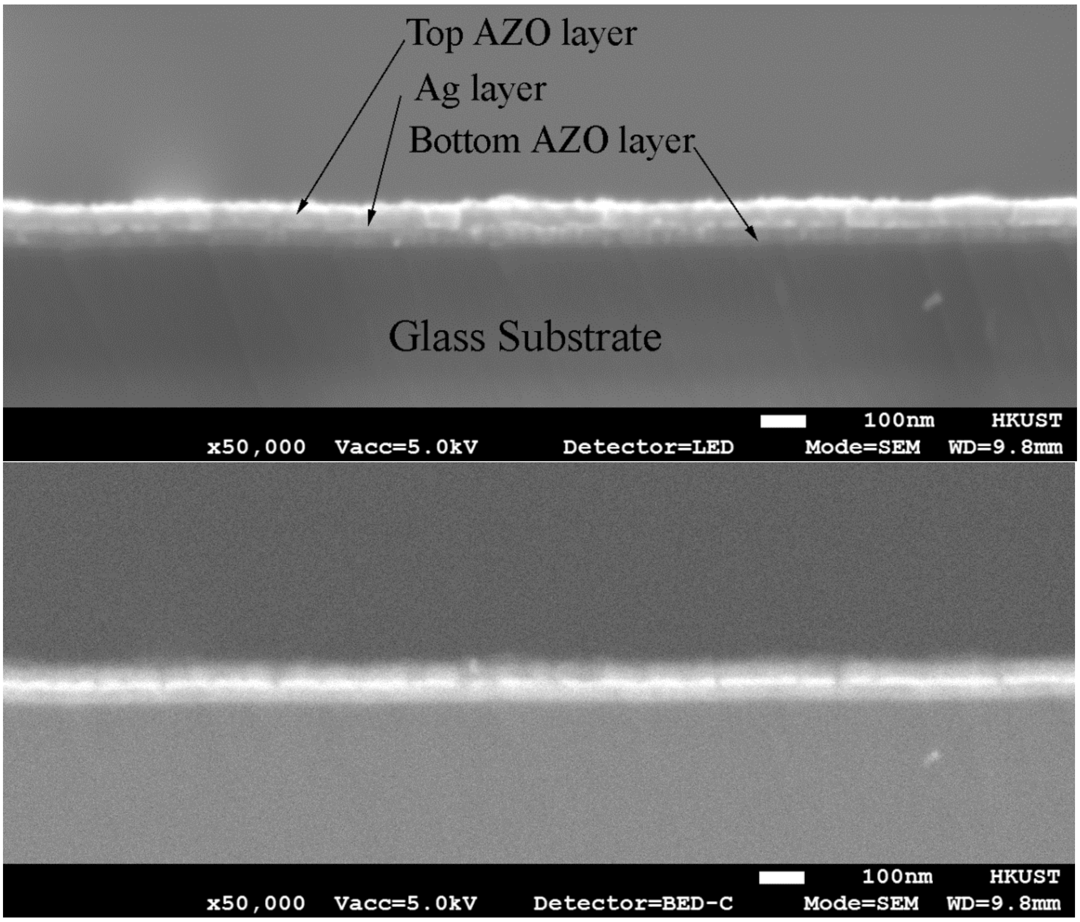

Figure 6.6 SEM cross section images of the AZO/Ag (15 nm)/AZO sample on glass substrate

6.4.3 Electrical properties analysis

The sheet resistance (Rs) of the coated trilayers which was determined as a function of the thickness of the Ag layer is shown in Figure 6.7. As shown in the figure, the sheet resistance decreases with increasing thickness of the Ag inner layer. The lowest Rs value of about 3.21 Ω/sq is acquired with a trilayer structure of AZO (30 nm)/Ag (15 nm)/AZO (30 nm). As determined by the equation in

Section 5.3.3, the resistivity of Ag is much lower than that of AZO; therefore, the total resistivity of the trilayers is mainly determined by the thickness of the Ag layer.

In the figure, it can also be noticed that the sheet resistance shows a sharp decrease when the thickness of the Ag layer is between 5 and 9 nm; after that, the sheet resistance slowly decreases. The results may indicate that the Ag inner layer started to form a continuous film at a thickness of around 9-10 nm, which is consistent with the XRD and SEM results.

For the sample with an Ag layer of 5 nm, separate Ag particles were randomly distributed onto the AZO substrate; only some bonded to others. Here, the electric conduction net of the Ag particles is incomplete, the free electrons could not be easily transmitted and not all of them could contribute to the electrical conductivity, so the sheet resistance is low. When the thickness of the Ag layer was 9 nm, the Ag particles would form a complete electric conduction net, the free electrons could be freely transmitted, and most of the free electrons helped to improve the electrical conductivity. With further increases in the thickness of the Ag layer, the number of free electrons would gradually increase and the sheet resistance would gradually decrease and finally approach the conductivity of the Ag block.

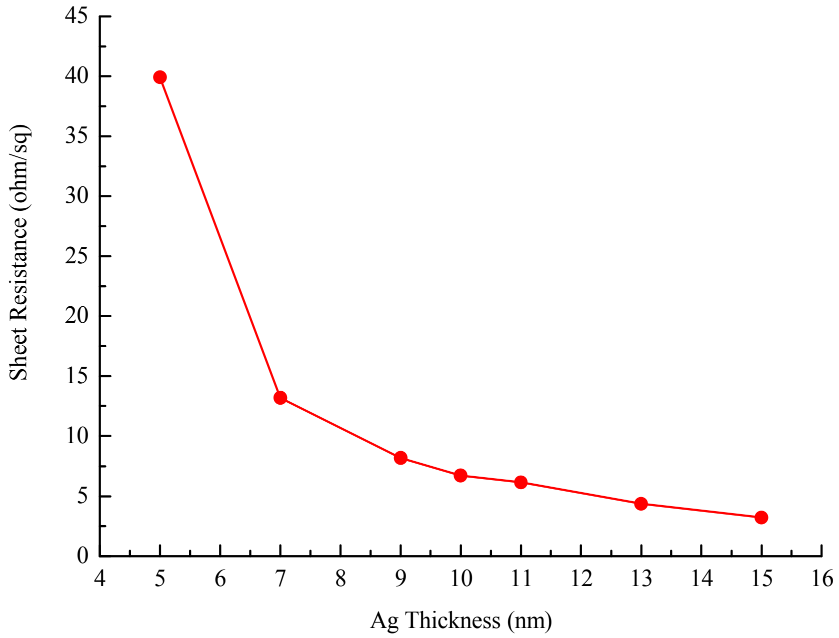

Figure 6.7 Sheet resistances of the AZO/Ag/AZO coated samples on glass substrate

6.4.4 Visible transmittance analysis

The optical transmittance spectra of the AZO/Ag/AZO samples with Ag layers that are 5, 7, 9, 10, 11, 13 and 15 nm in thickness are shown in Figure 6.8. As shown in the figure, the visible transmittance first increases with increases in the thickness of the Ag layer, and then decreases with further increases in the thickness of the Ag layer. The average visible transmittance (from 400 to 800 nm) of the samples is 73.5%, 78.7%, 82.1%, 81.2%, 76.4%, 70.6% and 60.0%, respectively. The highest average visible transmittance of the prepared samples can be obtained with an Ag layer of 9-10 nm, and the highest visible transmittance point is 89.8% in the whole visible region. It can also be noticed that transmittance of the coated samples in the near IR region decreases with increasing thickness of the Ag layer when the Ag layer is less than 9 nm in thickness.

As explained in Section 5.3.4, the optical features that can be influenced by the evolution of the Ag film vary with deposition time. As shown in Figure 6.4(a), Ag particles are deposited as islands that are randomly distributed on the AZO substrate, and the separated islands would scatter the incident light, thus reducing the light transmittance. As seen in Figure 6.4(b), the gap between the aggregated particles is reduced, thus reducing the scattering property. In Figures 6.4(c) and 6.4(d), the Ag islands have coalesced into a continuous film, which would serve as a reflection film and thus the transmittance would gradually decrease. Therefore, the AZO/Ag/AZO coated film shows the highest visible transmittance at a critical thickness of the Ag layer when the Ag particles start to form a continuous film, which is around 9-10 nm.

It can also be found that for the samples in which the Ag layers are thicker than 10 nm, the transmittance from 800 to 900 nm is inversely proportional to the thickness of the Ag layer. This trend in the NIR region is attributed to a significant increase in the reflection of IR photons by a high number of free electrons in the metal. The number of free electrons is increased with increasing thickness of the Ag layer, which is closely related to the electrical conductivity.

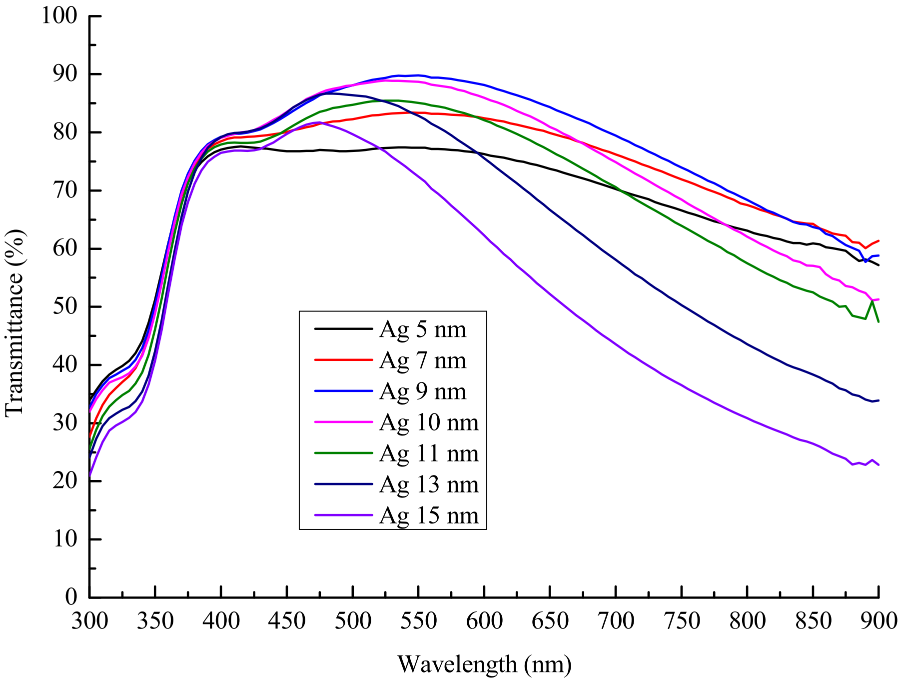

Figure 6.8 Visible transmittance spectra of the AZO/Ag/AZO coated samples with different thicknesses of the Ag layer on glass substrate

6.4.5 Ultraviolet protection factor analysis

The UPF values of the AZO/Ag/AZO coated samples with an Ag layer of 5 to 15 nm were 11.564, 11.618, 11.702, 12.177, 13.266, 14.247 and 15.34. Compared to the UPF of the uncoated glass which was 4.338, the UPFs of the AZO/Ag/AZO coated samples increased 166%-253%. The UPF values increased with increasing thickness of the Ag film.

6.4.6 Infrared properties analysis

The IR reflections of the AZO/Ag/AZO coated samples are shown in Figure 6.9. It can be observed that the IR reflections of all the coated samples are higher than that of the uncoated glass and increases with an increase in the thickness of the Ag layers. The sample with an Ag inlayer of 15 nm shows the highest IR reflection rate of 97% in the FIR range. In the figure, it can also be found that the IR reflection rate sharply increases when the thickness of the Ag layer is less than 10 nm, and after that, the IR reflection rate slightly increases with further increases in the thickness of the Ag layers. The results indicate that the Ag particles started to form a continuous film at a thickness of around 10 nm, which was also found in the XRD, SEM and visible transmittance results. In addition, it can also be observed that the IR reflection rate of all the samples sharply increases in the NIR region and slightly fluctuated in the MIR and FIR regions.

The IR transmission spectra of the AZO/Ag/AZO coated samples are shown in Figure 6.10. Similar to the results presented in Figure 5.7, the transmission spectra show the opposite tendency to the reflection spectra which can be explained by the energy conservation law: more reflected IR radiation means less radiation would penetrate the substance. Furthermore, all of the coated samples exhibit a lower transmission than the uncoated glass.

The AZO/Ag/AZO trilayers are metallic under low resistivity. The interactions between the electromagnetic waves and the metallicity are closely related to the electrical properties of the metal materials. The IR properties of metal film could be evaluated by using the renowned Hagen-Rubens relation [218]: $\varepsilon=4(\pi\varepsilon_0 c_0 \rho/\lambda)^{1/2}$, where ε is the IR emissivity, ε_0 is the permittivity of the electrons in vacuum, c_0 is the velocity of the light in vacuum, ρ is the resistivity and λ is the wavelength of the IR radiation. It is clear that the IR emissivity decreases with decreasing electrical resistivity. As $\varepsilon=1-r$, therefore, the IR reflection rate increases with decreasing electrical resistivity.

With reference to the sheet resistance and IR reflection results that are discussed in this chapter, it can be concluded that the IR reflection rate is inversely proportional to sheet resistance. When the Ag inner layer is less than 10 nm thick, the nano Ag particles become the scattering center, and thus the multilayer films show limitations in IR reflection at this time. After the forming of a continuous Ag layer, the multilayer films would act as an IR reflective mirror that could reflect most of the incident IR electromagnetic waves.

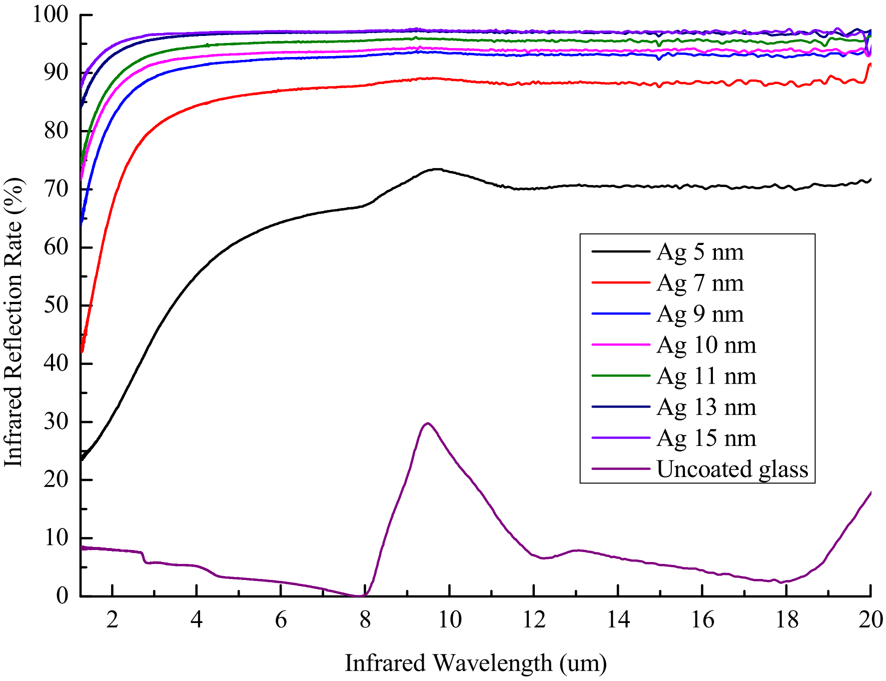

Figure 6.9 IR reflection spectra of uncoated glass and the prepared AZO/Ag/AZO samples on glass substrate

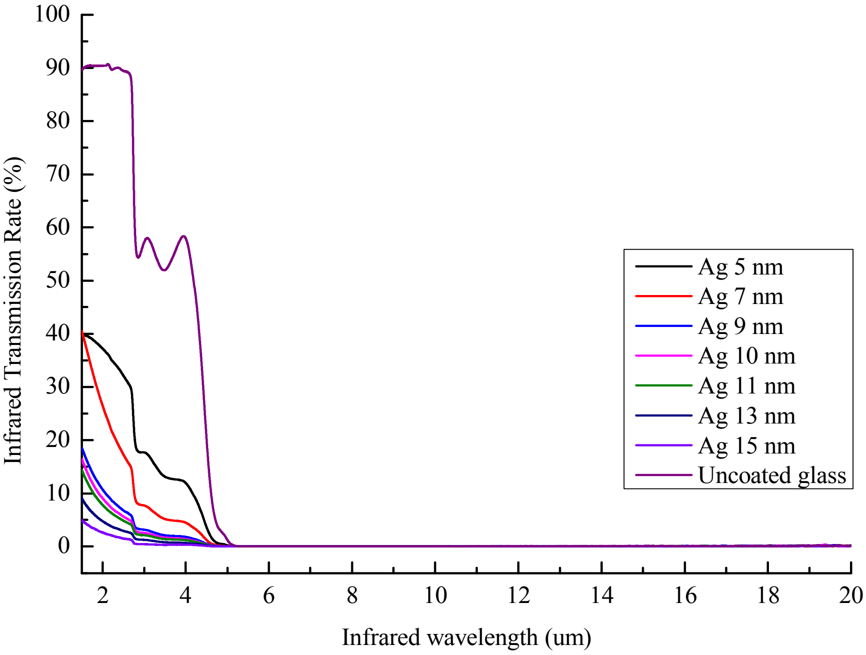

Figure 6.10 IR transmission spectra of uncoated glass and the AZO/Ag/AZO coated samples on glass substrate

6.5 Characterization of AZO/Ag/AZO films on flexible PET substrate

In this section, the characterization of AZO/Ag/AZO multilayer films deposited onto a flexible PET substrate will be discussed. The same procedure was used as that for the samples prepared on the glass substrate. The AZO layers were fixed at a thickness of 30 nm and the Ag layers were deposited at thicknesses of 5, 7, 9, 10, 11, 13 and 15 nm. In addition, the PET/AZO/Ag bi-layer films were also deposited and analyzed at the same thicknesses as those used with the glass substrate.

6.5.1 Crystal structure analysis

The XRD spectra of the AZO/Ag/AZO coated multilayer films plotted as a function of the thickness of the Ag layer are shown in Figure 6.11. In the spectra, the ZnO (002) and (103), and Ag (111) peaks can be detected, but the Ag (200) and (220) peaks are not found. It can also be observed that the ZnO and Ag peaks show similar changes to that of the peaks for films deposited onto glass with increases in the thickness of the Ag layer. All of these results indicate that slightly less crystallization takes place when the AZO/Ag/AZO films are deposited onto a PET substrate as opposed to deposition onto a glass substrate.

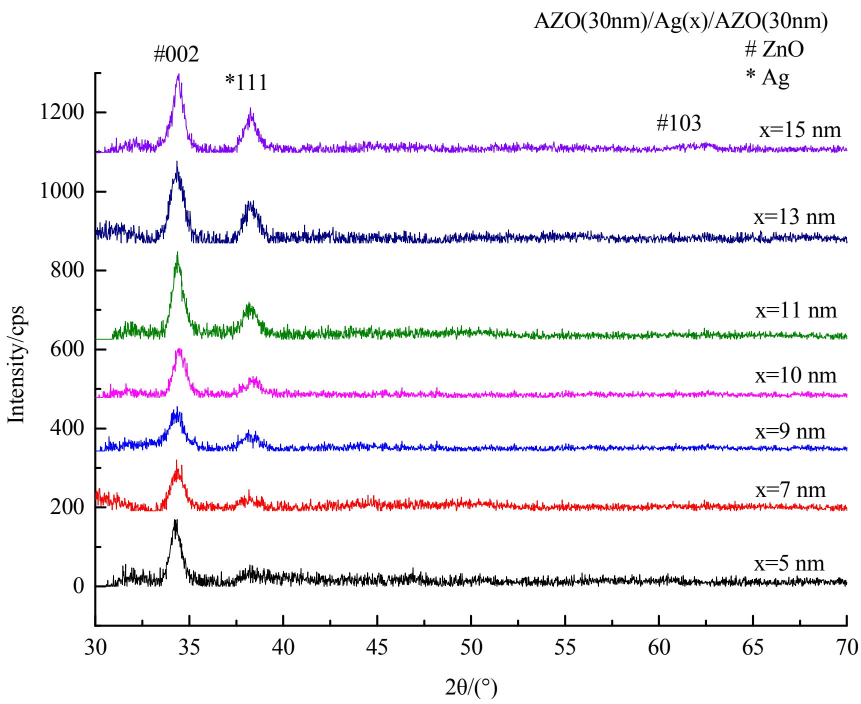

Figure 6.11 XRD spectra of AZO/Ag/AZO coated samples on PET substrate

6.5.2 Surface morphology analysis

The SEM and AFM imagings of the AZO/Ag films were carried out as a function of the thickness of the Ag layers, and the images are shown in Figure 6.12. The evolution of the Ag film is similar to that of the same film deposited onto a glass substrate and follows the Volmer-Weber model. However, the film surface is rougher than that of the film deposited onto a glass substrate, because the flexible PET substrate is not as stable as the rigid glass substrate.

A cross section image of the AZO/Ag/AZO multilayer with an Ag layer of 15 nm is shown in Figure 6.13. In the figure, the sandwich structure of the multilayer film is evident. The AFM imaging of the AZO/Ag/AZO multilayer films carried out as a function of the thickness of the Ag layer is shown in Figure 6.14. The roughness of the AZO/Ag/AZO coated samples is greater than that of the same films deposited onto glass, which is 5.85, 4.98, 3.3 and 5.04 nm, respectively.

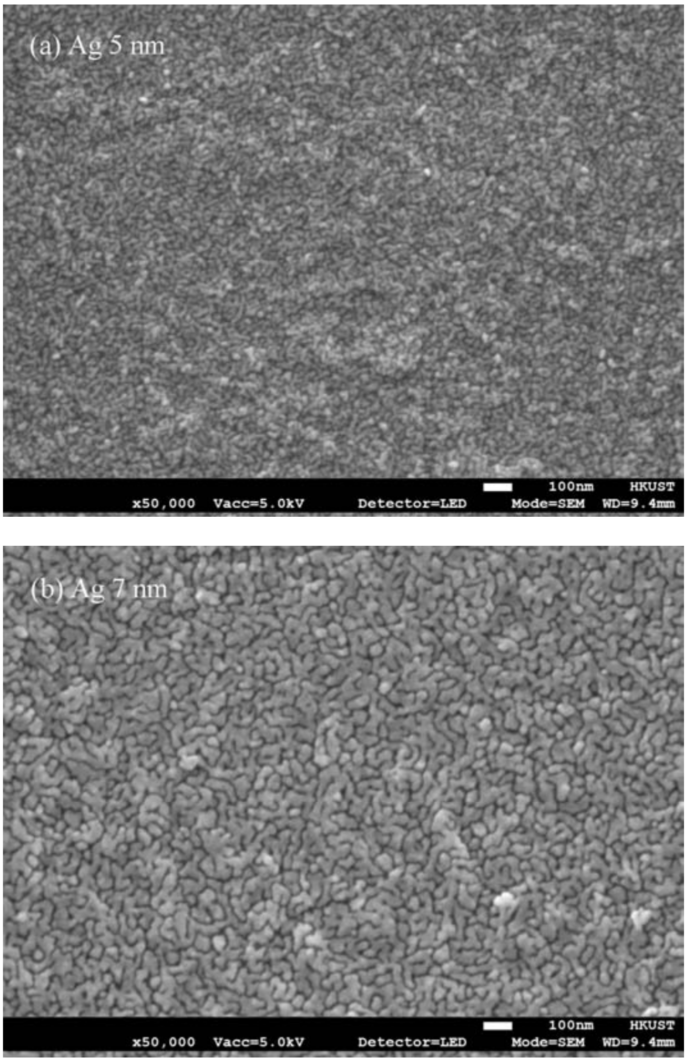

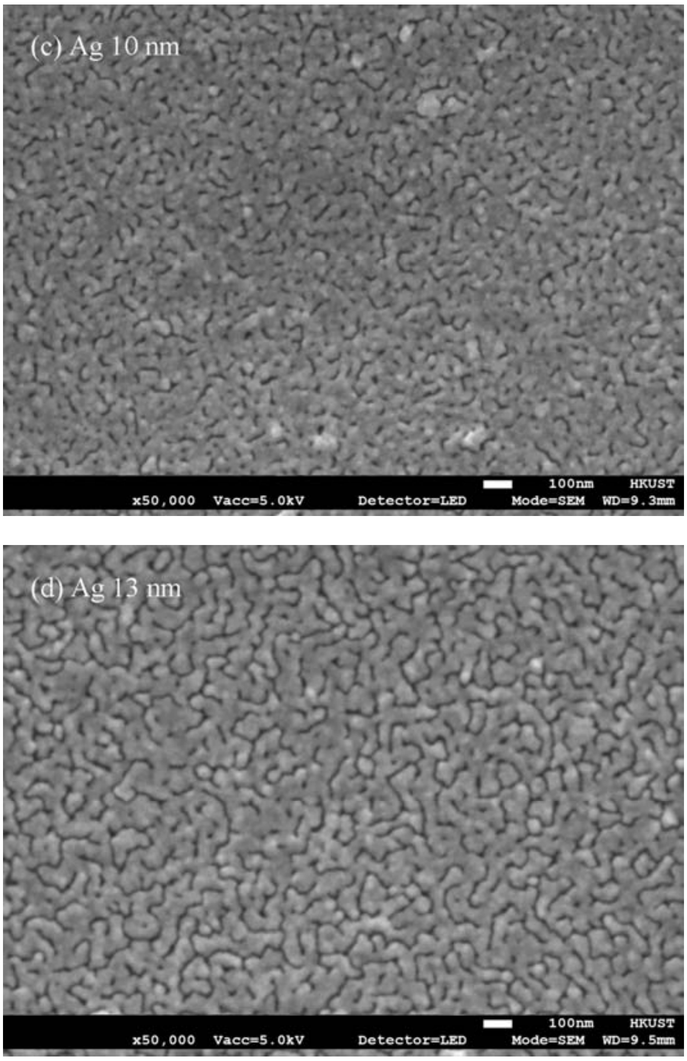

Figure 6.12 SEM images of AZO/Ag films with different thicknesses of Ag layer on PET substrate

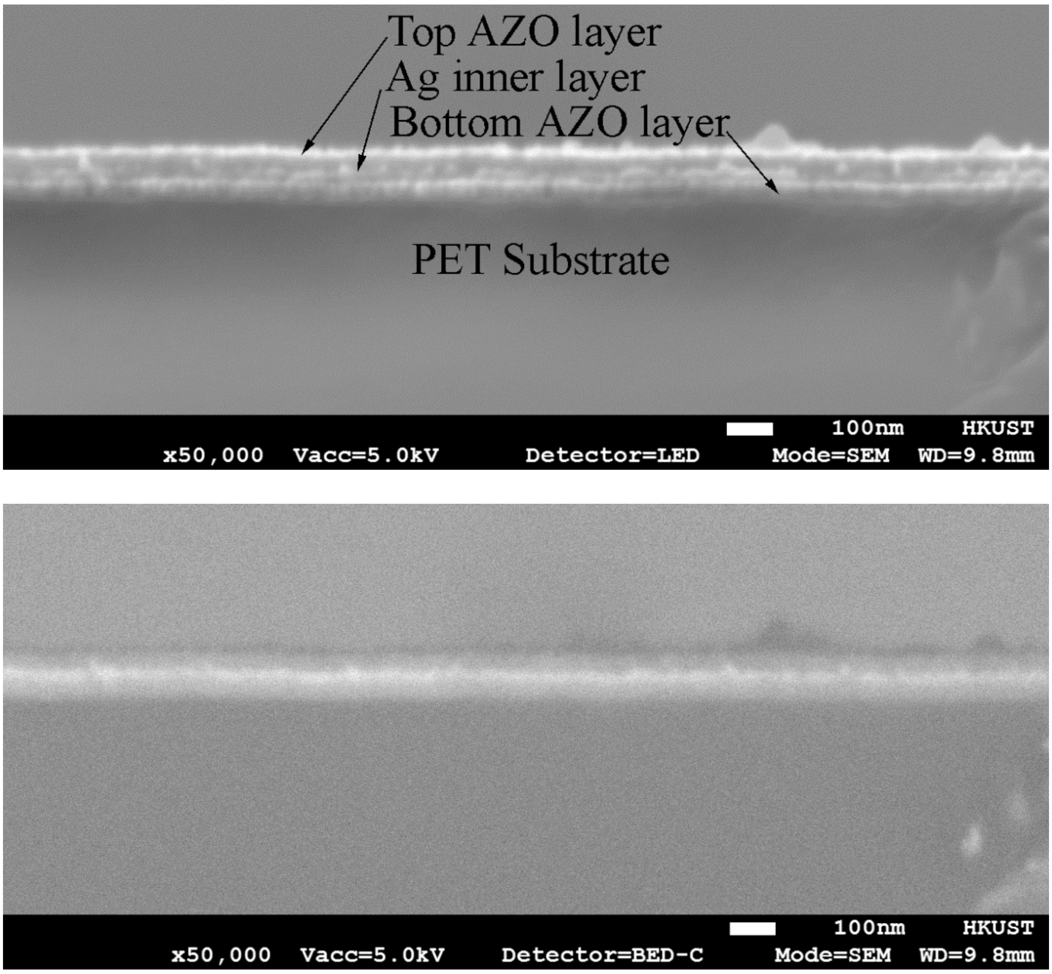

Figure 6.13 Cross section of SEM images of AZO/Ag (15 nm)/AZO film sample on PET substrate

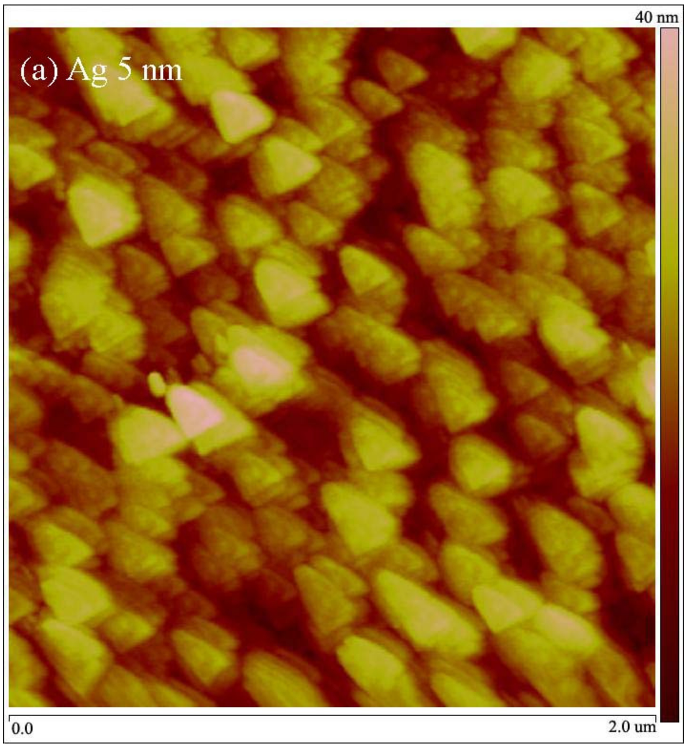
(a) Ag 5 nm
40 nm
0.0
2.0 um

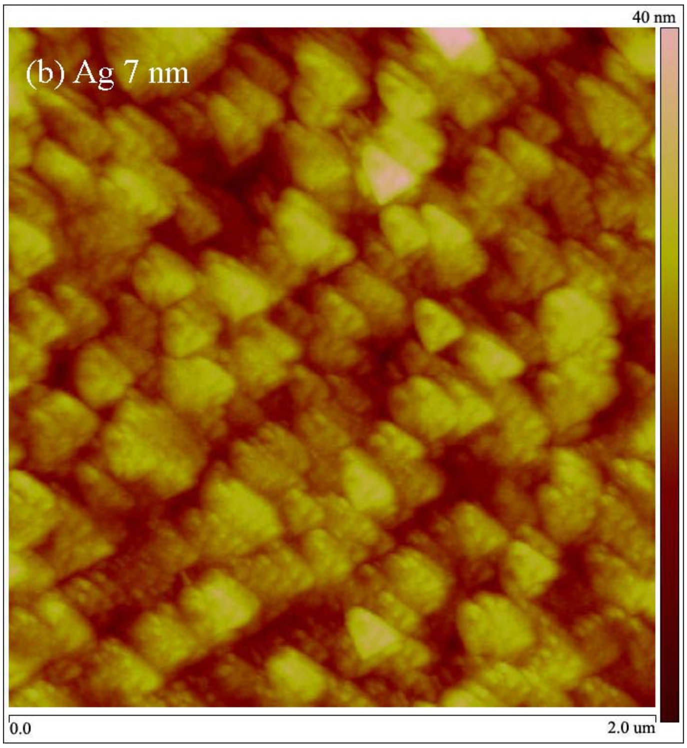
(b) Ag 7 nm
40 nm
0.0
2.0 um

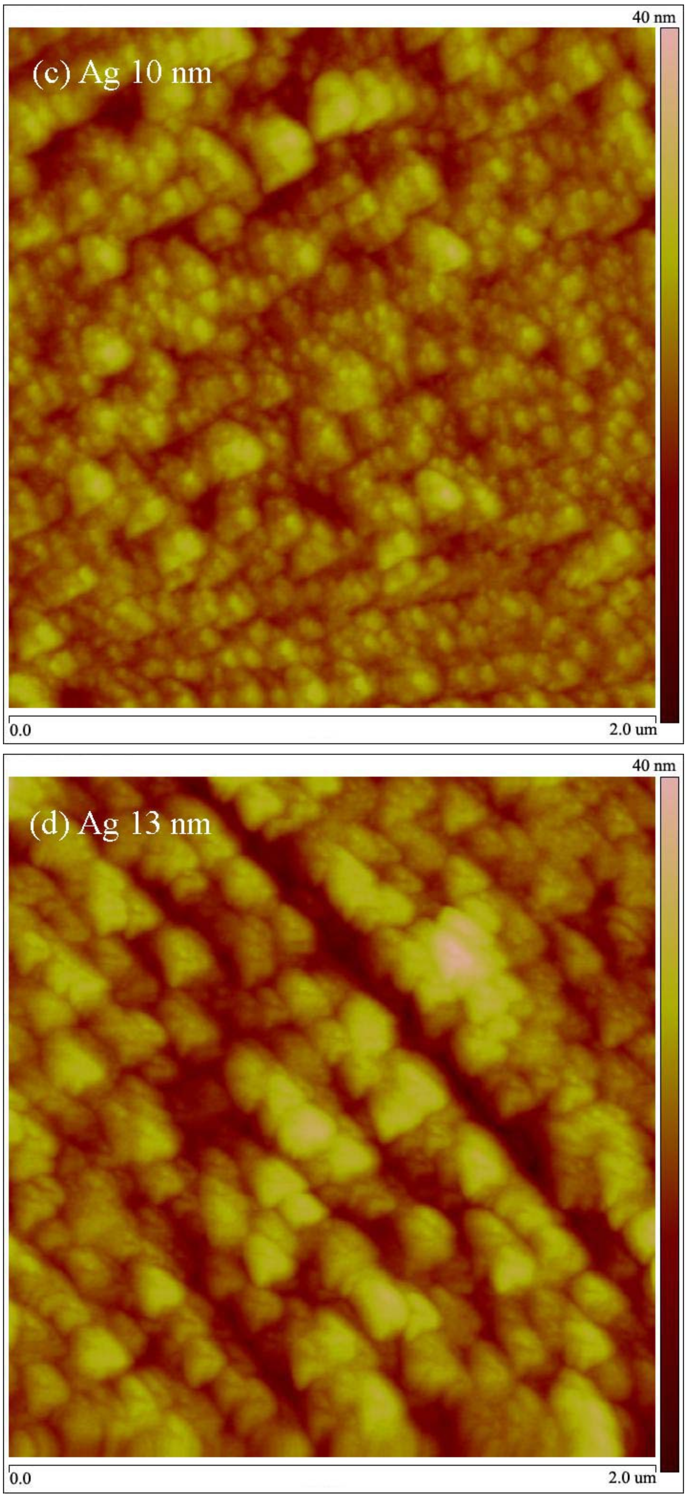

Figure 6.14 AFM images of AZO/Ag/AZO coated samples on PET substrate

6.5.3 Electrical properties analysis

The sheet resistance (Rs) of the coated multilayer films determined as a function of the thickness of the Ag layer is shown in Figure 6.15. The circumstances are the same as those for the films deposited onto glass; the sheet resistance significantly decreases when the Ag layer is less than 9 nm thick. After that, the sheet resistance slowly decreases with increasing thickness of the Ag layer. The lowest sheet resistance is 4.05 Ω/sq, which is obtained with a multilayer film that has an Ag inner layer of 15 nm in thickness. Moreover, the sheet resistance of the films is higher than that of the same films deposited onto glass with the same thickness of the Ag layer.

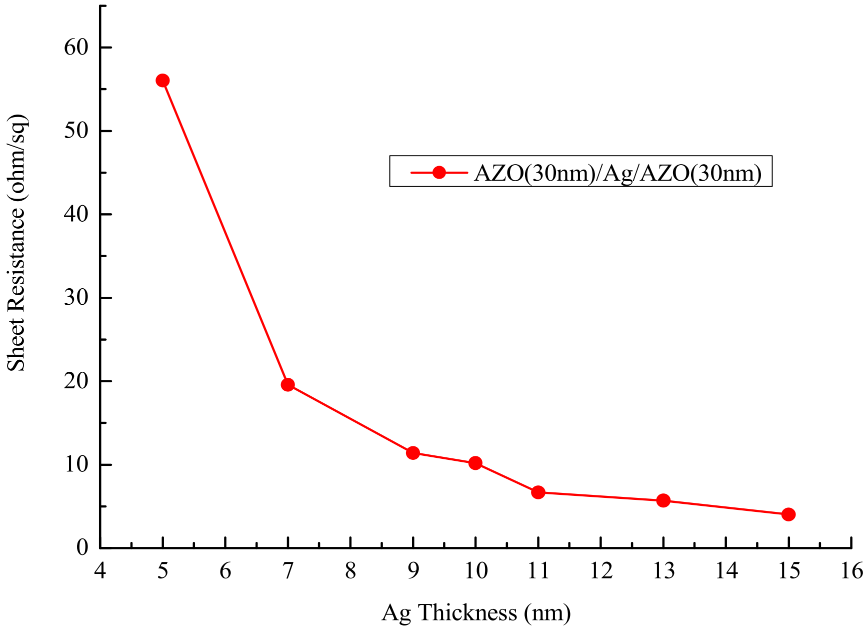

Figure 6.15 Sheet resistance of AZO/Ag/AZO coated samples on PET substrate

6.5.4 Visible transmittance analysis

The optical transmittance spectra of the studied AZO/Ag/AZO multilayer films are shown in Figure 6.16. In the figure, most of the samples show a significant increase in the transmittance in the UV region, and then maintain a transmittance of 75% - 80% in the visible region, and subsequently, the transmittance decreases to about 25% - 60% in the NIR region. The average visible transmittance (in a wavelength region of 400 to 800 nm) of the samples is 73.4%, 76.1%, 76.9%, 74.3%, 68.0%, 64.8% and 57.3%, respectively. It can be observed that the transmittance first increases and then decreases, and the sample with an Ag inner layer of 10 nm exhibits the highest visible transmittance of 85.6% at around 475 nm.

As explained in Section 6.4.4, the optical characteristics of the coated samples can be influenced by the evolution of the Ag film which varies with deposition time. At the beginning of the deposition, the Ag particles were deposited as separate islands that were randomly distributed on the AZO substrate, and the separate islands would scatter the incident light, thus reducing the light transmittance. With further sputtering, the gap between the Ag particles decreased, and the scattering property also decreased. Finally, the Ag islands coalesced into a continuous film, which served as a reflection film, and thus the transmittance would gradually decrease. According to this phenomenon, the critical thickness of the Ag layer should be around the highest visible transmittance point, which is about 10 nm in this study.

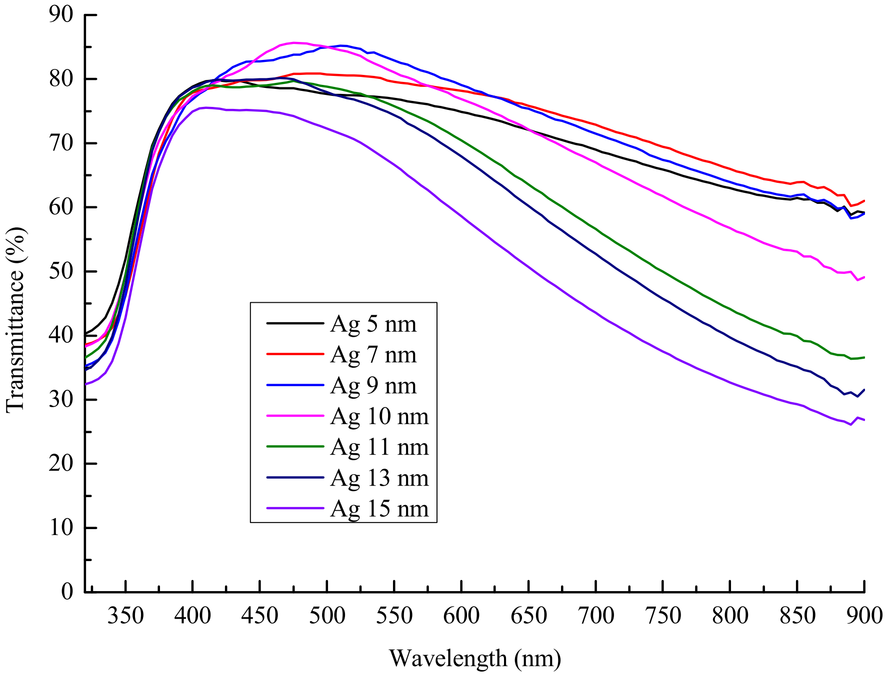

Figure 6.16 Visible transmittance spectra of the AZO/Ag/AZO coated samples with different thicknesses of Ag layer on PET substrate

6.5.5 Ultraviolet protection factor analysis

The UPF values of the AZO/Ag/AZO coated films with an Ag layer that ranged from 5 to 15 nm in thickness were 14.956, 15.396, 16.005, 16.224, 16.487, 16.764 and 17.889. Compared to the UPF value obtained from the uncoated PET which was 9.59, the UPF values of the AZO/Ag/AZO coated films increased by 56% - 86.5%. Additionally, the UPF values also increased with increasing thickness of the Ag film.

6.5.6 Infrared properties analysis

The IR reflection spectra of the AZO/Ag/AZO coated samples and uncoated PET are shown in Figure 6.17. In the figure, it is shown that the IR reflections of all the coated samples are higher than that of the uncoated PET and the IR reflection rates are increased with increases in the thickness of the Ag layer. Samples with an Ag inner layer of 15 nm show the highest IR reflection rate of about 96% in the wavelength region of 3-20 μm, which is much higher than that of bare PET of about 14% and slightly lower than the film with the same Ag layer but deposited onto a glass substrate (about 97%). As stated in Section 6.4.6, the IR reflection is inversely proportional to the sheet resistance. The sheet resistance of the films deposited onto the PET substrate is greater than that of the films deposited onto the glass substrate; therefore, the films deposited on glass exhibit a higher IR reflection rate.

As shown in the figure, the IR reflection of the coated samples with an Ag layer that is less than 9 nm in thickness is increased in the wavelength region around 1-6 μm, and after that, the IR reflection rates are maintained at a certain value or only slightly fluctuate. However, the IR reflection of the other film samples significantly increases from 1 to 3 μm and a similar IR reflection rate is maintained in the other IR regions. These results indicate that the evolution of the Ag film has a significant influence on the IR reflection, in that a continuous Ag inner layer can improve the IR reflection quickly and to the maximum point in the NIR region. Moreover, the samples with a discontinuous Ag layer can only obtain the highest rate of IR reflection in the MIR region.

The IR transmission spectra of the film samples are shown in Figure 6.18. The fluctuation in the spectra in the NIR region may have been caused by film interference and equipment noise. Similar to the results provided in Section 6.4.6, the transmission spectra show an opposite tendency to that of the reflection spectra, and all of the coated film samples exhibit a lower transmission than the uncoated PET.

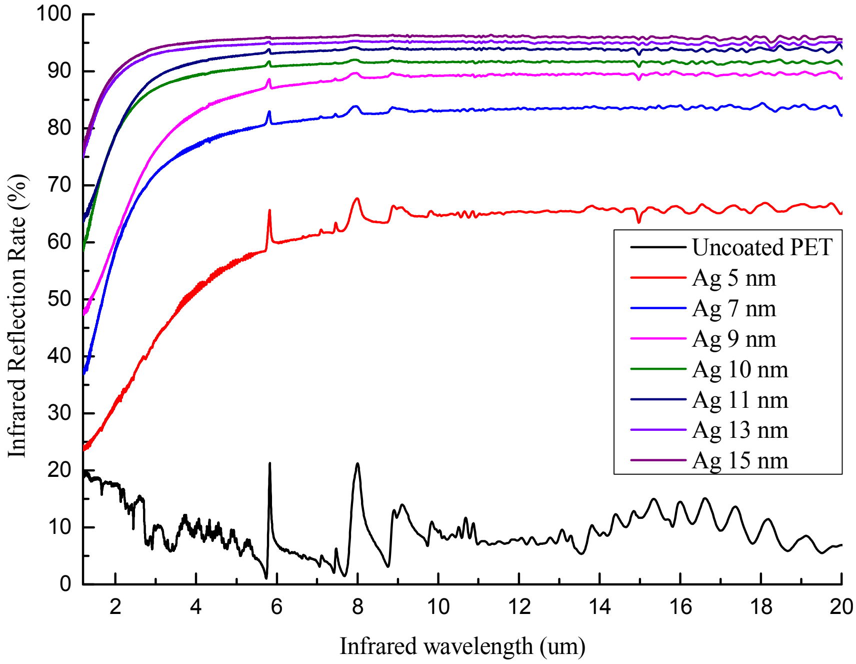

Figure 6.17 IR reflection spectra of uncoated PET and the AZO/Ag/AZO samples on PET substrate

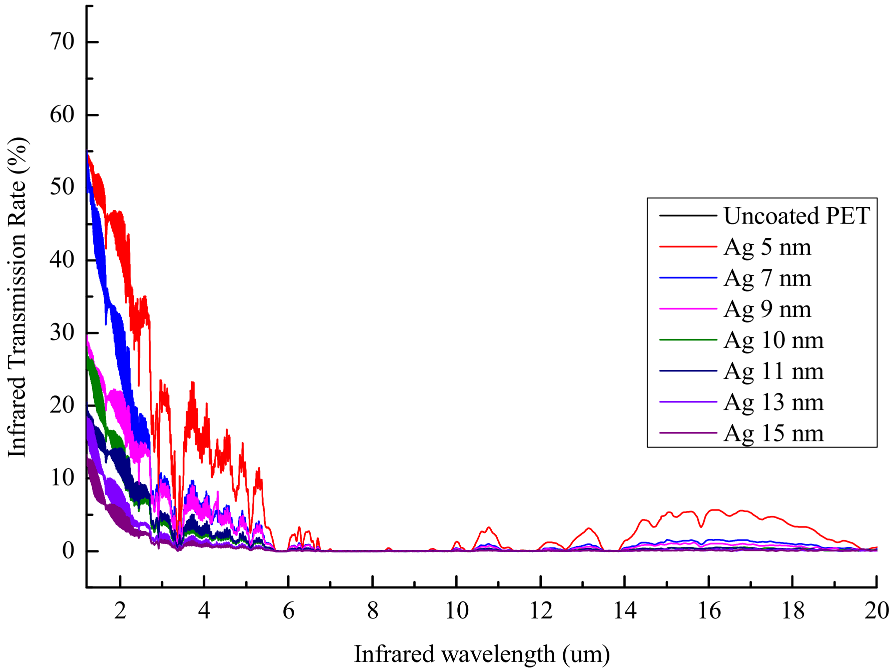

Figure 6.18 IR transmission spectra of uncoated PET and the AZO/Ag/AZO samples on PET substrate

6.6 Thickness of Ag layer based on optical properties

The IR reflection rates at a wavelength of 10 μm and the average visible transmittances of the AZO/Ag/AZO coated samples deposited onto glass substrates are shown in Figure 6.19. In the figure, when the Ag layer is less than 10 nm in thickness, the IR reflection rate significantly increases with increasing thickness of the Ag layer. The IR reflection rate is quite high at 97% - 98% when the Ag layer is about 13 nm in thickness, and slightly fluctuates with further increases in the thickness of the Ag layer. In the visible transmittance curve, the transmittance is shown to first improve and reaches its highest transmittance value of around 9-10 nm and then gradually decreases with increases in the thickness of the Ag layer.

The IR reflection rates at a wavelength of 10 μm and average visible transmittances of the AZO/Ag/AZO coated samples deposited onto a PET substrate are shown in Figure 6.20. The same is observed as the films deposited onto glass substrates. The IR reflection rate is relatively high at 96% - 97% when the thickness of the Ag layer is about 13 nm, and the highest visible transmittance is obtained when the thickness of the Ag layer is around 8-9 nm.

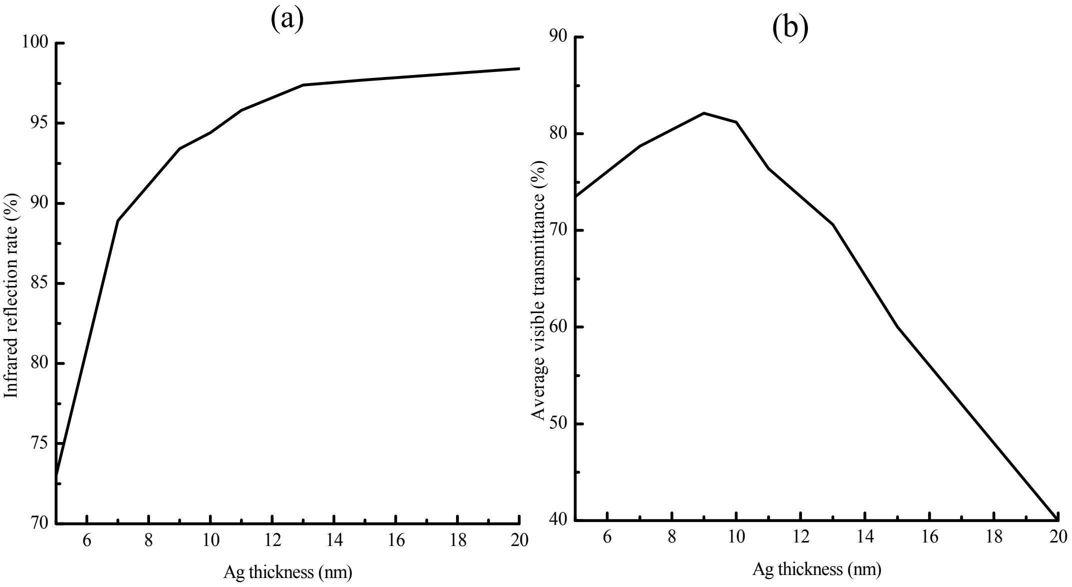

Figure 6.19 IR reflection rates at wavelength of 10 μm (a) and average visible transmittances (b) of the AZO/Ag/AZO coated samples on glass substrate

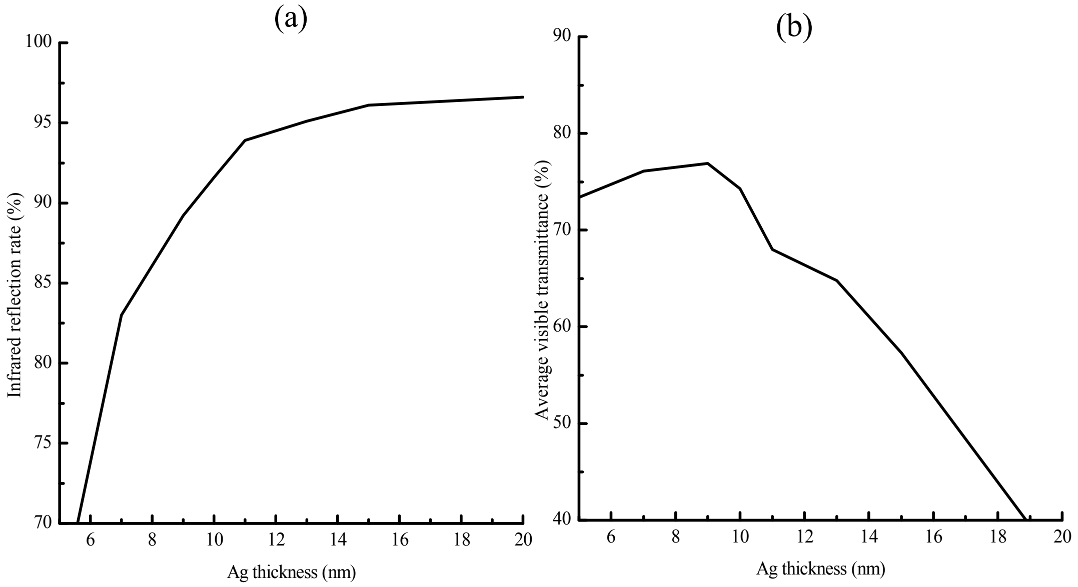

Figure 6.20 IR reflection rates at wavelength of 10 μm (a) and average visible transmittances (b) of the AZO/Ag/AZO coated samples on PET substrate

These results indicate that for the preparation of non-transparent products, an AZO/Ag/AZO multilayer coating with AZO and Ag layers that are 30 and 13 nm in thickness respectively can provide high IR reflection. For transparent products, an AZO/Ag/AZO multilayer coating with AZO and Ag layers that are 30 and 9 nm in thickness can provide an acceptable amount of IR reflection and high visible light transmittance.

6.7 Summary

In this chapter, it has been proven that an AZO/Ag/AZO multilayer film with

AZO layers that are 30 nm in thickness provides the most ideal IR transmitting properties. The crystal structure, surface morphology, electrical properties, visible transmittance, UPF values and IR properties of the AZO/Ag/AZO coated multilayer films that are deposited onto glass and PET substrates have been systematically investigated. The results indicate that the thickness of the Ag layer can significantly affect the properties of the coated multilayer films and the Ag layer starts to form a continuous film at a thickness of around 10 nm. The thickness of the Ag layer is inversely proportional to the film sheet resistance and directly proportional to the IR reflection of the film. The film with an Ag inner layer of 15 nm shows the highest rate of IR reflection of 97% on the glass substrate and 96% on the PET substrate. The AZO/Ag/AZO coated multilayer film with AZO and Ag layers that are 30 and 13 nm in thickness respectively can provide a similar high rate of IR reflection of 96% - 98% with further increases in the thickness of the Ag layer. Moreover, this would also show a high average visible transmittance of 80% with an Ag inner layer of 9-10 nm. The high IR reflectivity, both on rigid and flexible substrates, renders this RF magnetron sputtered AZO/Ag/AZO multilayer film a promising candidate in the development of high IR reflective textiles.

The AZO/Ag/AZO multilayer film exhibits high IR reflection, but the metal-Ag used in the multilayer film is very expensive, and therefore, there is the need for more reasonably priced products with an acceptable amount of IR reflection.

Therefore, it is necessary to fabricate this kind of film to substitute for the more costly AZO/Ag/AZO multilayer film. Under this context, the possibility of using an AZO/Cu/AZO multilayer film will be investigated in the next chapter.

Chapter 7 Exploring substitution of Ag with Cu as inner layer in AZO/metal/AZO films[iv]

7.1 Introduction

As shown in Chapter 6, AZO/Ag/AZO multilayer films have excellent IR reflection both on glass and flexible PET substrates. To fulfill the possibility of obtaining a film that has a lower cost yet provide an acceptable amount of IR reflection, an AZO/Cu/AZO multilayer film has been prepared and analyzed in this study. The various thicknesses of the AZO/Cu/AZO multilayer films that were deposited onto glass substrates will be outlined in this chapter. Then, the crystal structure, surface morphology, electrical properties, visible transmittance, UPF and IR transmittance/reflection properties of the coated films after deposition will be discussed.

7.2 Preparation of AZO/Cu/AZO films

Seven AZO/Cu/AZO samples were prepared for testing. For all of the samples, both the bottom and top AZO layers were fixed at a thickness of 30 nm and the Cu inner layer was deposited at thicknesses of 5, 7, 9, 11, 13 and 15 nm. Based on the capabilities of the deposition system used in this study, the deposition parameters

---

[iv] *Parts of this chapter have been published in the* ***Journal of Materials Science: Materials in Electronics.***

of the AZO and Cu layers are listed in Table 7.1.

Table 7.1 Deposition parameters of AZO/Cu/AZO films on glass substrate

	AZO Layer	Cu Layer
Base pressure	5×10^{-4} Pa	5×10^{-4} Pa
RF power	150 W	50 W
Ar flow rate	40 sccm	30 sccm
Working pressure	0.5 Pa	0.3 Pa

7.3 Characterization of AZO/Cu/AZO multilayer films

7.3.1 Crystal structure analysis

The XRD spectra of the AZO/Cu/AZO coated multilayer films are shown in Figure 7.1. In the spectra, strong ZnO (002) and weak ZnO (103) peaks can be detected in all of the samples, which indicate a polycrystalline structure of the AZO layers. However, the intensity of the Cu peak is not obvious in some of the spectra; the Cu (111) peak can only be observed when the thickness of the Cu layer is greater than 11 nm. Moreover, the intensity of the Cu (111) peaks increases with increases in the thickness of the Cu layer, as expected. This phenomenon may also lend support to the possibility that the Cu inner layer formed a continuous film when it was greater than 11 nm in thickness. It can also be noticed that the intensity of the ZnO (002) peaks is slightly reduced with increases in the thickness of the Cu layer, which can be easily observed in the

AZO/Cu (15 nm)/AZO sample. This is caused by increases in the Cu (111) peak intensity which partially suppressed the intensity of the ZnO peaks.

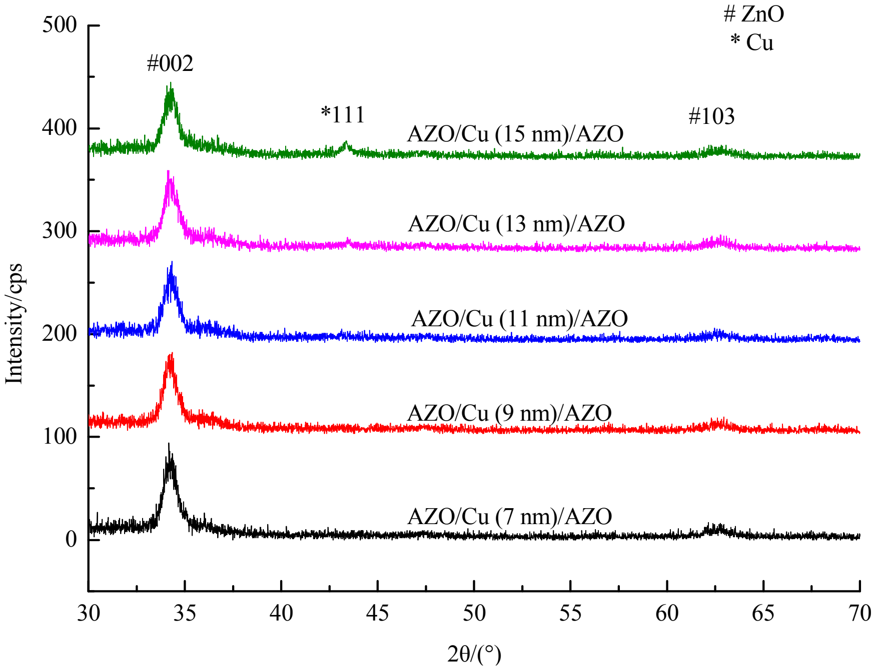

Figure 7.1 XRD spectra of AZO/Cu/AZO samples on glass substrate

7.3.2 Surface morphology analysis

The AFM images of the AZO/Cu/AZO film samples are shown in Figure 7.2. In Figure 7.2 (Cu layer with thickness of 7 nm), the size of the AZO particles is not uniform and large particles can be seen in the images. In Figure 7.2 (Cu layer with thickness of 9 nm), the size of the AZO particles is still not uniform, but there are fewer large particles observed. In Figure 7.2 (Cu layer with thickness of 11 nm), the surface of the top AZO layer is flat and the size of the particles is uniform. In Figure 7.2 (Cu layer with thickness of 13 nm), the top AZO layer has a rough surface again and some large particles can also be observed. The surface roughness of the samples with a Cu inner layer of 7-13 nm was 3.89, 2.25, 1.92 and 1.97 nm (determined by using NanoScope Analysis software V1.2). This is because the roughness of the multilayer film is affected by the evolution of the Cu inner layer in that it first decreased with increasing Cu thickness, until reaching its lowest point at a critical thickness of the Cu layer, and then slightly increased with further increases in the thickness of the Cu layer.

The trilayer structure of the AZO/Cu (15 nm)/AZO film sample is presented in Figure 7.3. In the figure, the continuous structure of the Cu inner layer and the sandwich structure of the multilayer film are clearly evident.

SEM imaging of the prepared AZO/Cu film samples was carried out as a function of the thickness of the Cu inner layer, see Figure 7.4 for images. The imaging showed that the morphology of the Cu inner layer changes with increasing thickness of the Cu layer. First, when the Cu layer is very thin (7 nm), the Cu particles are in an irregular strip shape, and the Cu layer is discontinuous. Secondly, when the Cu layer is increased to a thickness of 9 nm, the Cu particles bond to each other and some of the particles turn into an oval or circle shape. Thirdly, when the Cu inner layer is increased to 11 nm in thickness, most of the Cu particles bond together into an oval or circle shape and the Cu layer becomes a continuous flat film. Finally, with a further increase to the thickness of the Cu inner layer to 13 nm, the layer is still continuous and there is more surface roughness. The evolution of the Cu particles indicates that the growth of the deposited Cu film follows the Volmer-Weber model, which is the same for the evolution of an Ag inner layer as discussed in Chapter 6.

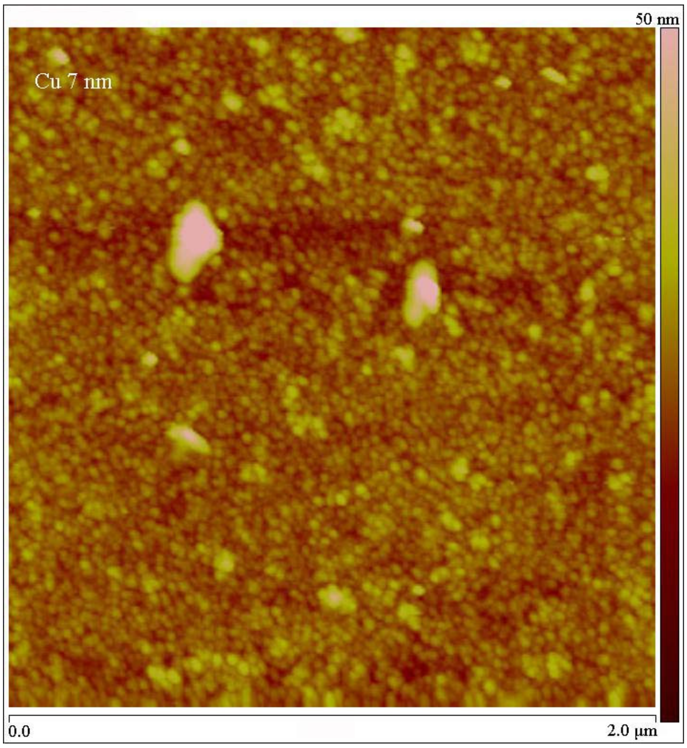

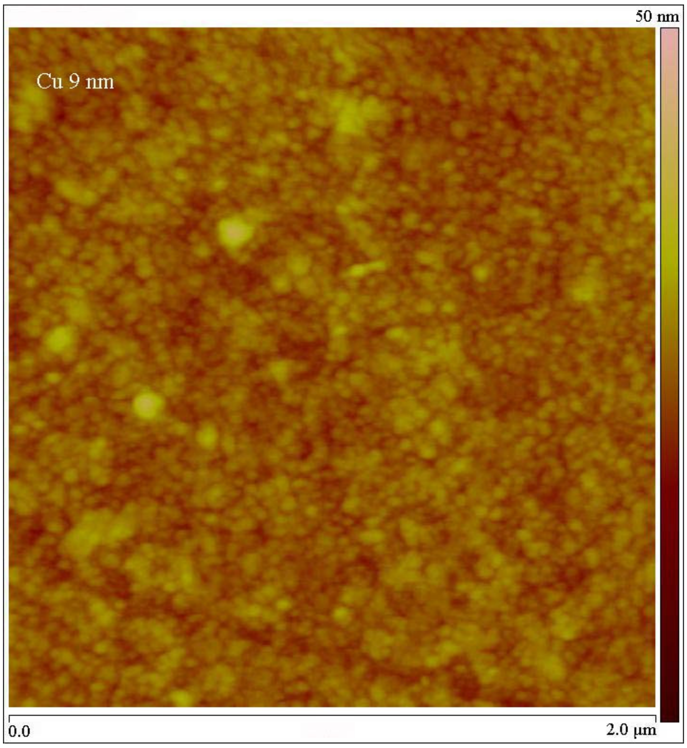

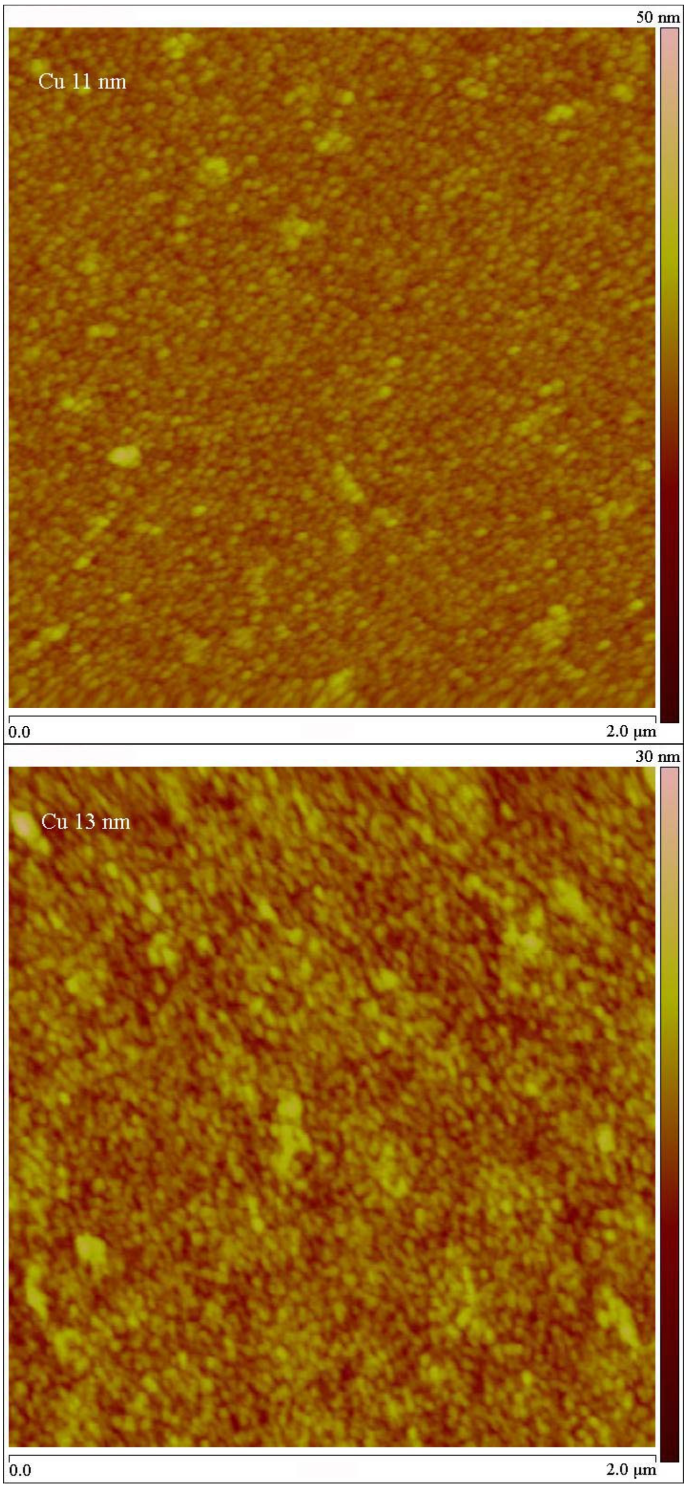

Figure 7.2 AFM images of AZO/Cu/AZO samples with Cu inner layers of different thicknesses on glass substrate

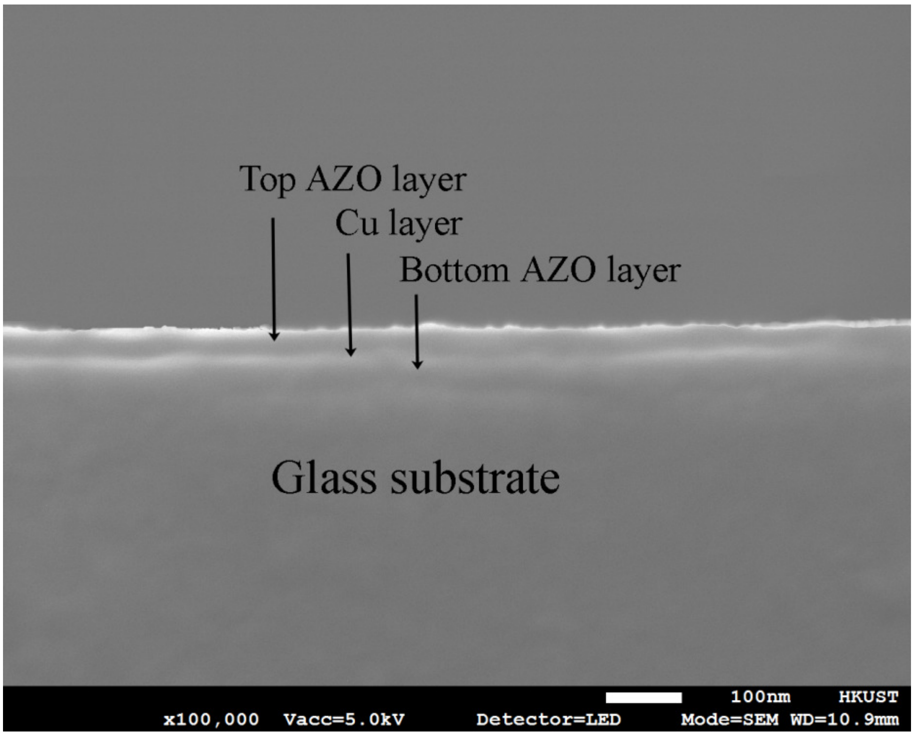

Figure 7.3 Cross section image of AZO/Cu/AZO sample with Cu inner layer of 15 nm on glass substrate

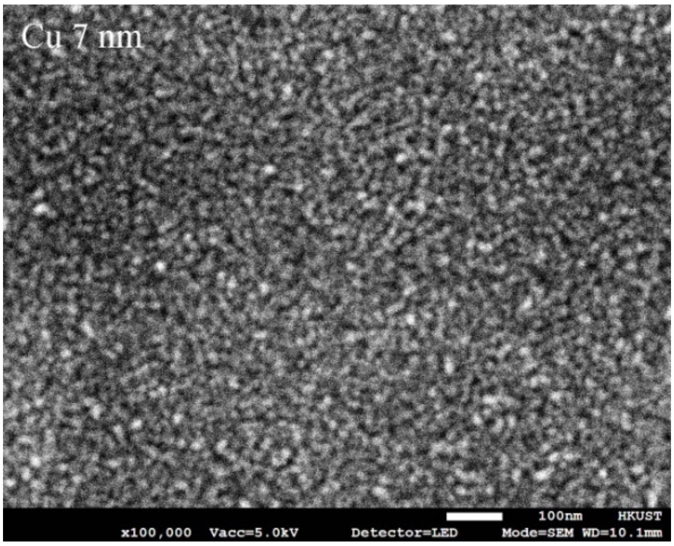

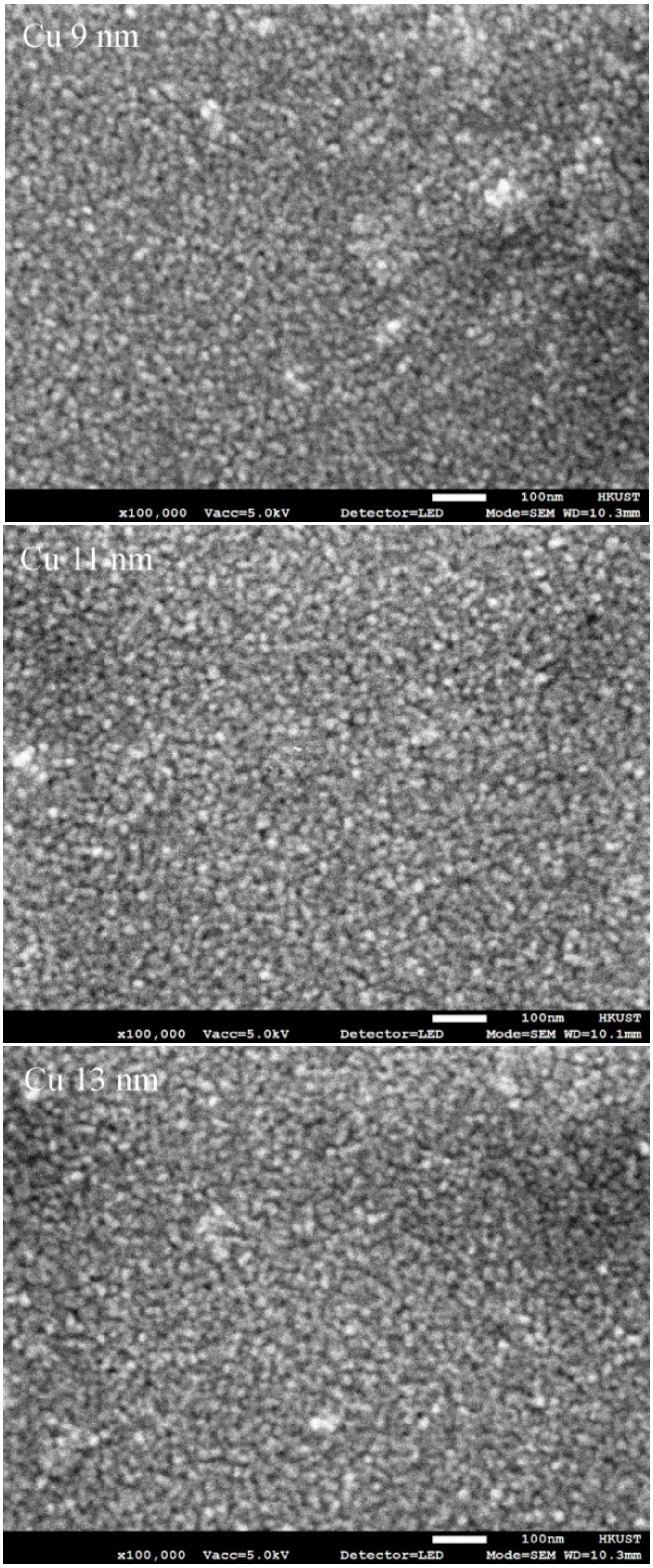

Figure 7.4 SEM images of AZO/Cu samples with different thicknesses of Cu layer on glass substrate

7.3.3 Electrical property analysis

The sheet resistance of the coated multilayer films was determined as a function of the thickness of the Cu layer, see Figure 7.5. As shown in the figure, the sheet resistance decreases with increases in the thickness of the Cu inner layer, as expected, and the lowest sheet resistance is 16.6 Ω/sq, obtained by the film with a Cu inner layer of 15 nm. It can also be noticed that the sheet resistance presents a sharp decrease when the thickness of the Cu layer is less than 11 nm. After that, the resistance is slightly decreased with further increases in the thickness of the Cu layer, which may indicate that the Cu inner layer formed a continuous film when its thickness was greater than 11 nm. This continuous film helps to improve the electrical conductivity. Before forming the continuous film, the Cu particles formed an incompletely electric conduction net, and not all could contribute to the electrical conductivity, so the sheet resistance was high.

The multilayer films were prepared by using RF magnetron sputtering at room temperature. The conductivity of the AZO films was low and the sheet resistance of pure AZO (60 nm; larger than 1.0×10^6 Ω/sq) was much larger than that of all the other prepared samples. Therefore, the total resistance of the multilayer films is determined by the Cu inner layer, and the resistance of the multilayer film is largely reduced with the addition of the Cu inner layer.

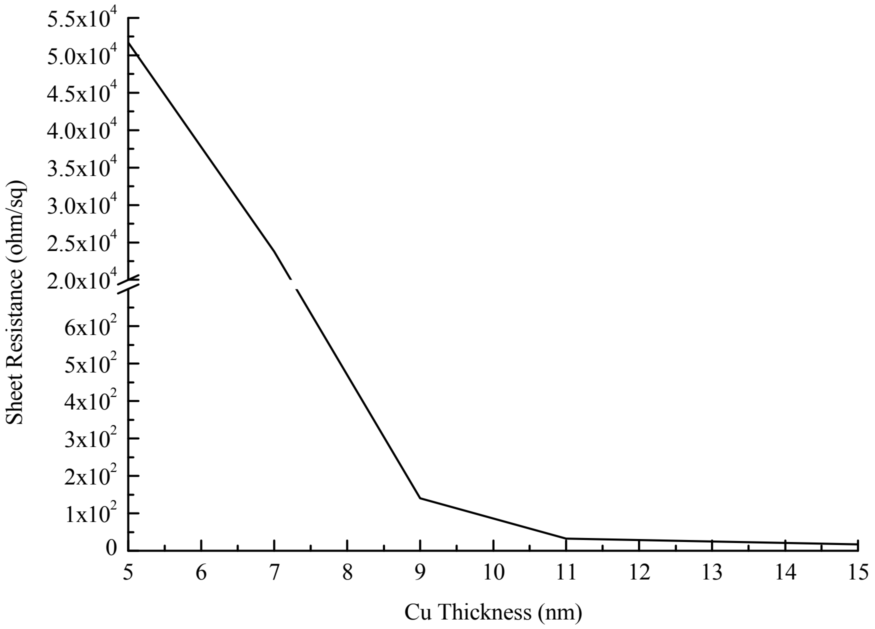

Figure 7.5 Sheet resistances of the AZO/Cu/AZO samples on glass substrate

7.3.4 UV-VIS transmittance analysis

The UV-VIS transmittance spectra of the prepared AZO/Cu/AZO multilayer films are presented in Figure 7.6. In the figure, most of the samples show a significant transmittance increase in the UV to the visible regions, and then maintain a transmittance of 60% - 80% in the visible region. The average visible transmittance (in a wavelength region of 400 to 800 nm) of the prepared samples is 74.2%, 72.5%, 68.9%, 72.2%, 68.8% and 61.1%. The average visible transmittance of the film samples is decreased with increases to the thickness of the Cu layer, except for the film sample with a Cu inner layer of 11 nm, which shows an abrupt increase in visible transmittance. This phenomenon can be explained by the formation of a continuous Cu inner layer. As stated by other researchers [219], before forming the continuous film, the deposited Cu particles work as a scattering center and the visible transmittance would increase with increases in the thickness of the Cu layer. After forming the continuous film, the Cu layer would act as a reflective mirror, and the transmittance would gradually decrease with further increases in the thickness of the Cu layer. In this study, the variation in the transmittance follows this tendency, except for the film samples with Cu inner layers that are 5 and 7 nm in thickness, and this may be resultant of film interference.

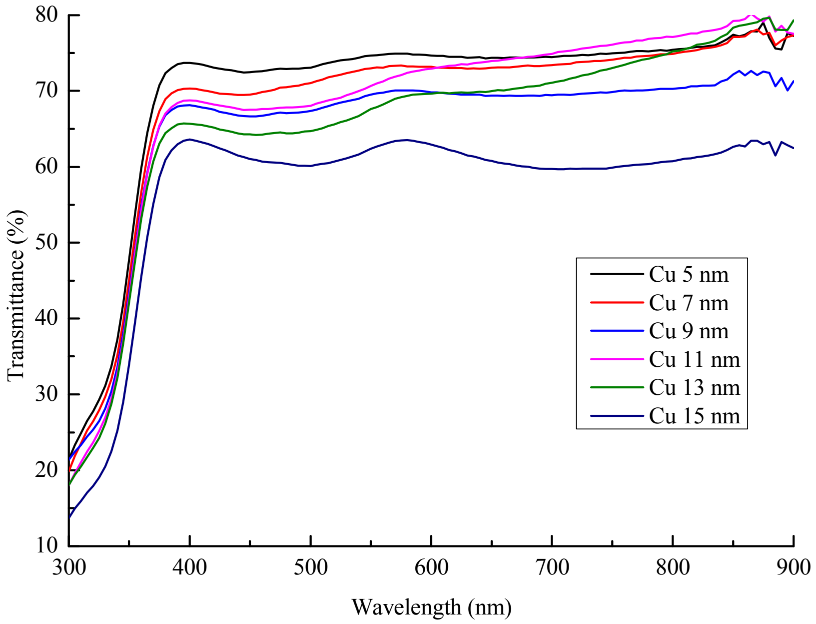

Figure 7.6 UV-VIS transmittance spectra of AZO/Cu/AZO samples on glass substrate

7.3.5 Ultraviolet protection factor analysis

The UPF values of the AZO/Cu/AZO coated samples with a Cu layer of 5 to 15 nm were 18.546, 19.093, 19.419, 21.12, 21.896 and 26.652. Compared to the UPF value of the uncoated glass which was 4.338, the UPF values of the AZO/Cu/AZO coated samples were increased about 323% - 626%. The UPF values of the AZO/Cu/AZO coated samples were higher than those of the AZO/Ag/AZO coated samples, which may be caused by the color difference between the two multilayer films.

7.3.6 Infrared properties analysis

The IR reflection and transmittance properties of the prepared samples are shown in Figure 7.7. In the figure, the samples with Cu inner layers that have a thickness of 5 and 7 nm have a low rate of IR reflection, and the sample with a Cu inner layer of 9 nm only shows a slight increase compared to the uncoated glass. However, the film samples with Cu inner layers of 11, 13 and 15 nm in thickness show a relatively high rate of IR reflection. The sample with a Cu inner layer of 15 nm shows the highest rate of IR reflection of about 67% in the FIR region.

IR reflection is caused by the interactions between IR electromagnetic waves and the free electrons in the multilayer films in that the free electrons can reflect the IR photons and the number of free electrons are directly determined by the sheet resistance. As stated in Section 7.3.1, in this study, AZO films are prepared at room temperature and their sheet resistance is very high. The sheet resistance of the multilayer films is mainly affected by the Cu inner layer. When the Cu inner layer has a thickness that is less than 11 nm, the electric conduction net of the Cu particles is incomplete. Therefore, there are fewer free electrons in the film. After forming the continuous film, most of the electrons would move about freely and contribute to the electrical conductivity; therefore, the concentration of free electrons is high when a continuous Cu layer is formed and would reflect more incident IR photons. In considering the relationship between the free electrons and film resistivity, it could be concluded that the IR reflection rate is inversely proportional to the film sheet resistance and directly proportional to the thickness of the Cu layer.

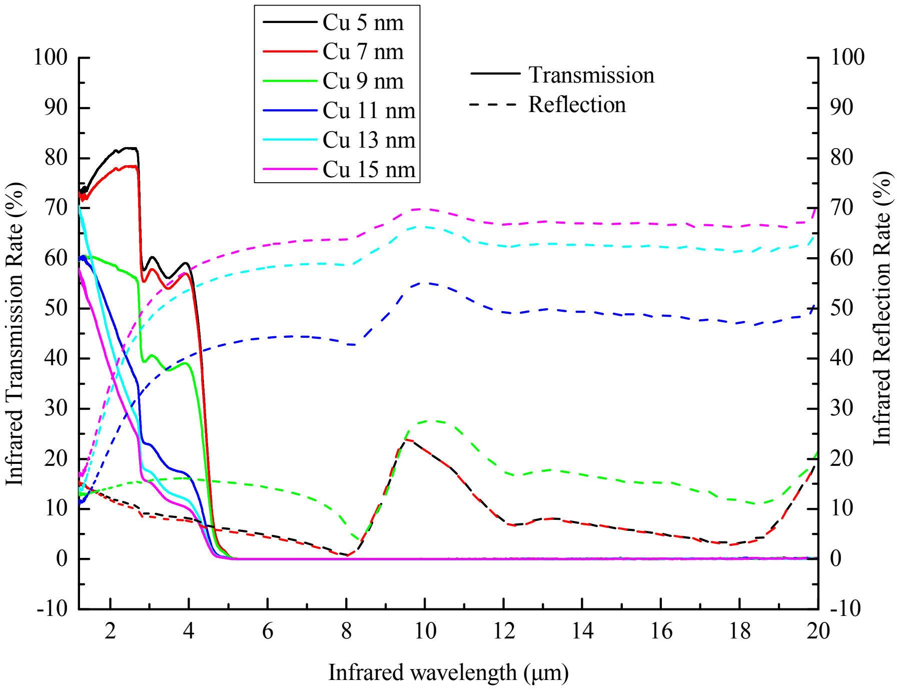

Figure 7.7 IR transmittance and reflection spectra of AZO/Cu/AZO samples on glass substrate

In the IR transmittance spectra, the transmittance of the coated samples is lower than that of the uncoated glass, and the IR transmittance decreases to zero when the IR wavelength is longer than 5 μm, which is caused by the high IR absorption of the uncoated glass in this wavelength region. The sample with a Cu inner layer of 15 nm shows the lowest IR transmittance, which is contrary to the IR reflection result. These results can also be explained by the law of energy conservation in that as more IR electromagnetic waves penetrate a substance, fewer IR electromagnetic waves would be reflected.

7.4 Summary

In this chapter, the crystal structure, electrical conductivity, visible transmittance, surface morphology and IR reflection of AZO/Cu/AZO coated multilayer films have been systematically investigated. The results indicate that the thickness of the Cu inner layer can significantly affect the properties of the prepared multilayer films and the Cu inner layer starts to form a continuous film at a thickness of around 11 nm. The thickness of the Cu inner layer is inversely proportional to the film sheet resistance and directly proportional to the IR reflection of the film. The film with a Cu inner layer that is 15 nm in thickness exhibits the highest rate of IR reflection of 67% and the lowest sheet resistance of 16.6 Ω/sq. In addition, the samples show a transmittance of 60% - 80% in the visible region. The IR reflectivity of the AZO/Cu/AZO multilayer films is not as high as that of the AZO/Ag/AZO films, but considered as an acceptable substitute for the latter with a more reasonable price. The application of these multilayer films on textiles will be discussed in the next chapter.

Chapter 8 Application of developed films for high infrared reflective textiles[v]

8.1 Introduction

As found in the previous chapters, AZO/Ag/AZO multilayer films exhibit an IR reflection rate of 96% - 97% when the Ag inner layer has a thickness that is greater than 13 nm and the AZO/Cu/AZO multilayer film has an IR reflection rate of 67% with a Cu inner layer that is 15 nm in thickness. In this chapter, a discussion will revolve around the deposition of AZO/Ag/AZO multilayer films onto polyester fabrics to fabricate high IR reflective textiles, and the properties of the high IR reflective textiles will be systematically investigated. After that, the deposition of the AZO/Cu/AZO multilayer films onto polyester fabrics to fabricate high IR reflective textiles with an acceptable IR reflective function at a reasonable cost will be outlined.

8.2 Fabrication of high infrared reflective polyester fabrics with AZO/Ag/AZO multilayer films

AZO/Ag/AZO multilayer films were deposited onto polyester fabric (75D/180T 90*90, 64.50 g/m^2) by using an RF magnetron sputtering apparatus. Prior to

---

[v] *Parts of this chapter have been published in* ***Ceramics international*** and the ***Journal of Materials Science: Materials in Electronics.***

deposition, the fabric substrates were ultrasonically cleaned in a detergent bath, followed by rinsing in an acetone solution and then dried in nitrogen gas. The polyester samples were then cut into 6 cm by 6 cm squares and conditioned in accordance with ASTM D1776-08 before sputtering and measurement. The deposition parameters of the AZO/Ag/AZO multilayer films are the same as those listed in Table 6.1. In this study, both the bottom and top AZO layers are fixed at a thickness of 30 nm and the Ag inner layers are deposited at thicknesses of 5, 7, 10, 13, 15 and 20 nm. In order to observe the evolution of the Ag inner layer, Fabric/AZO/Ag bi-layer films were also prepared by using the same deposition parameters as those listed in Table 6.1, only without depositing the top AZO layer. In the bi-layer film, the AZO layer is also fixed at a thickness of 30 nm. The Ag layer is varied in thickness from 5 to 13 nm. Images of the AZO/Ag/AZO (with Ag inner layer of 10 and 15 nm) coated polyester fabrics are shown in Figure 8.1.

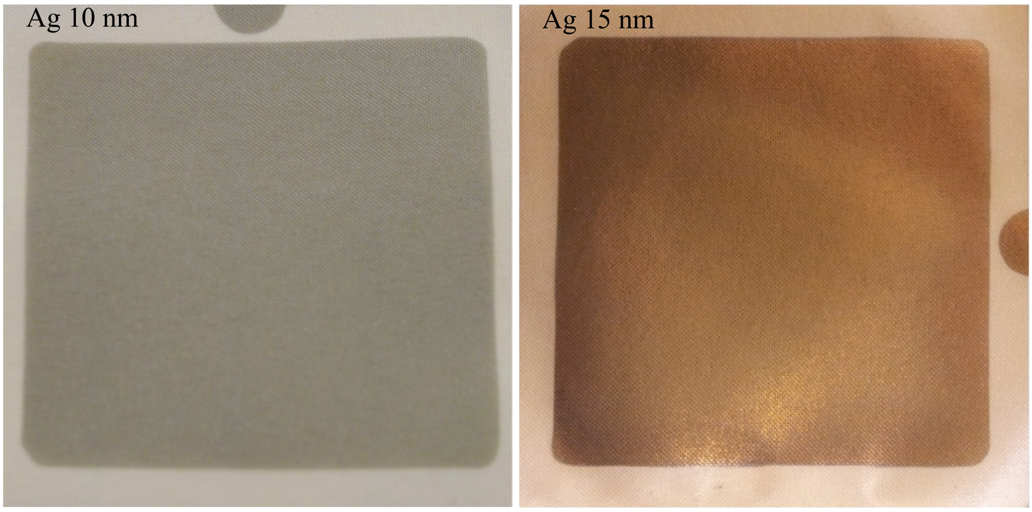

Figure 8.1 Images of AZO/Ag/AZO coated polyester fabrics

8.3 Fabrication of high infrared reflective polyester fabrics with AZO/Cu/AZO multilayer films

AZO/Cu/AZO multilayer films were deposited onto polyester fabric with the same deposition parameters as those listed in Table 7.1. The AZO layers were also fixed at a thickness of 30 nm, and the Cu layers were deposited at thicknesses of 15, 20, and 40 nm.

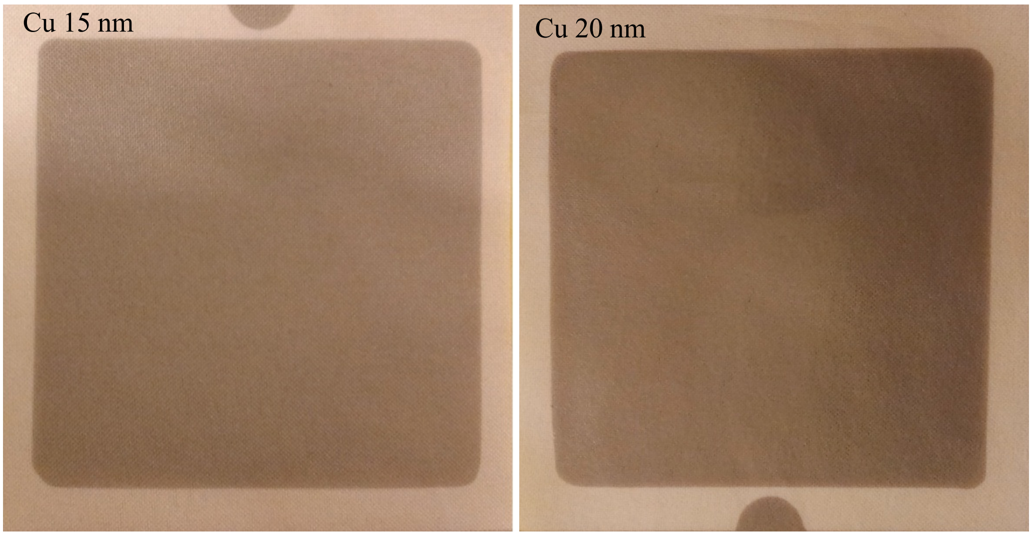

Figure 8.2 Images of AZO/Cu/AZO coated polyester fabrics

8.4 Characterization of AZO/Ag/AZO coated high infrared reflective polyester fabrics

8.4.1 XRD analysis

The XRD spectra of the AZO/Ag/AZO and AZO/Ag coated multilayer films are plotted as a function of the thickness of the Ag layer, as shown in Figure 8.3. In the figure, the ZnO (002) peaks can be detected in every AZO/Ag/AZO sample, which proves a well-defined wurtzite ZnO structure in the multilayer films. The intensity of the ZnO (002) peaks of the AZO/Ag/AZO film samples is also greater than that of the AZO/Ag film samples, as expected, and this is because a thicker film means greater intensity of crystallization. In addition, the intensity of the Ag (111) peaks is increased with increases in the thickness of the Ag layer both in the AZO/Ag/AZO and AZO/Ag film samples. In the AZO/Ag XRD spectra, obvious ZnO (002) peaks can only be observed when the Ag layers have a thickness of 10 and 13 nm, which indicates that the top Ag layer also affects the crystallization of the bottom AZO layer, in that the increased crystallization of the top Ag layer enhances the crystallization of the bottom AZO film.

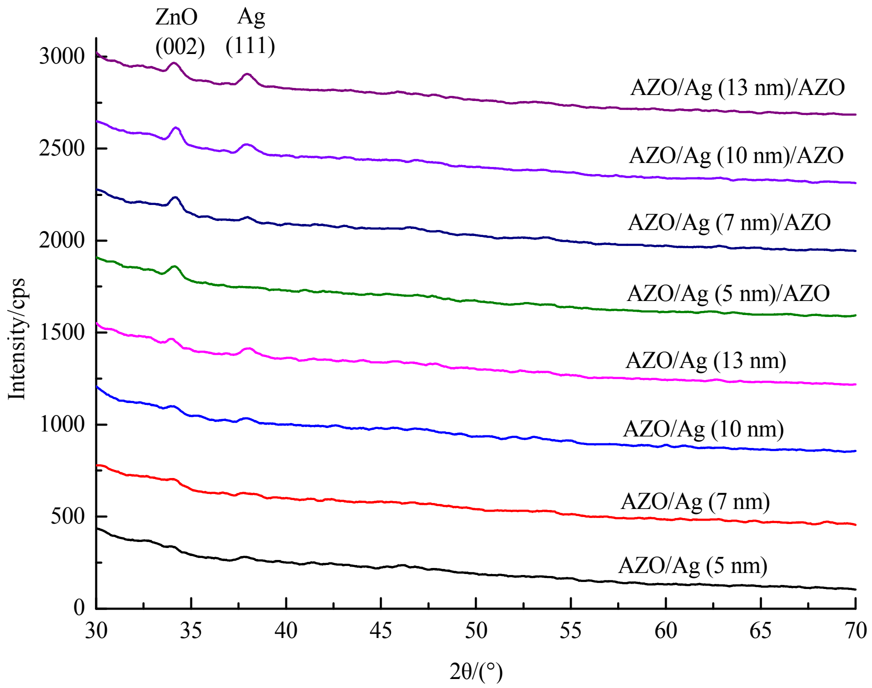

Figure 8.3 XRD spectra of the AZO/Ag/AZO and AZO/Ag coated polyester fabrics

8.4.2 Surface morphology analysis

SEM imaging of the deposited AZO/Ag films was carried out as a function of the thickness of the Ag layer, see Figure 8.4 for images. First, the Ag particle size is smaller than that seen in the other three images. There are gaps between the particles and almost no bonding between each other. The Ag particles are separate islands deposited onto an AZO substrate at this stage, see Figure 8.4(a). Then, the Ag particles begin to bond to each other and their size is increased, and so the gaps between them subsequently decrease. The surface of the Ag film is wavy at this thickness, as seen in Figure 8.4(b). Following that, the Ag particles agglomerate into large particles, and start to form a continuous flat film, and the particles bond well to each other, see Figure 8.4(c). Finally, the particle size of the continuous film is increased further, see Figure 8.4(d). By analyzing the images in Figure 8.4, it can be deduced that the evolution of the Ag film is consistent with the Volmer-Weber model, which is also the case for the same films deposited onto glass and PET substrates.

The SEM image of AZO/Ag (15 nm)/AZO coated polyester fabric is presented in Figure 8.5. In the figure, a layer of nano-scaled particles can be observed on the prepared polyester fabric surface. Moreover, the size of the particles is about 50 nm as estimated by the bar in the SEM image, which would endow the deposited polyester fabric with the unique properties of the nanomaterials.

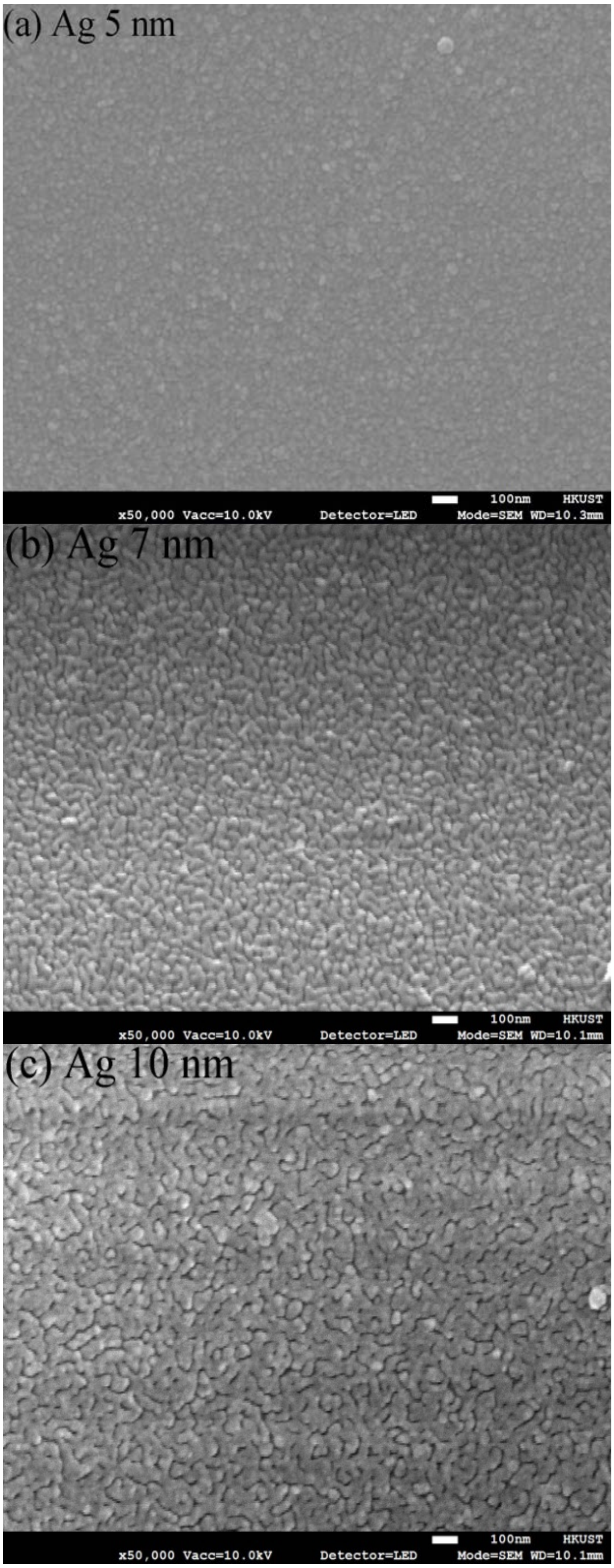
(a) Ag 5 nm
100nm HKUST
x50,000 Vacc=10.0kV Detector=LED Mode=SEM WD=10.3mm
(b) Ag 7 nm
100nm HKUST
x50,000 Vacc=10.0kV Detector=LED Mode=SEM WD=10.1mm
(c) Ag 10 nm
100nm HKUST
x50,000 Vacc=10.0kV Detector=LED Mode=SEM WD=10.1mm

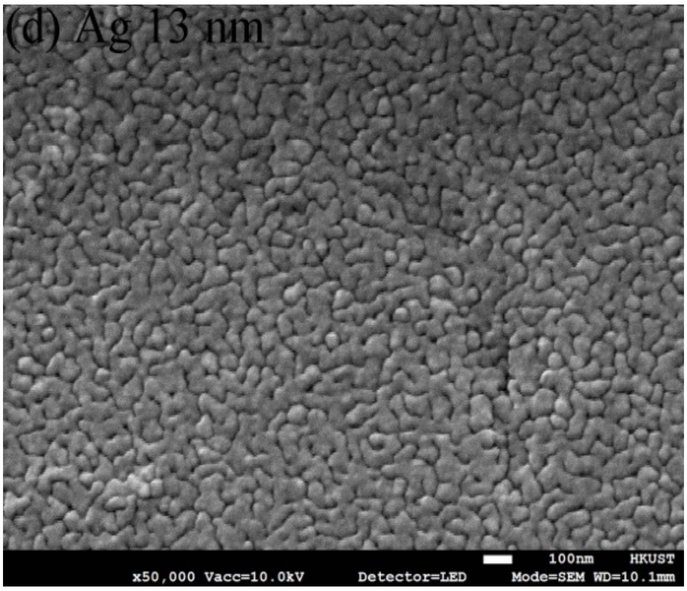

Figure 8.4 SEM images of AZO/Ag films with different thicknesses of Ag layer on polyester fabric

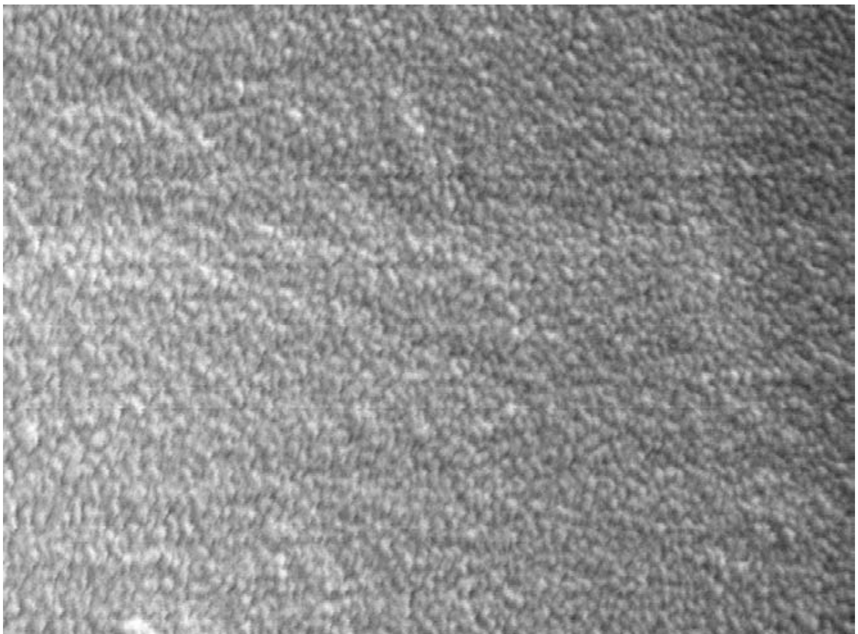

Figure 8.5 SEM image of AZO/Ag (15 nm)/AZO film deposited onto polyester fabric

8.4.3 Contact angle

Wettability is evaluated by water contact angle (CA) measurements of the uncoated polyester and coated polyester fabrics. Figure 8.6(a) shows the water CA on an uncoated polyester surface of about 52°. The CA is affected by the thickness of the coated films deposited onto a fabric [20], and in this study, the thickness of the AZO/Ag/AZO films varies minimally. Therefore, the CAs of different AZO/Ag/AZO coated samples change slightly, which is consistent with the testing results. The results, presented in Figure 8.6, show that the surface coated with nano-structured AZO/Ag (20 nm)/AZO trilayers obtains high hydrophobicity with a water CA of about 91.5° (Figure 8.6b).

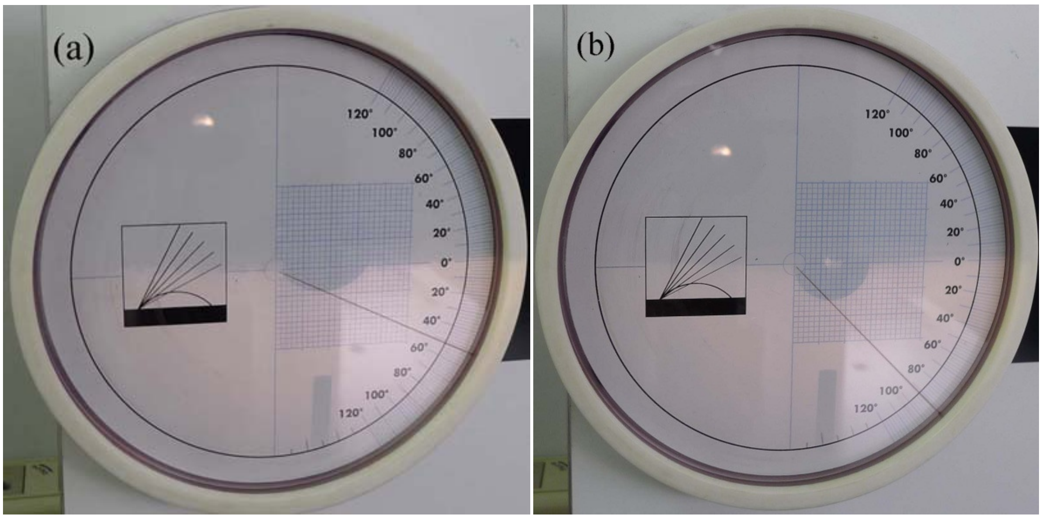

Figure 8.6 CAs of the uncoated and AZO/Ag/AZO coated polyester fabric

8.4.4 Air permeability

The air permeability was evaluated in accordance with ISO 9237:1995, and both uncoated and coated polyester fabrics were tested. The air permeability of the uncoated polyester fabric was 20 ml/s/cm^2 at 100 Pa. The values of the AZO/Ag/AZO coated polyester fabrics determined as a function of the thickness of the Ag layer from 5 to 20 nm were 19.6, 19.2, 18.4, 18, 17.1 and 15.4 ml/s/cm^2 at 100 Pa. As shown in the results, the air permeability decreased with increasing thickness of the deposited trilayers. The fabric air permeability was largely determined by the spaces between the yarn, and the deposited nano particles reduced those spaces, thus causing a reduction in the air permeability. However, the deposited particles are nano-sized, so they can only block a small amount of the space, and therefore, the air permeability of the coated fabric was only slightly reduced. This is supported by the fact that the highest reduction in the rate of the air permeability of the coated fabrics is only about 23%.

8.4.5 Visible transmittance analysis

Figure 8.7 shows the transmittance of UV radiation and visible light through the uncoated and AZO/Ag/AZO coated polyester fabrics. The transmittance of the uncoated fabric is about 2.7% in a wavelength range of 400-800 nm. The transmittance shows that the uncoated polyester fabric is close-knitted in that there is a low transmittance of visible light. Although the AZO/Ag/AZO multilayer films deposited onto transparent substrates show a visible transmittance above 80% and the transmittance in the Ag layers with different thicknesses provides different results, the tight fabric substrate blocks most of the visible light; therefore the visible transmittance of the AZO/Ag/AZO coated polyester fabrics is only about 1.7% in the same wavelength, which has a reduction of 1% compared to the uncoated fabric. Moreover, there are only very minimal transmittance differences among the different coated samples which are caused by the non-transparency of the polyester fibers.

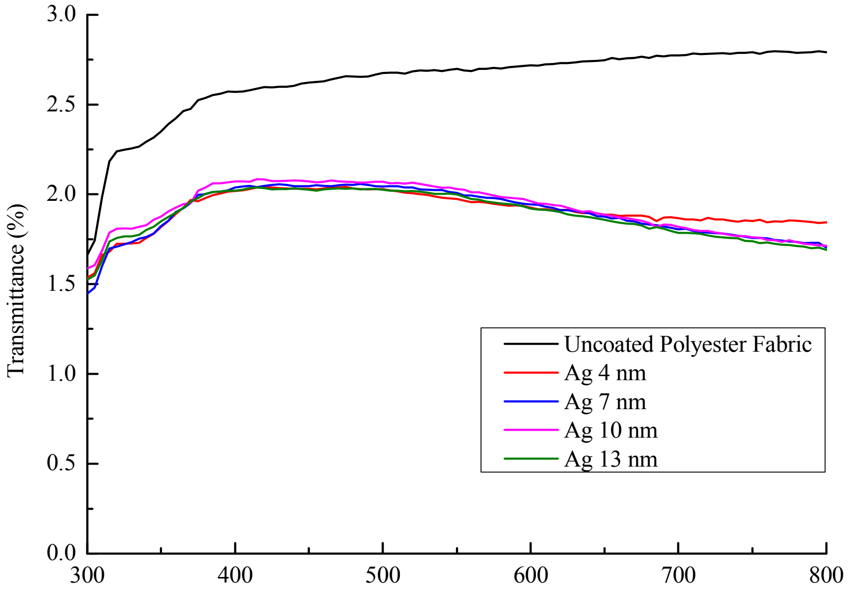

Figure 8.7 Visible transmittance of the coated and uncoated polyester fabric

8.4.6 Ultraviolet protection factor analysis

The UPF values of the AZO/Ag/AZO coated polyester fabrics that were determined as a function of the Ag layer with thicknesses that ranged from 5 to 20 nm were 30.26, 30.66, 34.49, 35.01, 40.64 and 46.67, respectively. Whereas the UPF value of the uncoated polyester fabric was only 20.09, it was determined that the UPF values of the AZO/Ag/AZO coated polyester fabrics increased by 50.64%, 52.63%, 71.67%, 74.29%, 102.29% and 132.3%, respectively. Among all of the UPF values, the values significantly increased when the Ag layer had a thickness of 10 nm. The significant variation is caused by the formation of a continuous Ag layer at a thickness of around 10 nm. When the Ag layer is less than 10 nm, there are gaps between each particle, and the film can be penetrated by UV radiation. After the continuous Ag film is formed, most of the UV radiation is blocked. Therefore, UV penetration decreases with increases in the thickness of the Ag film, and so, the UPF values are gradually increased.

In accordance with AATCC 183-2010, fabrics with UPF values in the range of 15-24 were classified as having “Good Protection”; those between 25 and 39 were considered to have “Very Good Protection” and 40 or greater were considered as having “Excellent UV Protection”. The results in this study prove that AZO/Ag/AZO (AZO: 30 nm; Ag: 15 and 20 nm) coated polyester fabrics provide “Excellent UV Protection”.

8.4.7 Infrared properties of AZO/Ag/AZO coated polyester fabrics

The IR properties of the AZO/Ag/AZO coated polyester fabrics are shown in Figures 8.8 and 8.9. In Figure 8.8, the coated fabrics exhibit a high rate of IR reflection when the Ag layer is thicker than 10 nm. Moreover, the IR reflection rate increases with increases in the thickness of the Ag layers. These results are consistent with the findings presented in Sections 6.4 and 6.5 in that the Ag inner layer started to form a continuous layer at a thickness of around 10 nm. As shown in the figure, the coated fabrics with Ag inner layers that have a thickness of 5 and 7 nm only show a slightly higher rate of IR reflection than that of the uncoated polyester fabric, whereas the coated fabrics with an Ag inner layer of 10 nm exhibit a much higher IR reflection, which is about 95% - 96% in the FIR region.

As stated in Section 6.6, the AZO/Ag/AZO multilayer films have a relatively high IR reflection when the Ag layer is about 13 nm, and the IR reflection rate is only improved slightly with further increases in the thickness of the Ag layer. This is consistent with the IR reflection spectra shown in Figure 8.8 and obvious differences in the IR reflection can only be observed in the NIR region among the samples with Ag inner layers of 13, 15 and 20 nm in thickness.

As shown in Figure 8.9, the IR transmittance of the coated fabrics is lower than that of the uncoated polyester fabric, and decreases with increases in film thickness. The IR transmittance of the coated fabrics is higher than that of the films coated onto glass and PET substrates as shown in Figures 6.10 and 6.18, which is mainly caused by the space among the fabric yarns. These results could also explain for the IR reflection rate of the coated fabrics, which is slightly lower than that with the same AZO/Ag/AZO film coated onto glass and PET substrates.

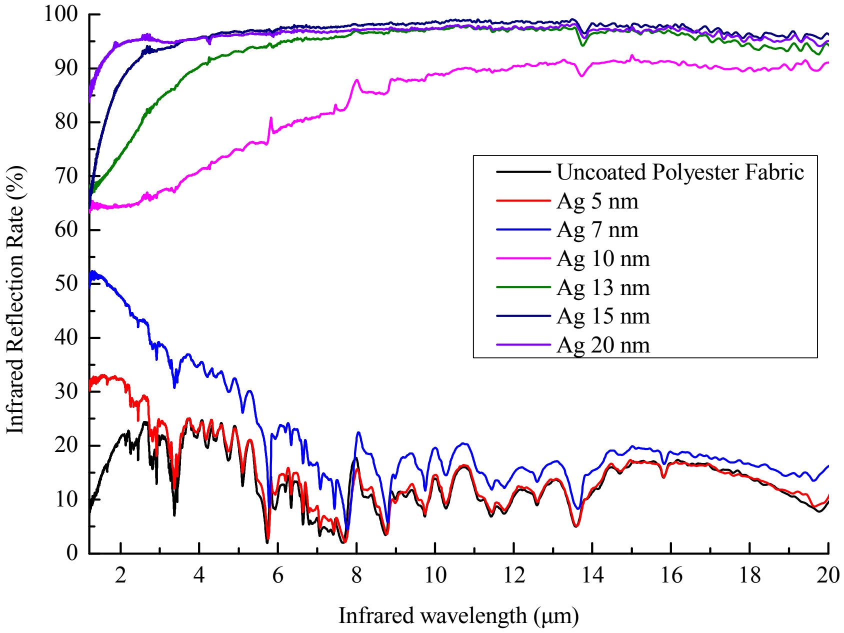

Figure 8.8 IR reflection spectra of the uncoated and AZO/Ag/AZO coated polyester fabric

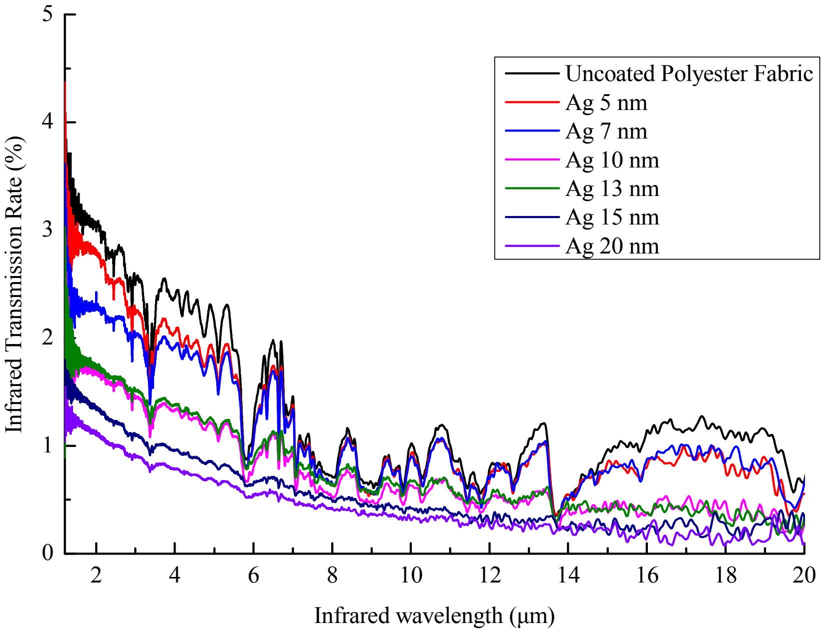

Figure 8.9 IR transmittance spectra of the uncoated and AZO/Ag/AZO coated polyester fabric

8.5 Characterization of AZO/Cu/AZO coated polyester fabrics

8.5.1 Contact angles, air permeability and UPFs of AZO/Cu/AZO coated polyester fabrics

The CAs among the AZO/Cu/AZO coated polyester fabrics only varied slightly, which was also the case for the AZO/Ag/AZO coated fabrics, and the highest value was about 85°. The air permeability of the AZO/Cu/AZO coated polyester fabrics determined as a function of the thickness of the Ag layer from 15 to 40 nm was 18.1, 17.5 and 15.9 $ml/s/cm^2$ at 100 Pa respectively. Compared to the AZO/Ag/AZO coated polyester fabrics, the CAs of the AZO/Cu/AZO coated polyester fabrics are smaller and air permeability is higher. The differences in CAs may be caused by the differences in the nature and crystallization of Ag and

Cu. And the differences in air permeability may be caused by the distortion of yarns or error of the testing process.

The UPF values of the AZO/Cu/AZO coated polyester fabrics determined as a function of the thickness of the Cu layer from 15 to 40 nm were 41.96, 48.437 and 49.008, respectively. Compared to the uncoated polyester (UPF=20.09), the UV protection of the AZO/Cu/AZO coated polyester fabrics increased by about 108.8%, 141.1% and 143.9%. The AZO/Cu/AZO coated fabrics have higher UPF values than those of AZO/Ag/AZO coated fabrics with the same film thickness, which is also true for the same films deposited onto glass substrates. Additionally, as evaluated from the UPF values, all of the AZO/Cu/AZO coated polyester fabrics exhibit excellent UV protection in accordance with AATCC 183-2010.

8.5.2 Infrared properties of AZO/Cu/AZO coated polyester fabrics

The IR properties of the AZO/Cu/AZO coated polyester fabrics are presented in Figures 8.10 and 8.11. In Figure 8.10, the AZO/Cu/AZO coated fabrics exhibit an IR reflection rate of 50% - 70% which is higher than that of the uncoated polyester fabric, and the IR reflection rate increases with increases in the thickness of the multilayer films, as expected. Similar to the AZO/Ag/AZO coated fabrics, the IR reflection rate of the AZO/Cu/AZO coated fabrics is slightly lower than that of the same films deposited onto glass substrates, which is also caused by IR penetration through the gaps found between the polyester yarns. These results are also consistent with the IR transmittance spectra presented in Figure 8.11, in which the IR transmittance is decreased with increasing thickness of the coated films.

The AZO/Cu/AZO coated polyester fabrics only showed an acceptable IR reflection which is lower than the IR reflection rate of the AZO/Ag/AZO coated polyester fabrics with the same film thickness. In considering the higher cost of Ag, AZO/Cu/AZO is a promising substitution for AZO/Ag/AZO multilayer films for products that do not demand the same quality and available at a more reasonable price.

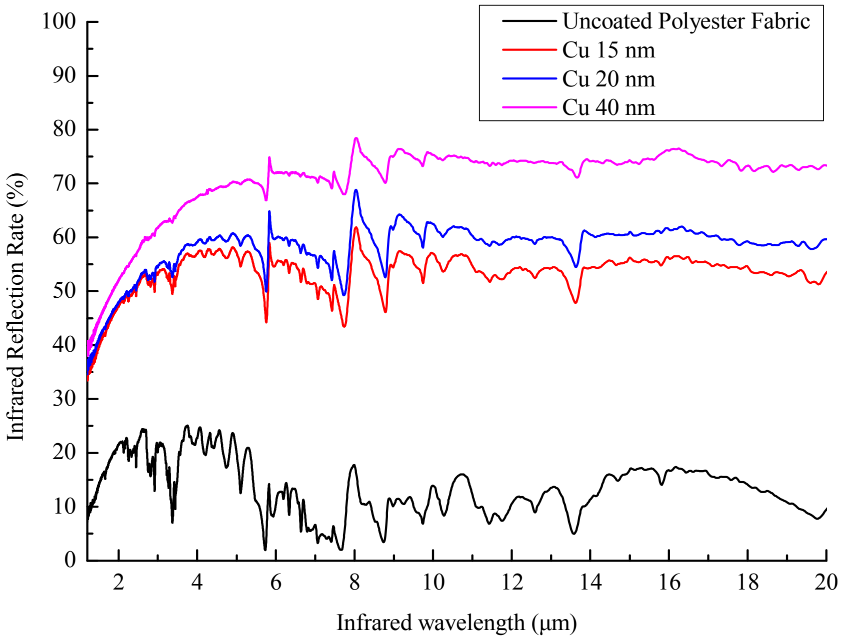

Figure 8.10 IR reflection spectra of the uncoated and AZO/Cu/AZO coated polyester fabric

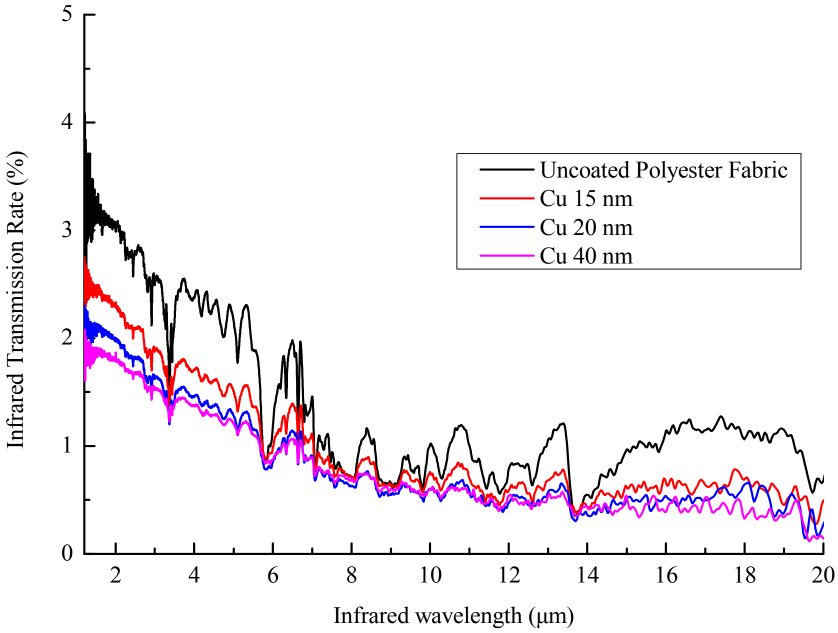

Figure 8.11 IR transmittance spectra of the uncoated and AZO/Cu/AZO coated polyester fabric

8.6 Summary

The deposition of AZO/Ag/AZO and AZO/Cu/AZO multilayer films onto polyester fabrics to fabricate high IR reflective textiles has been discussed in this chapter. The surface morphology, crystal structure, wettability, air permeability, UV radiation protection, visible transmittance and IR properties of the AZO/Ag/AZO coated polyester fabrics have been investigated. The results indicate that AZO/Ag/AZO coated polyester fabrics have the highest CA of about 91.5°, lowest air permeability, which is reduced by about 23% compared to the uncoated polyester fabric, and UPF values that range from 30.26 to 46.67, and visible transmittance of 1.5% - 2.0%. The samples coated with an Ag inner layer that has a thickness greater than 10 nm exhibit a high rate of IR reflection of 93% - 96% in the FIR region. Additionally, the AZO/Cu/AZO coated polyester fabrics have also been investigated. The results show that the AZO/Cu/AZO coated polyester fabrics have a lower CA, and higher UPF values than those of the AZO/Ag/AZO coated polyester fabrics with the same thickness of the inner metal layer, which may be caused by the differences in the nature and crystallization of Ag and Cu. The differences in air permeability may be caused by the distortion of yarns or error of the testing process. Moreover, the AZO/Cu/AZO coated polyester fabrics exhibit an acceptable rate of IR reflection of 50% - 70%.

The prepared polyester fabrics exhibit excellent IR reflectivity; these will be a good choice for the development of high IR reflective textiles. The conclusions of this study and suggestions for future research will be presented in the next chapter.

Chapter 9 Conclusions and Suggestions for Future Research

9.1 Conclusions

The purpose of this study is to fabricate high IR reflective textiles through the deposition of AZO/Ag/AZO multilayer films onto polyester fabric via RF magnetron sputtering. The deposition parameters and thickness of the AZO layers have been investigated towards the IR properties. The properties of the AZO/Ag/AZO multilayer structures are characterized after deposition onto glass and PET substrates. The influence of the Ag inner layer is studied and the evolution of the Ag inner layer in the deposition process has also been examined. After characterization of the AZO/Ag/AZO multilayer films, they have been applied onto polyester fabrics to fabricate high IR reflective textiles. In addition, the AZO/Cu/AZO multilayer films are also investigated for fabrication of products with an acceptable amount of IR reflection at a more reasonable price. The major findings that fulfill the objectives and represent significant contributions to the knowledge on film deposition are summarized as follows.

(1) High IR reflective textiles have been successfully prepared by depositing AZO/Ag/AZO multilayer films onto polyester fabrics through RF magnetron sputtering. The developed textiles show a high rate of IR reflection of about 95% 95% - 96%. Among all of the AZO and Ag based films, the AZO/Ag/AZO

multilayer shows the highest IR reflection. These results indicate that the surface of the bottom layer greatly affects the growth of the layer that is located on it. Furthermore, the bottom AZO layer helps the formation of a continuous Ag inner layer.

(2) The AZO films that are deposited onto glass substrates show a strong wurtzite wurtzite structure, and have low electrical conductivity, high visible transmittance and low IR reflection. The best average visible transmittance of the prepared AZO films is 84.8%. The electrical conductivity and IR reflectivity are directly proportional to the thickness of the AZO film. The AZO samples show an average IR reflection rate of approximately 30% in the the whole band range, which is 10% higher than that of glass. The AZO/Ag/AZO multilayer films deposited onto glass and PET substrates show show fine crystallization, high electrical conductivity, high visible transmittance and excellent IR reflection. The properties of the prepared AZO/Ag/AZO multilayer films are largely determined by the evolution of the Ag inner layer which follows the Volmer-Weber model in that Ag particle growth forms separate particles into a continuous film and the critical thickness of the Ag film is around 10 nm. The highest average visible transmittance of the AZO/Ag/AZO multilayer films is about 80%, which is obtained at a critical thickness of the Ag film. The electrical conductivity and IR reflectivity are directly proportional to the thickness of the Ag film; the

highest rate of the IR reflection of the prepared AZO/Ag/AZO multilayer films is about 96% - 97%.

(3) The AZO/Cu/AZO multilayer films deposited onto glass substrates exhibit an acceptable rate of IR reflection of about 67% with a Cu inner layer that has a thickness of 15 nm. The properties of the prepared AZO/Cu/AZO multilayer films are largely affected by the evolution of the Cu inner layer, which is also the case for the AZO/Ag/AZO films. The Cu inner layer starts to form a continuous film at a thickness of around 11 nm. The electrical conductivity and IR reflectivity are directly proportional to the thickness of the Cu film. To further improve the IR reflection of the AZO/Cu/AZO multilayer films, a much thicker Cu inner layer is required.

(4) The AZO/Ag/AZO and AZO/Cu/AZO coated polyester fabrics show good water repellency and air permeability, and excellent UV protection. These properties are affected by the thickness of the deposited films in that the water water repellency and UV protection would increase with increased film thickness. The air permeability would decrease with reduced film thickness. The high IR reflection and innovative functions of the nanomaterials render the AZO/Ag/AZO coated polyester fabrics as promising candidates for the future development of high IR reflective textiles. The AZO/Cu/AZO coated polyester fabrics exhibit an acceptable rate of IR reflection of 50% - 70%.

Therefore, they would be a proper substitution for AZO/Ag/AZO coated fabrics but at a more reasonable cost.

9.2 Suggestions for Future Research

In the present project, high IR reflective textiles have been fabricated by depositing AZO/Ag/AZO and AZO/Cu/AZO multilayer films onto polyester fabrics through RF magnetron sputtering. The created textiles have been proven to have high IR reflection, which could be used for heat shielding textiles. During the study, research opportunities have been revealed and identified. Therefore, the following recommendations are suggested to improve high IR reflective textiles in the future.

(1) Hitherto, only Ag and Cu have been investigated as the inner metal layer for the multilayer film in the present study due to the time limitations. It is well known that other alloys may create various new functions in this multilayer structure. The application of other types of alloy coatings is recommended for future studies.

(2) In this project, only one kind of polyester fabric has been used for deposition as the substrate fabric. Other fabric structures and types have not been evaluated in the present study, which can also affect the IR reflection

properties of coated textiles. Therefore, other fabric structures and types should also be considered in future studies.

(3) In this project, a preliminary study on high IR reflective textiles has been carried out. Applications of the developed textiles here are suggested for further investigation.

(4) It has been proven that AZO/Ag/AZO films have high IR reflection, which can be applied to the fabrication of heat shielding products. This also means that these films are a good candidate for IR stealth materials for the military, such as IR stealth suits and IR coatings for radar stealth, which could be studied in the future.

References

[1] N. H. Guo, X. Chen, S. P. Chen, W. Z. Zhu, "Solar heat reflective coatings," *Paint and Coatings Industry,* vol. 4, pp. 37-39, 1999.

[2] S. J. Tang, Z. Wang, Q. H. Meng, Y. Z. Fang, "Study on the Novel Infrared Reflective Materials and Application on the Films on Energy-saved Glass," *Information Recording Materials*, vol. 12, pp. 10-13, 2011.

[3] Y. M. Gao, L. Z. Chen, H. J. Qian, W. H. Miao, "Research and application of solar reflections coatings, " *Modern Paint and Finishing*, vol. 5, pp. 14-17, 2006.

[4] X. Zhang, D. Qiao, X. Lu, "Infrared stealth properties of ITO films on polymer matrix composites substrates," *Development and Application of Materials,* vol. 25, pp. 24-27, 2010.

[5] L. Gong, Z. Ye, J. Lu, L. Zhu, J. Huang, X. Gu and B. Zhao, "Highly transparent conductive and near- infrared reflective ZnO:Al thin films," *Vacuum,* vol. 84, pp. 947-952, 2010.

[6] Y. Okuhara, T. Kato, H. Matsubara, N. Isu and M. Takata, "Near-infrared reflection from periodically aluminium-doped zinc oxide thin films," *Thin Solid Films*, vol. 519, pp. 2280-2286, 2011.

[7] F. Khan, S. H. Baek and J. H. Kim, "Influence of Ag doping on structural, optical, and photoluminescence properties of nanostructured AZO films by sol-

gel technique," *J. Alloys Compd.*, vol. 584, pp. 190-194, 2014.

[8] D. K. Kim and H. B. Kim, "Room temperature deposition of Al-doped ZnO thin films on glass by RF magnetron sputtering under different Ar gas pressure," *J. Alloys Compd.,* vol. 509, pp. 421-425, 2011.

[9] C. P. Liu and G. R. Jeng, "Properties of aluminum doped zinc oxide materials and sputtering thin films," *J. Alloys Compd.,* vol. 468, pp. 343-349, 2009.

[10] G. E. Fernandes, D. J. Lee, J. H. Kim, K. B. Kim and J. Xu, "Infrared and microwave shielding of transparent Al-doped ZnO superlattice grown via atomic layer deposition," *J. Mater. Sci.,* vol. 48, pp. 2536-2542, 2013.

[11] H. HartnAgel, A. Dawar, A. Jain and C. JAgadish, *Semiconducting transparent thin films.* Bristol: Institute of Physics Pub, 1995.

[12] M. Girtan, "Comparison of ITO/metal/ITO and ZnO/metal/ZnO characteristics as transparent electrodes for third generation solar cells," *Sol. Energy Mater. Sol. Cells.,* vol. 100, pp. 153-161, 2012.

[13] Y. Y. Liu, R. H. Wang, H. F. Lu, L. Li, Y. Y. Kong, K. H. Qi and J. H. Xin, "Artificial lotus leaf structures from assembling carbon nanotubes and their applications in hydrophobic textiles," *J. Mater. Chem.,* vol. 17, pp. 1071-1078, 2007.

[14] R. H. Guo, S. Q. Jiang, C. Yuen and M. Ng, "Effect of copper content on the

properties of Ni-Cu-P plated polyester fabric," *J. Appl. Electrochem.,* vol. 39, pp. 907-912, 2009.

[15] R. H. Guo, S. Q. Jiang, C. Yuen and M. Ng, "Surface characterisation of electroless copper plated polyester fibres," *Surf. Eng.,* vol. 25, pp. 101-105, 2009.

[16] R. H. Guo, S. Q. Jiang, C. Yuen and M. Ng, "An alternative process for electroless copper plating on polyester fabric," *J. Mater. Sci. - Mater. Electron.*, vol. 20, pp. 33-38, 2009.

[17] M. Kuhr, S. Bauer, U. Rothhaar and D. Wolff, "Coatings on plastics with the PICVD technology," *Thin Solid Films,* vol. 442, pp. 107-116, 2003.

[18] S. X. Jiang, W. F. Qin, R. H. Guo and L. Zhang, "Surface functionalization of nanostructured silver-coated polyester fabric by magnetron sputtering," *Surf. Coat. Technol.,* vol. 204, pp. 3662-3667, 2010.

[19] Q. F. Wei, Q. Li, D. Y. Hou, Z. T. Yang and W. D. Gao, "Surface characterization of functional nanostructures sputtered on fiber substrates," *Surf. Coat. Technol.,* vol. 201, pp. 1821-1826, 2006.

[20] S. X. Jiang, W. F. Qin, X. M. Tao, Z. M. Zhang, C. Yuen, J. Xiong, C. W. Kan, L. Zhang, R. H. Guo and S. M. Shang, "Surface characterization of sputter silver-coated polyester fiber," *Fibers Polym.,* vol. 12, pp. 616-619, 2011.

[21] J. Yip, S. Jiang and C. Wong, "Characterization of metallic textiles deposited

by magnetron sputtering and traditional metallic treatments," *Surf. Coat. Technol.,* vol. 204, pp. 380-385, 2009.

[22] Q. Wei, Q. Xu, Y. Cai and Y. Wang, "Evaluation of the interfacial bonding between fibrous substrate and sputter coated copper," *Surf. Coat. Technol.,* vol. 202, pp. 4673-4680, 2008.

[23] C. H. Hou, J. M. Sun and B. L. Zhan, "Study on the heat insulation effect of infrared radiation coatings," *Journal of Zhengzhou University*, vol. *28*, pp. 54-56, 2007.

[24] C. Yao, S. L. Zhao and G. Y. Miao, "The property and application of nano transparent heat insulating films," *Paint & Coatings industry,* vol. 37, pp. 29-32, 2007.

[25] Y. Zhao and X. R. Kong, "Preparation of ITO nano particles and their composite film with infrared property," *Journal of Beijing University of Chemical Technology*, vol. 36, pp. 4-7, 2009.

[26] S. X. Li, W. G. Yang and F. Guo, "Study on thermal infrared shielding camouflage coatings," *Modern paint and finishing*, vol. 12, pp. 7-14, 2009.

[27] C. Y. Ma, Y. S. Li and Y. Q. Duan, "Preparation of near IR reflective materials by hollow balotini enwrapped TiO_2," *J. Cent. South Univ.,* vol. 35, pp. 806-809, 2004.

[28] G. S. Zheng, "The application of infrared reflection pigment," *Shanghai Coatings,* vol. 46, pp. 19-23, 2008.

[29] X. Y. Zhang and Y. J. Zhang, "Preparation of high near-infrared reflectance ceramic pigment by sol-gel method," *Journal of Synthetic Crystals,* vol. 44, pp. 417-420, 2013.

[30] D. G. Su, F. Ye and M. F. Zhong, "Preparation of infrared reflection phthalocyanine covered TiO_2 pigment," *Electroplating & Finishing*, vol. 30, pp. 75-77, 2011.

[31] F. Giovannetti, S. Föste, N. Ehrmann and G. Rockendorf, "High transmittance, low emissivity glass covers for flat plate collectors: Applications and performance," *Solar Energy*, vol. 104, pp.52-59, 2014.

[32] Z. R. Wang and Z. R. Yu, "The study of ITO coating infrared emissivity at 8 to 14 um," *Infrared Technology*, vol. 21, pp. 41-45, 1999.

[33] G. L. Ma, Q. X. Cao and Y. X. Huang, "Materials of infrared and radar multifunctional camouflage-doped semiconductor oxide," *Infrared Technology*, vol. 25, pp. 77-80, 2003.

[34] X. H. Li, L. Chen, X. X. Meng, and Y. P. Sun, "The study of foreign infrared stealth coating materials," *Infrared Technology*, vol. 16, pp. 5-11, 1994.

[35] L. G. Feng, Y. P. Cai, X. S. Sun and J. Liu, "Infrared absorption properties of

cylinder powder metal," *Journal of Sichuan University*, vol. 32, pp. 467-470, 1995.

[36] D. F. Pi, G. M. Wang and H. B. Fang, "The study of wide spectrum infrared stealth materials," *Semiconductor Technology*, vol. 3, pp. 51-53, 1996.

[37] M. Y. Zhang, J. S. Yao and Z. F. Chen, "The mechanism study of ITO wide spectrum stealth materials," *Minning and Metallurgical Engineering,* vol. 23, pp. 67-69, 2003.

[38] Y. Yang, Y. M. Zhou, J. H. Ge, Y. J. Wang and Y. X. Zhu, "Preparation, characterization, and infrared emissivity property of optically active polyurethane/TiO_2/SiO_2 multilayered microspheres," *J. Solid State Chem.,* vol. 184, pp. 2617-2622, 2011.

[39] C. Hu, G. Xu, X. Shen, C. Shao and X. Yan, "The epoxy-siloxane/Al composite coatings with low infrared emissivity for high temperature applications," *Appl. Surf. Sci.,* vol. 256, pp. 3459-3463, 2010.

[40] Y. Zhu, Y. Zhou, T. Zhang, M. He, Y. Wang, X. Yang and Y. Yang, "Preparation and characterization of lactate-intercalated Co-Fe layered double hydroxides and exfoliated nanosheet film with low infrared emissivity," *Appl. Surf. Sci.,* vol. 263, pp. 132-138, 2012.

[41] X. Yan and G. Xu, "Synergy effect of silane and CTAB on corrosion- resistant

property of low infrared emissivity Cu/polyurethane coating formed on tinplate," *Surf. Coat. Technol.,* vol. 204, pp. 1514-1520, 2010.

[42] X. Yan and G. Xu, "Effect of surface modification of Cu with Ag by ball-milling on the corrosion resistance of low infrared emissivity coating," *Mater. Sci. Eng., B: Solid-State Materials for Advanced Technology,* vol. 166, pp. 152-157, 2010.

[43] G. Wu and D. Yu, "Preparation and characterization of a new low infrared-emissivity coating based on modified aluminum," *Prog. Org. Coat.,* vol. 76, pp. 107-112, 2013.

[44] L. Yuan, X. L. Weng, J. L. Xie, W. F. Du and L. J. Deng, "Solvothermal synthesis and visible/infrared optical properties of Al/Fe_3O_4 core-shell magnetic composite pigments," *J. Alloys Compd.,* vol. 580, pp. 108-113, 2013.

[45] K. Kato, H. Omoto, T. Tomioka and A. Takamatsu, "Visible and near infrared light absorbance of Ag thin films deposited on ZnO under layers by magnetron sputtering," *Sol. Energy Mater. Sol. Cells.,* vol. 95, pp. 2352-2356, 2011.

[46] M. Del Re, R. Gouttebaron, J. P. Dauchot and M. Hecq, "Study of the optical properties of AlN/ZrN/AIN low-e coating," *Surf. Coat. Technol.,* vol. 180-81, pp. 488-495, 2004.

[47] J. H. Lee, S. H. Lee, K. L. Yoo, N. Y. Kim and C. K. Hwangbo, "Deposition of multi-period low-emissivity filters for display application by RF magnetron sputtering," *Surf. Coat. Technol.,* vol. 158, pp. 477-481, 2002.

[48] M. Yuste, R. E. Galindo, S. Carvalho, J. M. Albella and O. Sanchez, "Improving the visible transmittance of low-e titanium nitride based coatings for solar thermal applications," *Appl. Surf. Sci.,* vol. 258, pp. 1784-1788, 2011.

[49] K. Chiba, T. Takahashi, T. Kageyama and H. Oda, "Low-emissivity coating of amorphous diamond-like carbon/Ag-alloy multilayer on glass," *Appl. Surf. Sci.,* vol. 246, pp. 48-51, 2005.

[50] R. Meszaros, B. Merle, M. Wild, K. Durst, M. Göken and L. Wondraczek, "Effect of thermal annealing on the mechanical properties of low-emissivity physical vapor deposited multilayer-coatings for architectural applications," *Thin Solid Films,* vol. 520, pp. 7130-7135, 2012.

[51] E. Ando and M. Miyazaki, "Moisture resistance of the low-emissivity coatings with a layer structure of Al-doped ZnO/Ag/Al-doped ZnO," *Thin Solid Films,* vol. 392, pp. 289-293, 2001.

[52] E. Ando, S. Suzuki, N. Aomine, M. Miyazaki and M. Tada, "Sputtered silver-based low-emissivity coatings with high moisture durability," *Vacuum,* vol. 59, pp. 792-799, 2000.

[53] H. Liu, Y. S. Wang and J. H. Zhu, "Infrared stealth material," *Chinese Journal of Colloid & polymer*, vol. 20, 41-42, 2002.

[54] Y. Wang, G. Xu, H. Yu, C. Hu, X. Yan, T. Guo and J. Li, "Comparison of anti-corrosion properties of polyurethane based composite coatings with low infrared emissivity," *Appl. Surf. Sci.,* vol. 257, pp. 4743-4748, 2011.

[55] L. Yuan, X. Weng and L. Deng, "Influence of binder viscosity on the control of infrared emissivity in low emissivity coating," *Infrared Phys. Technol.,* vol. 56, pp. 25-29, 2013.

[56] H. Zhang, "The research and practice of infrared camouflage fabric," 2006.

[57] N. Li, "Study of sunlight infrared reflective thermal insulation materials," 2010.

[58] H. Zhang, T. Hu and J. Zhang, "Transmittance of infrared radiation through fabric in the range 8-14 μm," *Text. Res. J.,* vol. 80, pp. 1516-1521, 2010.

[59] W. L. Xu, T. W. Shyr and M. Yao, "Textiles' properties in the infrared irradiation," *Text. Res. J.,* vol. 77, pp. 513-519, 2007.

[60] M. Z. Li, Q. Zhang, Y. D. Yu and Y. C. Lin, "Sunshade cloth with thermal insulation and UV protection," *Dyeing and Finishing*, vol. 37, pp. 28-30, 2011.

[61] W. Haidinger, *Handbuch der bestimmenden mineralogy.* Wien: Braumüller and Seidel, 1845.

[62] W. L. BrAgg, "The arrangement of atoms in crystals," *The London, Edinburgh, and Dublin Philosophical Magazine and Journal of Science,* vol. 40, pp. 169-189, 1920.

[63] Y. Nishi and R. Doering, *Handbook of semiconductor manufacturing technology, Second Edition.* Boca Raton: CRC Press, 2008.

[64] F. Kröger, *The chemistry of imperfect crystals: imperfection chemistry of crystalline solids,* vol. 2, 1974.

[65] S. Fernandez, A. Martinez-Steele, J. J. Gandia and F. B. Naranjo, "Radio frequency sputter deposition of high- quality conductive and transparent ZnO: Al films on polymer substrates for thin film solar cells applications," *Thin Solid Films,* vol. 517, pp. 3152-3156, 2009.

[66] T. Yamada, A. Miyake, H. Makino, N. Yamamoto and T. Yamamoto, "Effect of thermal annealing on electrical properties of transparent conductive Ga-doped ZnO films prepared by ion-plating using direct-current arc discharge," *Thin Solid Film*s, vol. 517, pp. 3134-3137, 2009.

[67] M. Lee, J. Lim, J. Bang, W. Lee and J. Myoung, "Effect of the thickness and hydrogen treatment on the properties of Ga-doped ZnO transparent conductive films," *Appl. Surf. Sci.*, vol. 255, pp. 3195-3200, 2008.

[68] M. Allegrezza, M. Canino, M. Bellettato and C. Summonte, "Transparent Conducting Oxides for High Temperature Processing," *Energy Procedia,* vol. 44,

pp. 23-31, 2014.

[69] B. Oh, M. Jeong, D. Kim, W. Lee and J. Myoung, "Post-annealing of Al-doped ZnO films in hydrogen atmosphere," *J. Cryst. Growth*, vol. 281, pp. 475-480, 2005.

[70] P. Nunes, D. Costa, E. Fortunato and R. Martins, "Performances presented by zinc oxide thin films deposited by r.f. magnetron sputtering," *Vacuum*, vol. 64, pp. 293-297, 2002.

[71] W. Yang, Z. Wu, Z. Liu, A. Pang, Y. Tu and Z. C. Feng, "Room temperature deposition of Al-doped ZnO films on quartz substrates by radio-frequency magnetron sputtering and effects of thermal annealing," *Thin Solid Films*, vol. 519, pp. 31-36, 2010.

[72] H. Chang, F. Wang, J. Chao, C. Huang and H. Liu, "Effects of thickness and annealing on the properties of Ti-doped ZnO films by radio frequency magnetron sputtering," *Current Applied Physics*, vol. 11, pp. S185-S190, 2011.

[73] J. Kang, M. Lee, D. W. Kim, Y. S. Lim, W. Seo and H. Choi, "The annealing effect on damp heat stability of AGZO thin films prepared by DC moving magnetron sputtering," *Current Applied Physics*, vol. 11, pp. S333-S336, 2011.

[74] C. S. Moon, Y. M. Chung, W. S. Jung and J. G. Han, "The low temperature process design for Al doped ZnO film synthesis on polymer," *Surf. Coat. Technol.,*

vol. 201, pp. 5035-5038, 2007.

[75] S. Fernandez and F. B. Naranjo, "Optimization of aluminum-doped zinc oxide films deposited at low temperature by radio-frequency sputtering on flexible substrates for solar cell applications," *Sol. Energy Mater. Sol. Cells.,* vol. 94, pp. 157-163, 2010.

[76] C. Guillén and J. Herrero, "TCO/metal/TCO structures for energy and flexible electronics," *Thin Solid Films,* vol. 520, pp. 1-17, 2011.

[77] Y. S. Jung, Y. W. Choi, H. C. Lee and D. W. Lee, "Effects of thermal treatment on the electrical and optical properties of silver-based indium tin oxide/metal/ indium tin oxide structures," *Thin Solid Films,* vol. 440, pp. 278-284, 2003.

[78] J. Kim, J. Yun, S. Jee, Y. C. Park, M. Ju, S. Han, Y. Kim, J. Kim, W. A. Anderson, J. Lee and J. Yi, "Rapid thermal annealed Al-doped ZnO film for a UV detector," *Mater Lett,* vol. 65, pp. 786-789, 2011.

[79] C. H. Tseng, C. H. Huang, H. C. Chang, D. Y. Chen, C. P. Chou and C. Y. Hsu, "Structural and optoelectronic properties of Al-doped zinc oxide films deposited on flexible substrates by radio frequency magnetron sputtering," *Thin Solid Films,* vol. 519, pp. 7959-7965, 2011.

[80] M. Sibinski, K. Znajdek, S. Walczak, M. Sloma, M. Gorski and A. Cenian, "Comparison of ZnO:Al, ITO and carbon nanotube transparent conductive layers

in flexible solar cells applications," *Materials Science and Engineering b-Advanced Functional Solid-State Materia,* vol. 177, pp. 1292-1298, 2012.

[81] X. Diez-Betriu, R. Jimenez-Rioboo, J. Sanchez-Marcos, E. Cespedes, A. Espinosa and A. de Andres, "Amorphous-nanocrystalline Al doped ZnO transparent conducting thin films," *J. Alloys Compd.,* vol. 536, pp. S445-S449, 2012.

[82] E. J. Yun, J. W. Jung, B. C. Lee and M. Jung, "Characterization of the properties of high- energy electron irradiated Al-doped ZnO thin films prepared by RF magnetron sputtering using Ar plasma," *Surf. Coat. Technol.,* vol. 205, pp. 5130-5134, 2011.

[83] W. Liu, S. Wu, C. Hung, C. Tseng and Y. Chang, "Improving the optoelectronic properties of gallium ZnO transparent conductive thin films through titanium doping," *J. Alloys Compd.*, vol. 616, pp. 268-274, 2014.

[84] A. S. Pugalenthi, R. Balasundaraprabhu, V. Gunasekaran, N. Muthukumarasamy, S. Prasanna and S. Jayakumar, "Effect of thickness on the structural, optical and electrical properties of RF magnetron sputtered GZO thin films," *Mat. Sci. Semicon. Proc.*, vol. 29, pp. 176-182, 2015.

[85] M. Wu, S. Yu, G. Chen, L. He, L. Yang and W. Zhang, "Structural, optical, and electrical properties of Mo-doped ZnO thin films prepared by magnetron sputtering," *Appl. Surf. Sci.*, vol. 324, pp. 791-796, 2015.

[86] X. Chen, J. Liu, J. Ni, Y. Zhao and X. Zhang, "Wide-spectrum Mg and Ga co-doped ZnO TCO thin films for solar cells grown via magnetron sputtering with H_2 introduction," *Appl. Surf. Sci.*, vol. 328, pp. 193-197, 2015.

[87] H. An, H. Ahn and J. Park, "High-quality, conductive, and transparent Ga-doped ZnO films grown by atmospheric-pressure chemical-vapor deposition," *Ceram. Int.*, vol. 41, pp. 2253-2259, 2015.

[88] J. Yi, "Investigation of Electrical and Optical Properties of Highly Transparent TCO/Ag/TCO Multilaye," *J. Nanosci. Nanotechno.*, vol. 15, pp. 2247-2252, 2015.

[89] J. Yun, N. Duraisamy, M. M. Kumar and J. Kim, "Optical and electrical properties of AZO/Ni/ITO transparent conductor," *Mater. Lett.*, vol. 143, pp. 215-218, 2015.

[90] J. N. Alexander, N. Sun, R. Sun, H. Efstathiadis and P. Haldar, "Development and characterization of transparent and conductive InZnO films by magnetron sputtering at room temperature," *J. Alloys Compd.*, vol. 633, pp. 157-164, 2015.

[91] S. K. Vishwanath, W. Jin, J. Kang and J. Kim, "Polymer assisted solution processing of Ti-doped indium oxide transparent conducting thin films for organic solar cells," *J. Alloys Compd.*, vol. 631, pp. 67-71, 2015.

[92] J. M. Kim, P. Thiyagarajan and S. W. Rhee, "Deposition of Al-doped ZnO films

on polyethylene naphthalate substrate with radio frequency magnetron sputtering," *Thin Solid Films,* vol. 518, pp. 5860-5865, 2010.

[93] M. Fahland, P. Karlsson and C. Charton, "Low resisitivity transparent electrodes for displays on polymer substrates," *Thin Solid Films,* vol. 392, pp. 334-337, 2001.

[94] M. Katayama, "TFT-LCD technology," *Thin Solid Films,* vol. 341, pp. 140-147, 1999.

[95] E. Fortunato, D. Ginley, H. Hosono and D. C. Paine, "Transparent conducting oxides for photovoltaics," *MRS Bulletin,* vol. 32, pp. 242-247, 2007.

[96] H. Hosono, "Recent progress in transparent oxide semiconductors: Materials and device application," *Thin Solid Films,* vol. 515, pp. 6000-6014, 2007.

[97] M. Fahland, T. Vogt, W. Schoenberger and N. Schiller, "Optical properties of metal based transparent electrodes on polymer films," *Thin Solid Films,* vol. 516, pp. 5777-5780, 2008.

[98] T. Minami, "Transparent conducting oxide semiconductors for transparent electrodes," *Semicond. Sci. Technol.,* vol. 20, pp. S35-S44, 2005.

[99] T. Dimopoulos, G. Z. Radnoczi, B. Pécz and H. Brückl, " Characterization of ZnO:Al/Au/ZnO:Al trilayers for high performance transparent conducting electrodes," *Thin Solid Films*, vol. 519, pp. 1470-1474, 2010.

[100] D. Kim, "Low temperature deposition of transparent conducting ITO/Au/ ITO films by reactive magnetron sputtering," *Appl. Surf. Sci.*, vol. 256, pp. 1774-1777, 2010.

[101] K. S. Alford and T.L., "Metallic conductivity and the role of copper in ZnO/Cu/ ZnO thin films for flexible electronics," *Appl. Phys. Lett.*, vol. 94, pp. 052104-052104, 2009.

[102] D. R. Sahu and J. Huang, "The properties of ZnO/Cu/ZnO multilayer films before and after annealing in the different atmosphere," *Thin Solid Films*, vol. 516, pp. 208-211, 2007.

[103] H. Roh, S. Cho and W. Lee, "Study on the durability against heat in ITO/Ag-alloy/ ITO transparent conductive multilayer system," *Phys. Status Solidi A*, vol. 207, pp. 1558-1562, 2010.

[104] J. Jeong and H. Kim, "Low resistance and highly transparent ITO-Ag-ITO multilayer electrode using surface plasmon resonance of Ag layer for bulk-heterojunction organic solar cells," *Sol. Energy Mater. Sol. Cells*, vol. 93, pp. 1801-1809, 2009.

[105] M. Chakaroun, A. El Amrani, B. Lucas, B. Ratier and M. Aldissi, "Organic optoelectronic devices-flexibility versus performance," *Eur. Phys. J-Appl. Phys.*, vol. 51, pp. 33206-33206, 2010.

[106] M. Bender, W. Seelig, C. Daube, H. Frankenberger, B. Ocker and J. Stollenwerk, "Dependence of film composition and thicknesses on optical and electrical properties of ITO-metal-ITO multilayers," *Thin Solid Films*, vol. 326, pp. 67-71, 1998.

[107] A. Klöppel, W. Kriegseis, B. K. Meyer, A. Scharmann, C. Daube, J. Stollenwerk and J. Trube, "Dependence of the electrical and optical behaviour of ITO-silver-ITO multilayers on the silver properties," *Thin Solid Films*, vol. 365, pp. 139-146, 2000.

[108] N. D. Theodore and T. L. Alford, "Improved conductivity and mechanism of carrier transport in zinc oxide with embedded silver layer," *J. Appl. Phys.*, vol. 103, pp. 013708-013708, 2008.

[109] S. Choa, C. Cho, W. Hwang, K. Tae Eun and H. Kim, "Mechanical integrity of flexible InZnO/Ag/InZnO multilayer electrodes grown by continuous roll-to-roll sputtering," *Sol. Energy Mater. Sol. Cells*, vol. 95, pp. 3442-3449, 2011.

[110] J. Kim, D. Sohn and E. Kim, "Polymer-based multi-layer conductive electrode film for plastic LCD applications," *Appl. Phys. A*, vol. 72, pp. 699-704, 2001.

[111] M. Chakaroun, B. Lucas, B. Ratier, C. Defranoux, J. P. Piel and M. Aldissi, "High quality transparent conductive electrodes in organic photovoltaic devices,"

Thin Solid Films, vol. 518, pp. 1250-1253, 2009.

[112] S. Song, T. Yang, Y. Xin, L. Jiang, Y. Li, Z. Pang, M. Lv and S. Han, "Effect of GZO thickness and annealing temperature on the structural, electrical and optical properties of GZO/Ag/GZO sandwich films," *Curr. Appl. Phys.*, vol. 10, pp. 452-456, 2010.

[113] J. Lewis, S. Grego, B. Chalamala, E. Vick and D. Temple, "Highly flexible transparent electrodes for organic light-emitting diode-based displays," *Appl. Phys. Lett.*, vol. 85, pp. 3450-3452, 2004.

[114] Y. Abe and T. Nakayama, "Transparent conductive film having sandwich structure of gallium-indium-oxide/silver/gallium-indium-oxide," *Mater. Lett.*, vol. 61, pp. 3897-3900, 2007.

[115] S. H. Mohamed, "Effects of Ag layer and ZnO top layer thicknesses on the physical properties of ZnO/Ag/Zno multilayer system," *J. Phys. Chem. Solid.*, vol. 69, pp. 2378-2384, 2008.

[116] F. Wang, M. Z. Wu, Y. Y. Wang, Y. M. Yu, X. M. Wu and L. J. Zhuge, "Influence of thickness and annealing temperature on the electrical, optical and structural properties of AZO thin films," *Vacuum,* vol. 89, pp. 127-131, 2013.

[117] C. Y. Hsu, T. F. Ko and Y. M. Huang, "Influence of ZnO buffer layer on AZO film properties by radio frequency magnetron sputtering," *Journal of the*

European Ceramic Society, vol. 28, pp. 3065-3070, 2008.

[118] J. J. Huang, Y. P. Wang, J. G. Lu, L. Gong and Z. Z. Ye, "Transparent conductive Al-Doped ZnO/Cu bilayer films grown on polymer substrates at room temperature," *Chin.Phys.Lett.,* vol. 28, pp. 127306, 2011.

[119] M. Chen, Z. L. Pei, X. Wang, Y. H. Yu, X. H. Liu, C. Sun and L. S. Wen, "Intrinsic limit of electrical properties of transparent conductive oxide films," *Journal of Physics d-Applied Physics,* vol. 33, pp. 2538-2548, 2000.

[120] K. Ellmer and R. Mientus, "Carrier transport in polycrystalline transparent conductive oxides: A comparative study of zinc oxide and indium oxide," *Thin Solid Films,* vol. 516, pp. 4620-4627, 2008.

[121] A. Suzuki, T. Matsushita, N. Wada, Y. Sakamoto and M. Okuda, "Transparent conducting Al-doped ZnO thin films prepared by pulsed laser deposition," *Jpn. J. Appl. Phys.,* vol. 35, pp. 56-59, 1996.

[122] D. K. Kim and H. B. Kim, "Dependence of the properties of sputter deposited Al-doped ZnO thin films on base pressure," *J. Alloys Compd.*, vol. 522, pp. 69-73, 2012.

[123] D. K. Kim and H. B. Kim, "Room temperature deposition of Al-doped ZnO thin films on glass by RF magnetron sputtering under different Ar gas pressure," *J. Alloys Compd.*, vol. 509, pp. 421-425, 2011.

[124] J. Su, C. Tang, Q. Niu, C. Zang, Y. Zhang and Z. Fu, "Microstructure, optical and electrical properties of Al-doped ZnO films grown by MOCVD," *Appl. Surf. Sci.*, vol. 258, pp. 8595-8598, 2012.

[125] P. H. Quang, N. D. Sang and D. Q. Ngoc, "Pulsed electron beam deposition of transparent conducting Al-doped ZnO films," *Thin Solid Films*, vol. 520, pp. 6455-6458, 2012.

[126] Y. Suzaki, H. Miyagawa, K. Yamaguchi and Y. Kim, "Fabrication of Al doped ZnO films using atmospheric pressure cold plasma," *Thin Solid Films*, vol. 522, pp. 324-329, 2012.

[127] X. Díez-Betriu, R. Jiménez-Rioboo, J. S. Marcos, E. Céspedes, A. Espinosa and A. de Andrés, "Amorphous-nanocrystalline Al doped ZnO transparent conducting thin films," *J. Alloys Compd.*, vol. 536, pp. S445-S449, 2012.

[128] H. B. Zhou, H. Y. Zhang, Z. G. Wang and M. L. Tan, "Highly conductive and transparent Al-doped ZnO films on glass substrate via incorporating hydrogen at low substrate temperatures," *Mater. Lett.*, vol. 74, pp. 96-99, 2012.

[129] J. Kim, J. Yun, S. Jee, Y. C. Park, M. Ju, S. Han, Y. Kim, J. Kim, W. A. Anderson, J. Lee and J. Yi, "Rapid thermal annealed Al-doped ZnO film for a UV detector," *Mater. Lett.*, vol. 65, pp. 786-789, 2011.

[130] Z. Li, Z. Chen, W. Huang, S. Chang and X. Ma, "The transparence comparison of Ga- and Al-doped ZnO thin films," *Appl. Surf. Sci.*, vol. 257, pp. 8486-8489, 2011.

[131] X. D. Liu, J. Liu, S. Chen and Z. Q. Li, "Electrical transport properties of Al-doped ZnO films," *Appl. Surf. Sci.*, vol. 263, pp. 486-490, 2012.

[132] S. Rahmane, M. S. Aida, M. A. Djouadi and N. Barreau, "Effects of thickness variation on properties of ZnO:Al thin films grown by RF magnetron sputtering deposition," *Superlattice. Microst.*, vol. 79, pp. 148-155, 2015.

[133] Q. You, H. Cai, K. Gao, Z. Hu, S. Guo, P. Liang, J. Sun, N. Xu and J. Wu, "Highly transparent and conductive Al-doped ZnO films synthesized by pulsed laser co-ablation of Zn and Al targets assisted by oxygen plasma," *J. Alloys Compd.*, vol. 626, pp. 415-420, 2015.

[134] O. Gürbüz and S. Güner, "Role of annealing temperature on electrical and optical properties of Al-doped ZnO thin films," *Ceram. Int.*, vol. 41, pp. 3968-3974, 2015.

[135] M. Raja, N. Muthukumarasamy, D. Velauthapillai, R. Balasundrapraphu, T. S. Senthil and S. Agilan, "Enhanced photovoltaic performance of quantum dot-sensitized solar cell fabricated using Al-doped ZnO nanorod electrode," *Superlattice. Microst.*, vol. 80, pp. 53-62, 2015.

[136] M. F. Malek, M. H. Mamat, M. Z. Musa, T. Soga, S. A. Rahman, S. A. H. Alrokayan, H. A. Khan and M. Rusop, "Metamorphosis of strain/stress on optical band gap energy of ZAO thin films via manipulation of thermal annealing process," *J. Lumin.*, vol. 160, pp. 165, 2015.

[137] W. Hsiao, S. Tseng, C. Chung, D. Chiang, K. Huang, K. Lin, L. Li and M. Chen, "Effect on structural, optical and electrical properties of aluminum-doped zinc oxide films using diode laser annealing," *Opt. Laser Technol.*, vol. 68, pp. 41-47, 2015.

[138] H. Kumarakurua, D. Chernsa and A. M.Collins, "The growth and conductivity of nanostructured ZnO films grown on Al-doped ZnO precursor layers by pulsed laser deposition," *Ceram. Int.,* vol. 40, pp. 8389-8395, 2014.

[139] Q. Shi, K. S. Zhou, M. J. Dai, H. J. Hou, S. S. Lin, C. B. Wei and F. Hu, "Room temperature preparation of high performance AZO films by MF sputtering," *Ceram. Int.,* vol. 39, pp. 1135-1141, 2013.

[140] M. A. Martínez, J. Herrero and M. T. Gutiérrez, "Deposition of transparent and conductive Al-doped ZnO thin films for photovoltaic solar cells," *Sol. Energy Mater. Sol. Cells,* vol. 45, pp. 75-86, 1997.

[141] U. Betz, M. K. Olsson, J. Marthy, M. F. Escola and F. Atamny, "Thin films engineering of indium tin oxide: Large area flat panel displays application," *Surf. Coat. Technol.,* vol. 200, pp. 5751-5759, 2006.

[142] C. A. Hoel, T. O. Mason, J. F. Gaillard and K. R. Poeppelmeier, "Transparent conducting oxides in the ZnO-In_2O_3-SnO_2 system," *Chem. Mater.,* vol. 12, 3569-3579, 2010.

[143] K. Seal, M. A. Nelson, Z. C. Ying, D. A. Genov, A. K. Sarychev and V. M. Shalaev, "Growth, morphology, and optical and electrical properties of semicontinuous metallic films," *PHYSICAL REVIEW B; Phys.Rev.B,* vol. 67, pp. 035318, 2003.

[144] C. Guillén and J. Herrero, "Transparent conductive ITO/Ag/ITO multilayer electrodes deposited by sputtering at room temperature," *Opt. Commun.,* vol. 282, pp. 574-578, 2009.

[145] Y. S. Park, K. H. Choi and H. K. Kim, "Room temperature flexible and transparent ITO/Ag/ITO electrode grown on flexile PES substrate by continuous roll-to-roll sputtering for flexible organic photovoltaics," *J.Phys.D-Appl.Phys.,* vol. 42, pp. 235109, 2009.

[146] J. A. Jeong and H. K. Kim, "Low resistance and highly transparent ITO-Ag-ITO multilayer electrode using surface plasmon resonance of Ag layer for bulk-heterojunction organic solar cells," *Sol. Energy Mater. Sol. Cells.,* vol. 93, pp. 1801-1809, 2009.

[147] Y. S. Jung, Y. W. Choi, H. C. Lee and D. W. Lee, "Effects of thermal treatment on the electrical and optical properties of silver-based indium tin

oxide/metal/indium tin oxide structures," *Thin Solid Films,* vol. 440, pp. 278-284, 2003.

[148] C. Guillen and J. Herrero, "Transparent electrodes based on metal and metal oxide stacked layers grown at room temperature on polymer substrate," *Physica Status Solidi a-Applications and Materials Science,* vol. 207, pp. 1563-1567, 2010.

[149] D. R. Sahu, S. Lin and J. Huang, "Investigation of conductive and transparent Al-doped ZnO/Ag/Al-doped ZnO multilayer coatings by electron beam evaporation," *Thin Solid Films,* vol. 516, pp. 4728-4732, 2008.

[150] K. H. Choi, H. J. Nam, J. A. Jeong, S. W. Cho, H. K. Kim, J. W. Kang, D. G. Kim and W. J. Cho, "Highly flexible and transparent InZnSnOx/Ag/InZnSnOx multilayer electrode for flexible organic light emitting diodes," *Appl. Phys. Lett.,* vol. 92, pp. 223302, 2008.

[151] N. F. Ren, L. J. Huang, M. Zhou and B. J. Li, "Introduction of Ag nanoparticles and AZO layer to prepare AZO/Ag/FTO trilayer films with high over all photo electric properties," *Ceram. Int.,* vol. 40, pp. 8693-8699, 2014.

[152] J. A. Jeong, Y. S. Park and H. K. Kim, "Comparison of electrical, optical, structural, and interface properties of IZO-Ag-IZO and IZO-Au-IZO multilayer electrodes for organic photovoltaics," *J. Appl. Phys.,* vol. 107, pp. 023111, 2010.

[153] H. K. Kyung, S. J. Yu, S. P. Yong and Won-Jae Lee, "Properties of AZO/Ag/AZO Multilayer Thin Film Deposited on Polyethersulfone Substrate," *Trans. Electr. Electron. Mater.*, vol. 14, pp. 9-11, 2013.

[154] M. Theuring, M. Vehse, K. von Maydell and C. Agert, "AZO-Ag-AZO transparent electrode for amorphous silicon solar cells," *Thin Solid Films*, vol. 558, pp. 294 -297, 2014.

[155] D. R. Sahu, S. Y. Lin and J. L. Huang, "Deposition of Ag-based Al-doped ZnO multilayer coatings for the transparent conductive electrodes by electron beam evaporation," *Sol. Energy Mater. Sol. Cells.,* vol. 91, pp. 851-855, 2007.

[156] D. R. Sahu, S. Y. Lin and J. L. Huang, "Study on the electrical and optical properties of Ag/Al-doped ZnO coatings deposited by electron beam evaporation," *Appl. Surf. Sci.,* vol. 253, pp. 4886-4890, 2007.

[157] H. K. Park, J. W. Kang, S. I. Na, D. Y. Kim and H. K. Kim, "Characteristics of indium-free GZO/Ag/GZO and AZO/Ag/AZO multilayer electrode grown by dual target DC sputtering at room temperature for low-cost organic photovoltaics," *Sol. Energy Mater. Sol. Cells.,* vol. 93, pp. 1994-2002, 2009.

[158] S. Sutthana, N. Hongsith and S. Choopun, "AZO/Ag/AZO multilayer films prepared by DC magnetron sputtering for dye-sensitized solar cell application," *Curr. Appl Phys.,* vol. 10, pp. 813-816, 2010.

[159] I. Crupi, S. Boscarino, V. Strano, S. Mirabella, F. Simone and A. Terrasi, "Optimization of ZnO:Al/Ag/ZnO:Al structures for ultra-thin high-performance transparent conductive electrodes," *Thin Solid Films,* vol. 520, pp. 4432-4435, 2012.

[160] H. Wu, R. Yang, C. Hsiung and C. Chu, "Influence of Ag thickness of aluminum-doped ZnO/Ag/aluminum-doped ZnO thin films," *Thin Solid Films,* vol. 520, pp. 7147-7152, 2012.

[161] J. H. Qi, Y. Li, T. T. Duong, H. J. Choi and S. G. Yoon, "Dye-sensitized solar cell based on AZO/Ag/AZO multilayer transparent conductive oxide film," *J. Alloys Compd.,* vol. 556, pp. 121-126, 2013.

[162] Y Y. S. Jung, C. W. Bark, H. W. Choi and K. H. Kim, "Characteristics of AZO/Cu/AZO multilayer thin films prepared on polyethersulfone substrate at room temperature," *Mol. Cryst. Liq. Cryst.,* vol. 564, pp. 121-129, 2012.

[163] S. M. Song, T. L. Yang, M. S. Lv, Y. H. Li, Y. Q. Xin, L. L. Jiang, Z. C. Wu and S. H. Han, "Effect of Cu layer thickness on the structural, optical and electrical properties of AZO/Cu/AZO tri-layer films," *Vacuum,* vol. 85, pp. 39-44, 2010.

[164] Y. P. Wang, J. G. Lu, X. Bie, Z. Z. Ye, X. Li, D. Song, X. Y. Zhao and W. Y. Ye, "Transparent conductive and near-infrared reflective Cu-based Al-doped ZnO multilayer films grown by magnetron sputtering at room temperature," *Appl. Surf.*

Sci., vol. 257, pp. 5966-5971, 2011.

[165] Y. S. Lin and Y. H. Huang, "Study of optoelectronics and microstructures on the AZO/nano-layer metals/AZO sandwich structures," *J. Mater. Sci. - Mater. Electron.,* vol. 24, pp. 3058-3062, 2013.

[166] J. K. Jeong, "The status and perspectives of metal oxide thin-film transistors for active matrix flexible displays," *Semicond.Sci.Technol.,* vol. 26, pp. 034008, 2011.

[167] T. M. Razykov, C. S. Ferekides, D. Morel, E. Stefanakos, H. S. Ullal and H. M. Upadhyaya, "Solar photovoltaic electricity: Current status and future prospects," *Sol. Energy,* vol. 85, pp. 1580-1608, 2011.

[168] C. J. Brabec, "Organic photovoltaics: Technology and market," *Sol. Energy Mater. Sol. Cells.,* vol. 83, pp. 273-292, 2004.

[169] S. Logothetidis, "Flexible organic electronic devices: Materials, process and applications," *Materials Science and Engineering b-Advanced Functional Solid-State Material,* vol. 152, pp. 96-104, 2008.

[170] M. Choi, Y. Kim and C. Ha, "Polymers for flexible displays: From material selection to device applications," *Prog. Polym. Sci. (Oxford),* vol. 33, pp. 581-630, 2008.

[171] E. J. Widjaja, G. Delporte, F. Vandevelde and B. Vanterwyngen, "Progress

toward roll-to-roll processing of inorganic monolithic electrochromic devices on polymeric substrates," *Sol. Energy Mater. Sol. Cells.,* vol. 92, pp. 97-100, 2008.

[172] F. C. Krebs, S. A. Gevorgyan and J. Alstrup, "A roll-to-roll process to flexible polymer solar cells: model studies, manufacture and operational stability studies," *J. Mater. Chem.,* vol. 19, pp. 5442-5451, 2009.

[173] F. Ruske, A. Pflug, V. Sittinger, W. Werner and B. Szyszka, "Process stabilisation for large area reactive MF-sputtering of Al-doped ZnO," *Thin Solid Films,* vol. 502, pp. 44-49, 2006.

[174] K. H. Choi, J. A. Jeong, J. W. Kang, D. G. Kim, J. K. Kim, S. I. Na, D. Y. Kim, S. S. Kim and H. K. Kim, "Characteristics of flexible indium tin oxide electrode grown by continuous roll-to-roll sputtering process for flexible organic solar cells," *Sol. Energy Mater. Sol. Cells.,* vol. 93, pp. 1248-1255, 2009.

[175] Y. Park, H. Kim, S. Jeong and W. Cho, "Highly flexible indium zinc oxide electrode grown on PET substrate by cost efficient roll-to-roll sputtering process," *Thin Solid Films,* vol. 518, pp. 3071-3074, 2010.

[176] W. R. Grove, "On the Electro-Chemical Polarity of Gases," *Abstracts of the Papers Communicated to the Royal Society of London (1843-1854),* vol. 6, pp. 168-169, 1850.

[177] D. M. Mattox, *Handbook of Physical Vapor Deposition (PVD) Processing.*

Oxford: William Andrew, 2010.

[178] L. W. Rieth, "Sputter deposition of zinc oxide thin films," 2001.

[179] M. Ohring, *The Materials Science of Thin Films.* Boston: Academic Press, 1992.

[180] B. Zhao, "Synthesis and characterization of hydrogenated amorphous carbon-based tribological coatings," 2010.

[181] J. A. Thornton, "Influence of apparatus geometry and deposition conditions on the structure and topography of thick sputtered coatings," *J. Vac. Sci. Technol.,* vol. 11, pp. 666, 1974.

[182] W. Liu, "Zinc oxide sputter deposition and modeling of copper-indium-gallium-diselenide-based thin film solar cells," 2007.

[183] R. X. Wang, X. M. Tao, Y. Wang, G. F. Wang and S. M. Shang, "Microstructures and electrical conductance of silver nanocrystalline thin films on flexible polymer substrates," *Surf. Coat. Technol.,* vol. 204, pp. 1206-1210, 2010.

[184] O. Baghriche, C. Ruales, R. Sanjines, C. Pulgarin, A. Zertal, I. Stolitchnov and J. Kiwi, "Ag-surfaces sputtered by DC and pulsed DC-magnetron sputtering effective in bacterial inactivation: Testing and characterization," *Surf. Coat. Technol.,* vol. 206, pp. 2410-2416, 2012.

[185] X. Y. Zhao, "Sputter deposition of nanostructured antibacterial silver on polypropylene non-wovens," *Surf. Eng.,* vol. 24, pp. 70-74, 2008.

[186] Q. F. Wei, L. Y. Yu, N. Wu and S. J. Hong, "Preparation and characterization of copper nanocomposite textiles," *J. Ind. Text.,* vol. 37, pp. 275-283, 2008.

[187] B. Y. Deng, Q. F. Wei and W. D. Gao, "Physical properties of Al-doped ZnO films deposited on nonwoven substrates by radio frequence magnetron sputtering," *J. Coat. Technol. Res.,* vol. 5, pp. 393-397, 2008.

[188] B. Y. Deng, X. Yan, Q. F. Wei and W. D. Gao, "AFM characterization of nonwoven material functionalized by ZnO sputter coating," *Mater. Charact.,* vol. 58, pp. 854-858, 2007.

[189] H. Agura, A. Suzuki, T. Matsushita, T. Aoki and M. Okuda, "Low resistivity transparent conducting Al-doped ZnO films prepared by pulsed laser deposition," *Thin Solid Films,* vol. 445, pp. 263-267, 2003.

[190] S. Y. Kuo, W. C. Chen, F. I. Lai, C. P. Cheng, H. C. Kuo, S. C. Wang and W. F. Hsieh, "Effects of doping concentration and annealing temperature on properties of highly-oriented al-doped ZnO films," *J. Cryst. Growth,* vol. 287, pp. 78-84, 2006.

[191] Y. S. Kim and W. P. Tai, "Electrical and optical properties of Al-doped ZnO thin films by sol-gel process," *Appl. Surf. Sci.,* vol. 253, pp. 4911-4916, 2007.

[192] M. Wimmer, F. Ruske, S. Scherf and B. Rech, "Improving the electrical and optical properties of DC-sputtered ZnO:Al by thermal post deposition treatments," *Thin Solid Films,* vol. 520, pp. 4203-4207, 2012.

[193] J. L. Zhao, X. M. Li, J. M. Bian, W. D. Yu and X. D. Gao, "Structural, optical and electrical properties of ZnO films grown by pulsed laser deposition (PLD)," *J. Cryst. Growth,* vol. 276, pp. 507-512, 2005.

[194] W. S. Yan, T. M. Ong, H. P. Zhou and S. Xu, "The fabrication and application of ZnO:Al thin films in low-frequency inductively coupled plasma fabricated silicon solar cell," *Thin Solid Films*, vol. 520, pp. 6900-6904, 2012.

[195] C. Charpentier, P. Prod'Homme, and P.R. Cabarrocas, "Microstructural, optical and electrical properties of annealed ZnO:Al thin films," *Thin Solid Films*, vol. 531, pp. 424-429, 2013.

[196] R. Wen, L. Wang, X. Wang, G. Yue, Y. Chen and D. Peng, "Influence of substrate temperature on mechanical, optical and electrical properties of ZnO:Al films," *J. Alloys Compd.,* vol. 508, pp. 370-374, 2010.

[197] J. L. Zhao, X. W. Sun, H. Ryu and Y. B. Moon, "Thermally stable transparent conducting and highly infrared reflective Ga-doped ZnO thin films by metal organic chemical vapor deposition," *Opt. Mater.,* vol. 33, pp. 768-772, 2011.

[198] F. S. Li, Y. Z. Zhang, C. X. Wu, Z. X. Lin, B. B. Zhang and T. L. Guo,

"Improving efficiency of organic light-emitting diodes fabricated utilizing AZO/Ag/AZO multilayer electrode," *Vacuum,* vol. 86, pp. 1895-1897, 2012.

[199] Y. Chen, P. W. Wang, J. Hsu and C. Lee, "Post-annealing properties of aluminum-doped zinc oxide films fabricated by ion beam co-sputtering," *Vacuum,* vol. 87, pp. 227-231, 2013.

[200] S. Flickyngerova, M. Netrvalova, L. Prusakova, I. Novotny, P. Sutta and V. Tvarozek, "Modification of AZO thin-film properties by annealing and ion etching," *Vacuum,* vol. 84, pp. 215-217, 2009.

[201] N. Ohta, D. Ohba, S. Sato, Z. Tang, H. Shimizu and H. Shirai, "Rapid thermal-plasma annealing of ZnO:Al films for silicon thin-film solar cells," *Thin Solid Films,* vol. 519, pp. 6920-6927, 2011.

[202] S. Y. Kuo, K. C. Liu, F. I. Lai, J. F. Yang, W. C. Chen, M. Y. Hsieh, H. I. Lin and W. T. Lin, "Effects of RF power on the structural, optical and electrical properties of Al-doped zinc oxide films," *Microelectron. Reliab.,* vol. 50, pp. 730-733, 2010.

[203] Y. C. Lin, M. Z. Chen, C. C. Kuo and W. T. Yen, "Electrical and optical properties of ZnO:Al film prepared on polyethersulfone substrate by RF magnetron sputtering," *Colloids Surf. Physicochem. Eng. Aspects,* vol. 337, pp. 52-56, 2009.

[204] Z. L. Pei, X. B. Zhang, G. P. Zhang, J. Gong, C. Sun, R. F. Huang and L. S. Wen, "Transparent conductive ZnO:Al thin films deposited on flexible substrates prepared by direct current magnetron sputtering," *Thin Solid Films,* vol. 497, pp. 20-23, 2006.

[205] M. Wimmer, F. Ruske, S. Scherf and B. Rech, "Improving the electrical and optical properties of DC-sputtered ZnO:Al by thermal post deposition treatments," *Thin Solid Films,* vol. 520, pp. 4203-4207, 2012.

[206] W. S. Yan, T. M. Ong, H. P. Zhou and S. Xu, "The fabrication and application of ZnO:Al thin films in low-frequency inductively coupled plasma fabricated silicon solar cell," *Thin Solid Films,* vol. 520, pp. 6900-6904, 2012.

[207] T. Wang, X. Diao and P. Ding, "Orthogonal optimization for room temperature magnetron sputtering of ZnO:Al films for all-solid electrochromic devices," *Appl. Surf. Sci.,* vol. 257, pp. 3748-3752, 2011.

[208] H. Zhu, J. Hupkes, E. Bunte and S. M. Huang, "Study of ZnO:Al films for silicon thin film solar cells," *Appl. Surf. Sci.,* vol. 261, pp. 268-275, 2012.

[209] X. D. Liu, J. Liu, S. Chen and Z. Q. Li, "Electrical transport properties of Al-doped ZnO films," *Appl. Surf. Sci.,* vol. 263, pp. 486, 2012.

[210] E. Fortunato, P. Nunes, A. Marques, D. Costa, H. Águas, I. Ferreira, M. E. V. Costa, M. H. Godinho, P. L. Almeida, J. P. Borges and R. Martins, "Transparent,

conductive ZnO:Al thin film deposited on polymer substrates by RF magnetron sputtering," *Surface and Coatings Technology,* vol. 151-152, pp. 247-251, 2002.

[211] R. Wen, L. Wang, X. Wang, G. Yue, Y. Chen and D. Peng, "Influence of substrate temperature on mechanical, optical and electrical properties of ZnO:Al films," *J. Alloys Compd.,* vol. 508, pp. 370-374, 2010.

[212] N. R. Yogamalar and A. C. Bose, "Absorption-emission study of hydrothermally grown Al:ZnO nanostructures," *J. Alloys Compd.,* vol. 509, pp. 8493-8500, 2011.

[213] W. Song, R. E. Justice, C. A. Jones, V. H. Grassian and S. C. Larsen, "Synthesis, characterization, and adsorption properties of nanocrystalline ZSM-5," Langmuir, vol. 20, pp. 8301-8306, 2004.

[214] M. Suchea, S. Christoulakis, N. Katsarakis, T. Kitsopoulos and G. Kiriakidis, "Comparative study of zinc oxide and aluminum doped zinc oxide transparent thin films grown by direct current magnetron sputtering," *Thin Solid Films,* vol. 515, pp. 6562-6566, 2007.

[215] E. Martin, M. Yan, M. Lane, J. Ireland, C. R. Kannewurf and R. Chang, "Properties of multilayer transparent conducting oxide films," *Thin Solid Films,* vol. 461, pp. 309-315, 2004.

[216] D. Y. Zhang, H. Yabe, E. Akita, P. P. Wang, R. Murakami and X. P. Song,

"Effect of silver evolution on conductivity and transmittance of ZnO/Ag thin films," *J. Appl. Phys.,* vol. 109, pp. 104318, 2011.

[217] M. Aliofkhazraei and N. Ali, *Two-Dimensional Nanostructures*. New York: CRC press, 2012.

[218] K. W. Sun, W. C. Zhou, X. F. Tang, Z. B. Huang, F. Luo and D. M. Zhu, "Effects of air annealing on the structure, resistivity, infrared emissivity and transmission of indium tin oxide films," *Surf. Coat. Technol.,* vol. 206, pp. 4095-4098, 2012.

[219] L. Gong, J. G. Lu and Z. Z. Ye, "Transparent conductive Ga-doped ZnO/Cu multilayers prepared on polymer substrates at room temperature," *Sol. Energy Mater. Solar Cells*., vol. 95, pp. 1826-1830, 2011.